Supporting Information

Carbonohydrazonoyl dicyanide−linked indole carboxamides as a new scaffold for transmembrane H^+/Cl^- transport

Akram Raza,[a] Sandip Chattopadhayay,[a] Debashis Mondal,[a,‡] and Pinaki Talukdar*[a]

[a] Department of Chemistry, Indian Institute of Science Education and Research Pune, Dr. Homi Bhabha Road, Pashan, Pune 411008, Maharashtra, India.

[‡] Department of Chemistry, University of Reading, Whiteknights, Reading, RG6, 6DX, UK.

Table of contents

1. General methods

All dry reactions were performed under the nitrogen atmosphere. All the chemicals and solvents were purchased from commercial sources, *Sigma–Aldrich*, *TCI*, *Avra*, *Spectrochem*, and *BLD* companies, and they were used as received. Dry solvents THF, CH_2Cl_2, and MeOH were purchased from *Spectrochem* company. For purification, column chromatography was carried over silica gel (100–200 mesh), which was directly purchased from *Rankem* company. The reaction progress was monitored by thin layer chromatography (TLC) *E. Merck* silica gel 60–F254 plates obtained commercially from *Sigma−Aldrich*. Deuterated solvents (DMSO–d_6, acetonitrile–d_3) were purchased from *Sigma–Aldrich* company for NMR characterization and all other NMR-related experiments. 8-Hydroxypyrene-1,3,6-trisulfonic acid trisodium salt (HPTS), lucigenin, and 5(6)-Carboxyfluorescein (CF) dyes were also purchased from *Sigma–Aldrich* company. Egg yolk phosphatidylcholine (EYPC) lipid was purchased from *Avanti Polar Lipids Inc*. as a solution dissolved in chloroform (25 mg/mL). 4-(2-Hydroxyethyl)piperazine-1-ethanesulfonic acid (HEPES), tris, phosphate, and citrate buffers, Triton X–100, NaOH, and all inorganic salts were purchased from *Sigma–Aldrich* as molecular biology grade. Gel–permeation chromatography was performed on a column of Sephadex G-50 gel (25×300 mm, V_0 = 25 mL). Large unilamellar vesicles (LUVs) were prepared from EYPC lipid using a mini extruder equipped with 100 nm or 200 nm pore size polycarbonate membrane (*Whatman Nuclepore*™) acquired from *Avanti Polar Lipids Inc*.

2. Physical measurements

The ^{1}H, ^{13}C, and ^{19}F NMR spectra were recorded on *Bruker* or *Jeol* (400 MHz for ^{1}H, 376.8 MHz for ^{19}F, and 101 MHz for ^{13}C NMR) spectrometers by using either residual solvent signals as an internal reference or from internal tetramethyl silane on the δ scale relative dimethyl sulfoxide (δ 2.50 ppm), acetonitrile (δ 1.94) for ^{1}H NMR and dimethyl sulfoxide (δ 39.50 ppm) for ^{13}C NMR. The chemical shifts (δ) are reported in ppm and coupling constants (J) in Hz. The following abbreviations are used: s (singlet), d (doublet), t (triplet), m (multiplet), and td (triplet of doublet) while describing ^{1}H NMR signals. The compound purity test was established by employing analytical HPLC (High-performance liquid chromatography) Agilent 1260 infinity II equipped with Luna@ 5 μm C18 100 Å reverse phase LC column (250 × 4.6 mm). High–resolution mass spectra (HRMS) were performed using *Waters SYNAPT G2*, a micro mass electron spray ionization–time of flight (ESI–TOF) spectrometer. Fluorescence spectra were recorded using Fluoromax–4 and Fluoromax+ from *Jobin Yvon Edison* (*Horiba Scientific*), equipped with an injector port and a micromagnetic stirrer. Infrared (IR) spectra

were recorded in cm^{-1} using a *Bruker* FT–IR spectrometer. The single crystal X–ray diffraction (SCXRD) data was collected on a *Bruker* Smart Apex Duo Diffractometer using Mo K*α* radiation at 297 K. The pH of the buffer solutions was measured using a *Helmer* pH meter. UV–Vis spectra were recorded on a *Shimadzu* UV–2600 UV–Vis spectrophotometer. Chloride concentration data in ppm was obtained by using an *Accumet* chloride–selective electrode. All fluorescence data were processed by *Origin 8.5*, and finally, all data were processed through *Chem Draw Professional 20*.

3. Synthesis

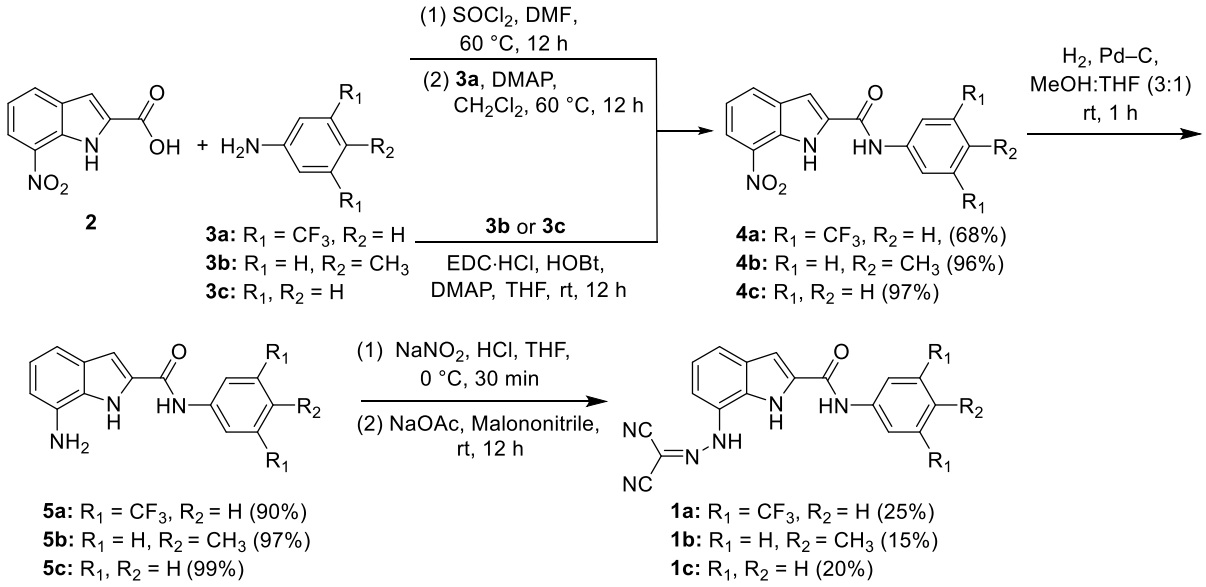

Scheme. S1 Synthetic scheme of **1a**–**1c**.

3.1 Synthesis of 2 (7–nitro–1*H*–indole–2–carboxylic acid): Compound **2** was synthesized in 4 steps using a standard protocol.[S1]

3.2.1 Synthesis of compound *N*–(3,5–bis(trifluoromethyl)phenyl)–7–nitro–1*H*-indole–2–carboxamide (4a): To synthesize compound **4a**, compound **2** (300 mg, 1.46 mmol) was initially dissolved in 20 mL $SOCl_2$ in a clean and dry 50 mL round–bottomed flask. A catalytic amount of DMF was added to it, and then the reaction mixture was refluxed for 12 h at 60 ºC. Reaction progress was monitored by TLC. After completion of the reaction, $SOCl_2$ was evaporated. The corresponding acid chloride was obtained as a solid yellowish product, which was immediately used for further reaction without any purification. Dry CH_2Cl_2 (10 mL) was added in a two–neck round–bottomed flask containing acid chloride under a nitrogen atmosphere. Solution of compound **3a**, 3,5–bis(trifluoromethyl)aniline (333 mg, 1.46 mmol),

and DMAP base (623 mg, 5.10 mmol) in CH_2Cl_2 (5 mL) were added dropwise into the two neck RB containing acid chloride solution. The reaction mixture was refluxed for 12 h at 60 °C. Completion of the reaction was monitored by TLC. The reaction mixture was transferred into a separating funnel, and the water layer was washed with CH_2Cl_2 (20 mL × 3). Subsequently, the collected CH_2Cl_2 layer was washed with a brine solution (20 mL). Finally, to remove the trace amount of water, Na_2SO_4 was added to the collected CH_2Cl_2 solution. Then, the CH_2Cl_2 was evaporated on the rota evaporator to get the crude product. The dried yellow crude product was further purified over silica gel (100–200 mesh) column chromatography at 20% ethyl acetate/pet ether to get pure yellow compound **4a** with a 68% (415 mg) yield. **^{1}H NMR (400 MHz, DMSO–*d*$_6$):** δ 11.57 (s, 1H), 11.18 (s, 1H), 8.49 (s, 2H), 8.29 (d, J = 8.0 Hz, 2H), 7.86 (s, 1H), 7.66 (d, J = 2.2 Hz, 1H), 7.38 (t, J = 7.9 Hz, 1H); **^{13}C NMR (101 MHz, DMSO–*d*$_6$):** δ 158.7, 140.4, 133.3, 133.1, 131.0, 130.9, 130.8, 130.6, 130.3, 129.0, 125.8, 124.0, 122.2, 121.7, 120.4, 120.2, 119.7, 119.7, 116.6, 116.6, 116.6, 116.6, 116.5, 108.0; **^{19}F NMR (376.8 MHz, DMSO−*d*$_6$):** −61.59; **HRMS (ESI):** Calc. $C_{17}H_{10}F_6N_3O_3$ $[M+H]^+$: 418.0621, Found: 418.0627; **IR (neat, *ν*/cm^{-1}):** 3463, 3352, 3115, 1646, 1556, 1474, 1375, 1330, 1277, 1175, 1122, 988, 936, 892, 831, 733, 690, 626.

3.2.2 Synthetic of compound 7–amino–*N*–(3,5-bis(trifluoromethyl)phenyl)–1*H*–indole–2–carboxamide (5a): In a 100 mL round−bottomed flask, the compound **4a** (320 mg, 0.77 mmol) was dissolved in 20 mL of dry MeOH/THF (3:1) solvent, and then the solution was degassed for 30 min using an N_2 gas balloon. Then, the catalytic amount of Pd–C (10%) was quickly added into RB, and the solution was stirred under an H_2 gas balloon for 1 h at room temperature. The reaction process was checked by TLC. After completion of the reaction, the reaction mixture was passed through a celite bed and washed with MeOH. Then, the crude product was purified using silica gel (100−200 mesh) column chromatography using 30% ethyl acetate/pet ether as a solvent system to get the pure compound **5a** with a 90% (267 mg) yield. **^{1}H NMR (400 MHz, DMSO−*d*$_6$):** δ 11.49 (s, 1H), 10.74 (s, 1H), 8.56 (s, 2H), 7.80 (s, 1H), 7.38 (d, J = 2.2 Hz, 1H), 6.91 (d, J = 8.0 Hz, 1H), 6.83 (t, J = 8.0 Hz, 1H), 6.42 (dd, J = 7.3, 0.8 Hz, 1H), 5.45 (s, 2H); **^{13}C NMR (101 MHz, DMSO−*d*$_6$):** δ 160.6, 141.1, 134.6, 131.2, 130.9, 130.6, 130.2, 129.3, 127.8, 127.4, 127.1, 124.7, 122.0, 121.6, 119.5, 119.0, 116.1, 116.1, 116.1, 116.1, 116.0, 109.5, 106.4, 105.3; **^{19}F NMR (376.8 MHz, DMSO−*d*$_6$):** −61.62; **HRMS (ESI):** Calc. $C_{17}H_{12}F_6N_3O$ $[M+H]^+$: 388.0879, Found: 388.0886. **IR (neat, *ν*/cm^{-1}):** 3327, 2924, 2854, 1654, 1563, 1551, 1471, 1441, 1422, 1378, 1351, 1275, 1243, 1176, 1130, 986, 936, 886, 835, 820, 778, 732, 700, 682.

3.2.3 Synthetic of compound (*N*–(2–((3,5-bis(trifluoromethyl) phenyl)carbamoyl)–1*H*-indol–7–yl) carbonohydrazonoyl dicyanide) (1a): To synthesize the final Compound **1a**,[S3] compound **5a** (200 mg, 0.52 mmol) was taken in a dry and clean 50 mL round–bottomed flask containing 200 μL HCl and 1 mL THF solution. After the addition of $NaNO_2$ (53 mg, 0.77 mmol) solution into the reaction mixture, it was stirred for 30 min at 0 °C. The required amount of NaOAc (338 mg, 4.13 mmol) and malononitrile (81 mg, 1.24 mmol) were added to it, and it was kept in stirring condition for 12 h. The reaction progress was monitored by TLC. After completion of the reaction, the crude mixture was extracted with ethyl acetate (10 mL × 3) and washed with brine (15 mL). Finally, a trace amount of moisture was removed using Na_2SO_4, and the solvent was evaporated by a rota evaporator. The dried mixture was purified over silica gel at 14% ethyl acetate/pet ether, and the purified compound **1a** was obtained with a 25% (60 mg) yield. **^{1}H NMR (400 MHz, acetonitrile−*d*$_3$):** δ 11.10 (s, 1H), 10.21 (s, 1H), 9.29 (s, 1H), 8.40 (s, 2H), 7.76 (s, 1H), 7.67 (dt, J = 8.0, 0.9 Hz, 1H), 7.38 (d, J = 2.2 Hz, 1H), 7.33 (dd, J = 7.7, 1.0 Hz, 1H), 7.21 (t, J = 7.9 Hz, 1H); **^{13}C NMR (101 MHz, DMSO−*d*$_6$):** δ 159.9, 140.7, 131.2, 131.1, 130.9, 130.6, 130.2, 129.5, 127.3, 126.2, 124.6, 121.9, 120.9, 120.2, 119.7, 119.6, 119.2, 116.5, 116.5, 116.4, 116.4, 116.4, 114.6, 112.2, 110.3, 105.3; **^{19}F NMR (376.8 MHz, DMSO−*d*$_6$):** −61.67; **HRMS (ESI):** Calc. $C_{20}H_{11}F_6N_6O$ $[M+H]^+$ 465.0893, Found: 465.0898; **IR (neat, *v*/cm^{-1}):** 3460, 3332, 3216, 3075, 2219, 1679, 1559, 1461, 1377, 1274, 1185, 1125, 935, 888, 830, 730.

3.3.1 Synthesis of 7–nitro–*N*–(*p*–tolyl)–1*H*–indole–2–carboxamide (4b): First, in a 50 mL round–bottomed flask, 7–nitro–1*H*–indole–2–carboxylic acid **2** (600 mg, 2.91 mmol) and **3b**, *p*−toluidine (310 mg, 2.91 mmol) were dissolved in 10 mL of dry THF. Then, into the reaction mixture, HOBt (430 mg, 3.20 mmol), EDC·HCl (730 mg, 3.78 mmol), and DMAP (900 mg, 7.28 mmol) were added sequentially. The reaction mixture was then stirred overnight at room temperature under an inert atmosphere. After completion of the reaction, the reaction mixture was washed with water (2 × 30 mL) and followed by brine solution (1 × 20 mL) while extracting the compound in $CHCl_3$ (100 mL). The organic layer was then dried over Na_2SO_4, and the solvent was evaporated in a rotary evaporator to get the crude product. The crude product was purified by silica gel column chromatography using 30% ethyl acetate/pet ether as a solvent system to get the pure compound **4b** with a 96% (825 mg) yield. The ^{1}H NMR and ^{13}C NMR data matched with the reported protocol.[S2] **^{1}H NMR (400 MHz, DMSO–*d*$_6$):** δ 11.50 (s, 1H), 10.60 (s, 1H), 8.27 (m, 1H), 8.24 (s, 1H) 7.68 (d, J = 8.3 Hz, 2H), 7.59 (d, J = 1.9 Hz, 1H), 7.36 (t, J = 7.4 Hz, 1H), 7.20 (d, J = 8.3 Hz, 2H), 2.30 (s, 3H); **^{13}C NMR (101 MHz,**

DMSO–d_6): δ 157.9, 135.9, 134.6, 133.1, 130.9, 130.7, 129.2, 128.9, 121.3, 120.3, 120.0, 107.2, 20.5; **HRMS (ESI):** Calc $C_{16}H_{14}N_3O_3$ $[M+H]^+$: 296.1030, Found: 296.1034; **IR (neat, ν/cm^{-1}):** 3735, 3458, 3339, 3121, 2918, 2384, 2311, 1741, 1649, 1600, 1518, 1398, 1283, 1236, 1106, 980, 819, 727, 626.

3.3.2 Synthesis of 7–amino–*N*–(*p*-tolyl)–1*H*–indole–2–carboxamide (5b): In a 100 mL round–bottomed flask, the compound **4b** (800 mg, 2.71 mmol) was solubilized in 40 mL MeOH/THF (3:1) solvent, and then the solution was purged with nitrogen gas for 30 min. Then, a catalytic Pd–C (10%) was added quickly to the solution, and the solution was stirred under an H_2 gas for 1 h at room temperature. The reaction progress was observed by TLC. After completion of the reaction, the reaction mixture was passed through a celite bed and washed with MeOH. The crude product was then purified by silica gel column chromatography using 40% ethyl acetate/pet ether as a solvent system to get the compound **5b** with a 97% (697 mg) yield. The ^{1}H NMR and ^{13}C NMR data matched with the reported protocol.[S2] **^{1}H NMR (400 MHz, DMSO–d_6):** δ 11.34 (s, 1H), 10.06 (s, 1H), 7.69 (d, J = 8.3 Hz, 2H), 7.31 (d, J = 1.9 Hz, 1H), 7.17 (d, J = 8.3 Hz, 2H), 6.87 (d, J = 7.9 Hz, 1H), 6.80 (t, J = 7.6 Hz, 1H), 6.39 (d, J = 7.2 Hz, 1H), 5.40 (s, 2H), 2.29 (s, 3H); **^{13}C NMR (101 MHz, DMSO–d_6):** δ 159.8, 136.5, 134.5, 132.4, 130.4, 129.1, 127.9, 126.6, 121.2, 120.2, 109.2, 105.9, 104.0, 20.5; **HRMS (ESI):** Calc. $C_{16}H_{16}N_3O$ $[M+H]^+$: 266.1288, Found: 266.1295. **IR (neat, ν/cm^{-1}):** 3392, 3280, 3208, 1709, 1632, 1609, 1586, 1549, 1517, 1425, 1405, 1356, 1329, 1284, 1258, 1200, 1106, 1018, 802, 780, 744, 727, 691.

3.3.3 Synthesis of compound (*N*–(2–(*p*–tolylcarbamoyl)–1*H*–indol–7–yl) carbonohydrazonoyl dicyanide) (1b): For the synthesis of final compound **1b**,[S3] in a 50 mL round–bottomed flask, compound **5b** (95 mg, 0.35 mmol) was taken, which was suspended in a mixture of 400 µL HCl and 1.6 mL THF solution. The $NaNO_2$ water solution (37 mg, 0.53 mmol) was added dropwise. The reaction was stirred for 30 min at 0 °C. After that, NaOAc (234 mg, 2.8 mmol) and malononitrile (59 mg, 0.89 mmol) were added. The reaction was stirred overnight. The reaction progress was monitored by TLC. After completion of the reaction, the crude mixture was extracted with ethyl acetate. (5 mL × 3) and washed with brine. The organic layer was dried over Na_2SO_4. The dried mixture was purified over silica gel at 14% ethyl acetate/pet ether. The purified compound was obtained with a 15% (18 mg) yield. **^{1}H NMR (400 MHz, acetonitrile−d_3):** δ 11.11 (s, 1H), 10.17 (s, 1H), 8.82 (s, 1H), 7.66–7.62 (m, 3H), 7.31–7.29 (m, 2H), 7.23–7.14 (m, 3H), 2.33 (s. 3H); **^{13}C NMR (101 MHz,**

DMSO−d_6): δ 159.1, 136.1, 132.9, 132.3, 129.7, 129.2, 127.6, 125.8, 120.7, 120.4, 119.9, 115.1, 111.8, 110.5, 104.1, 20.5; **HRMS (ESI):** Calc. $C_{19}H_{15}N_6O$ $[M+H]^+$: 343.1302, Found: 343.1310; **IR (neat, ν/cm^{-1}):** 3280, 2925, 2859, 2218, 1709, 1632, 1549, 1468, 1417, 1324, 1274, 814, 733, 644.

3.4.1 Synthesis of 7–nitro–*N*–phenyl–1*H*–indole–2–carboxamide (4c): For the first step, in a 50 mL round bottom flask, compound **2** (290 mg, 1.41 mmol) and **3c**, aniline (144 mg, 1.55 mmol) were dissolved in 10 mL dry THF. Then sequentially, HOBt (210 mg, 1.55 mmol), EDC.HCl (350 mg, 1.84 mmol) and DMAP (400 mg, 3.25 mmol) were added to the reaction mixture. The reaction mixture was then stirred overnight at room temperature under an inert atmosphere. After completion of the reaction, the reaction mixture was washed with water (2 × 15 mL) and followed by brine solution (1 × 15 mL) while extracting the compound in $CHCl_3$ (60 mL). The organic layer was then dried over Na_2SO_4, and the solvent was evaporated in a rotary evaporator to get the crude product. The crude product was purified by silica gel column chromatography using 10% ethyl acetate/pet ether as a solvent system to get compound **4c** with a 97% (383 mg) yield. **^{1}H NMR (400 MHz, DMSO–d_6):** δ 11.54 (s, 1H), 10.67 (s, 1H), 8.27 (t, J = 7.1 Hz, 2H), 7.80 (d, J = 7.9 Hz, 2H), 7.62 (d, J = 1.8 Hz, 1H), 7.43−7.35 (m, 3H), 7.15 (t, J = 7.4 Hz, 1H); **^{13}C NMR (101 MHz, DMSO–d_6):** δ 158.0, 138.5, 134.5, 133.1, 130.9, 130.8, 128.9, 128.8, 124.1, 121.4, 120.3, 120.1, 107.4; **HRMS (ESI):** Calc. $C_{15}H_{12}N_3O_3$ $[M+H]^+$: 282.0873, Found: 282.0885; **IR (neat, ν/cm^{-1}):** 3735, 3459, 3353, 3129, 2385, 2312, 1657, 1600, 1541, 1442, 1403, 1301, 1237, 1104, 983, 829, 742, 687, 629.

3.4.2 Synthesis of 7–amino–*N*–phenyl–1*H*-indole–2–carboxamide (5c): For synthesizing compound **5c**, first in 100 mL RB, compound **4c** (285 mg, 1.01 mmol) was taken and solubilized into a 20 mL Methanol/THF mixture (3:1). The resultant solution was purged with nitrogen gas for 30 min. After degassing, a catalytic amount of palladium on the carbon (10%) catalyst was added quickly, and the reaction was put for hydrogenation using a hydrogen gas for 1 h. The reaction progress was monitored by TLC. After completion of the reaction, the solvent mixture was passed through the celite bed and washed with methanol. Filtrate was dried as a grey solid compound and purified by column chromatography over silica gel in 30% ethyl acetate/pet ether to get compound **5c** with a 99% (252 mg) yield. **^{1}H NMR (400 MHz, DMSO–d_6):** δ 11.37 (s, 1H), 10.15 (s, 1H), 7.82 (dd, J = 8.6, 0.9 Hz, 2H), 7.39–7.35 (m, 2H), 7.33 (d, J = 2.2 Hz, 1H), 7.10 (t, J = 7.3 Hz, 1H), 6.88 (d, J = 7.8 Hz, 1H), 6.80 (t, J = 7.8 Hz, 1H), 6.39 (dd, J = 7.3, 0.8 Hz, 1H), 5.41 (s, 2H); **^{13}C NMR (101 MHz, DMSO–d_6):** δ 160.0, 139.1,

134.6, 130.3, 128.7, 127.9, 126.7, 123.5, 121.3, 120.1, 109.3, 106.0, 104.2; **HRMS (ESI):** Calc. $C_{15}H_{14}N_3O$ $[M+H]^+$: 252.1131, Found: 252.1142; **IR (neat, *ν*/cm^{-1}):** 3381, 3303, 3213. 3035, 2926, 1706, 1625, 1587, 1508, 1420, 1346, 1319, 1242, 1065, 1013, 869, 813, 733, 706, 659.

3.4.3 Synthesis of (*N*–(2–(phenylcarbamoyl)–1*H*–indol–7–yl) carbonohydrazonoyl dicyanide) (1c): To synthesize the final compound **1c**,[S3] initially, in a 50 mL round−bottomed flask, compound **5c** (95 mg, 0.37 mmol) was taken, which was suspended in a mixture of 300 μL HCl and 1.7 mL THF solution. A solution of $NaNO_2$ (39 mg, 0.56 mmol) in water was added dropwise at 0 °C, and the reaction was stirred for 30 min. After that, NaOAc (522 mg, 6.3 mmol) and malononitrile (62 mg, 0.94 mmol) were added. The reaction was stirred overnight at room temperature. The reaction progress was checked by TLC. After completion of the reaction, the crude mixture was extracted with ethyl acetate. The dried mixture was purified over silica gel at 12% ethyl acetate/pet ether. The purified **1c** was obtained with a 20% (25 mg) yield. **^{1}H NMR (400 MHz, acetonitrile−*d*$_3$):** *δ* 11.10 (s, 1H), 10.19 (s, 1H), 8.87 (s, 1H), 7.79–7.76 (m, 2H), 7.64–7.62 (m, 1H), 7.42–7.38 (m, 2H), 7.32–7.29 (m, 2H), 7.21–7.17 (m, 2H); **^{13}C NMR (101 MHz, DMSO−*d*$_6$):** *δ* 159.3, 138.7, 132.2, 132.1, 129.6, 128.8, 126.0, 126.0, 123.8, 120.7, 120.3, 119.9, 115.2, 112.0, 104.4; **HRMS (ESI):** Calc. $C_{18}H_{13}N_6O$ $[M+H]^+$: 329.1145, Found: 329.1149; **IR (neat, *ν*/cm^{-1}):** 3259, 2922, 2856, 2220, 1704, 1631, 1544, 1454, 1320, 1268, 1070, 820, 737, 688, 648.

4. Binding studies

4.1 2D NMR studies

Before performing anion binding studies, ^{1}H–^{1}H COSY 2D spectrum of compound **1a** was collected in acetonitrile–*d*$_3$ to understand the relative position of each proton peak in NMR spectrum.

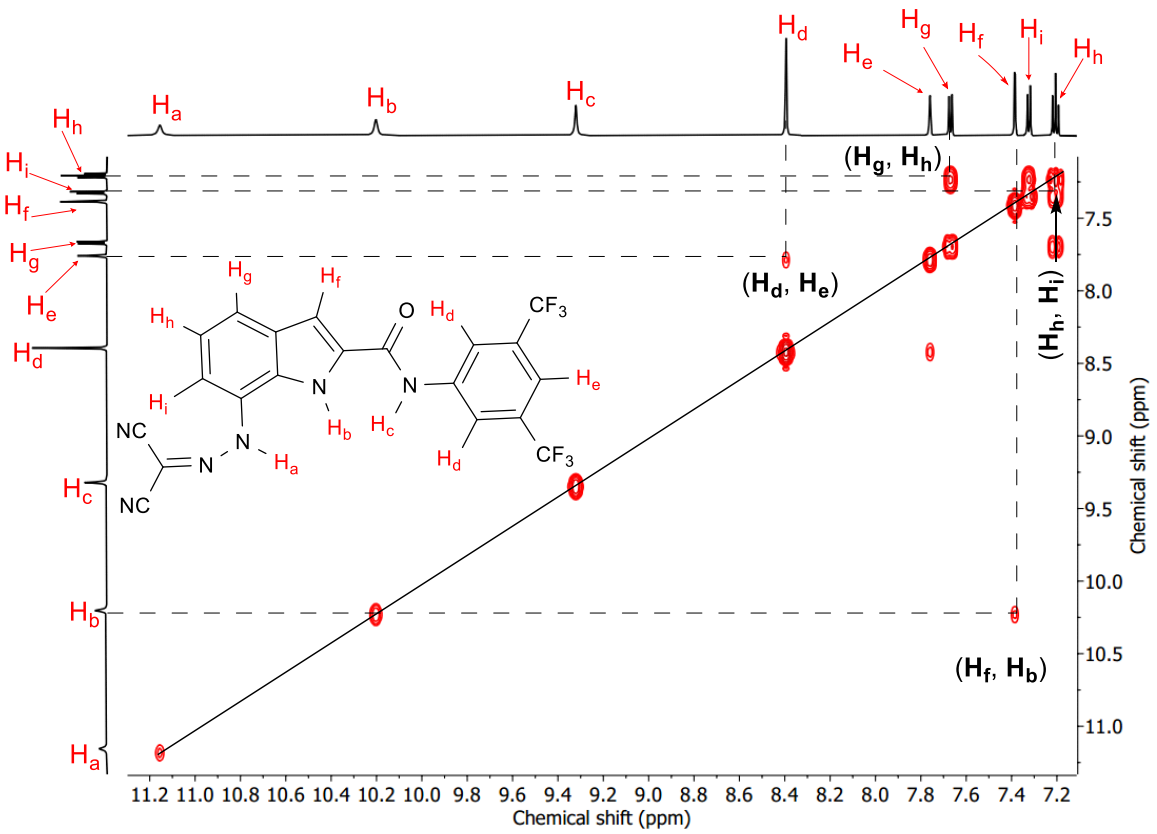

Fig. S1 ^{1}H–^{1}H COSY 2D NMR spectrum of compound **1a** (4 mM) in acetonitrile–d_3 at 25 °C (400 MHz).

4.2 ^{1}H NMR titration studies

^{1}H NMR titrations were carried out to investigate the ion binding process of the receptor in acetonitrile–d_3 solvent at 25 °C in Bruker 400 MHz NMR instrument. A solution of 2 mM compound **1a** in acetonitrile–d_3 was taken in an NMR tube. Alteration in the proton chemical shift was investigated upon sequential addition of the tetra butyl ammonium halide (TBAX, where $X^- = Cl^-, Br^-, I^-$) salt from a 200 mM stock solution. A sequential downfield shift of the protons H_a, H_b, H_c, H_d, and H_f was observed by increasing the equivalent of the TBAX salt, validating the involvement of these protons in the overall ion binding process. The binding constant was evaluated using the *BindFit program*[S4] by fitting the data into a 1:1 model. However, the addition of TBAI did not show any prominent change in the chemical shift, indicating compound **1a** cannot bind efficiently with the larger I^- ion in its binding pocket. Due to the insignificant shift in the ^{1}H NMR titration, we were unable to evaluate the binding constant by using the *BindFit program*.

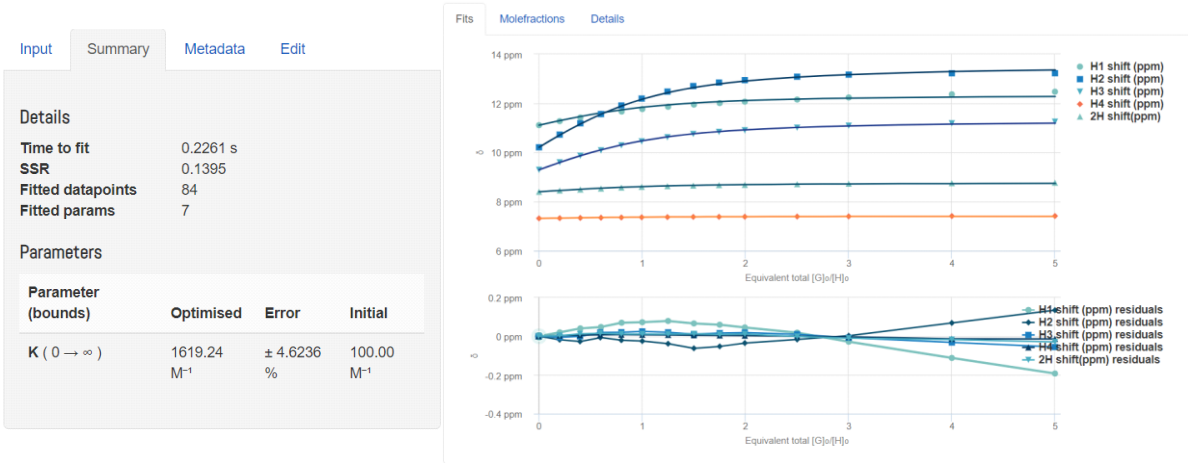

Fig. S2 Screenshot of the fitted data plot for a 1:1 model from supramolecular.org. The right–side graph shows an increase in the downfield chemical shift of different protons of **1a** upon the sequential addition of TBACl. The left side picture shows the calculated binding constant, which fits in the 1:1 compound–to–anion binding model. The *BindFit* webpage of this experiment is: http://app.supramolecular.org/bindfit/view/d33600bb-f080-434d-b34f-aaac4e5c8117

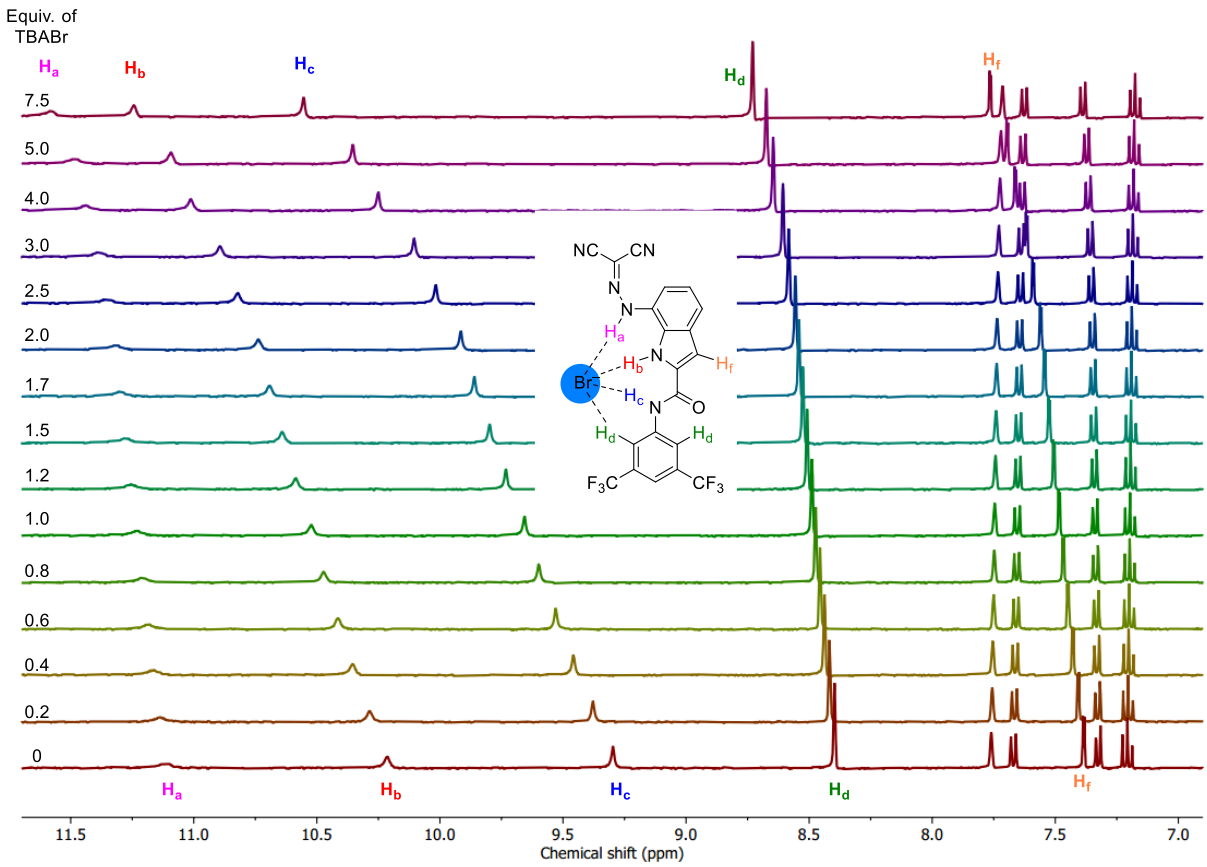

Fig. S3 The stacked plot of ^{1}H NMR titration experiment (400 MHz, acetonitrile–d_3) of compound **1a** (2 mM) with the sequential addition from TBABr salt at 25 °C.

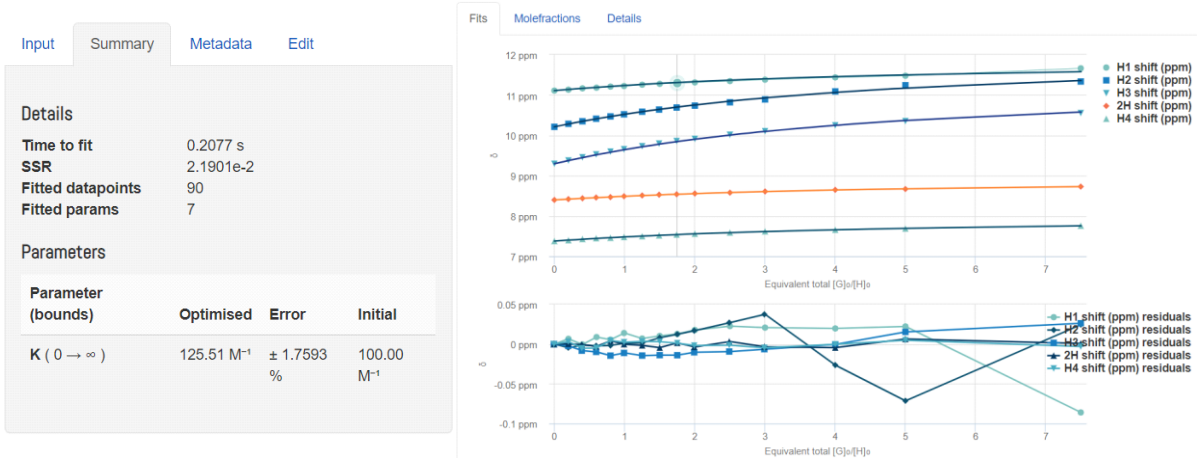

Fig. S4 Screenshot of the fitted data plot for a 1:1 model from supramolecular.org. The right−side graph shows an increase in the downfield chemical shift of different protons of compound **1a** upon the sequential addition of TBABr. The left side picture shows the calculated binding constant, which fits in the 1:1 compound–to–anion binding model. The Bindfit webpage of this experiment is: http://app.supramolecular.org/*BindFit*/view/d22a9a23-129f-4c76-b221-855ebd4a5cb1

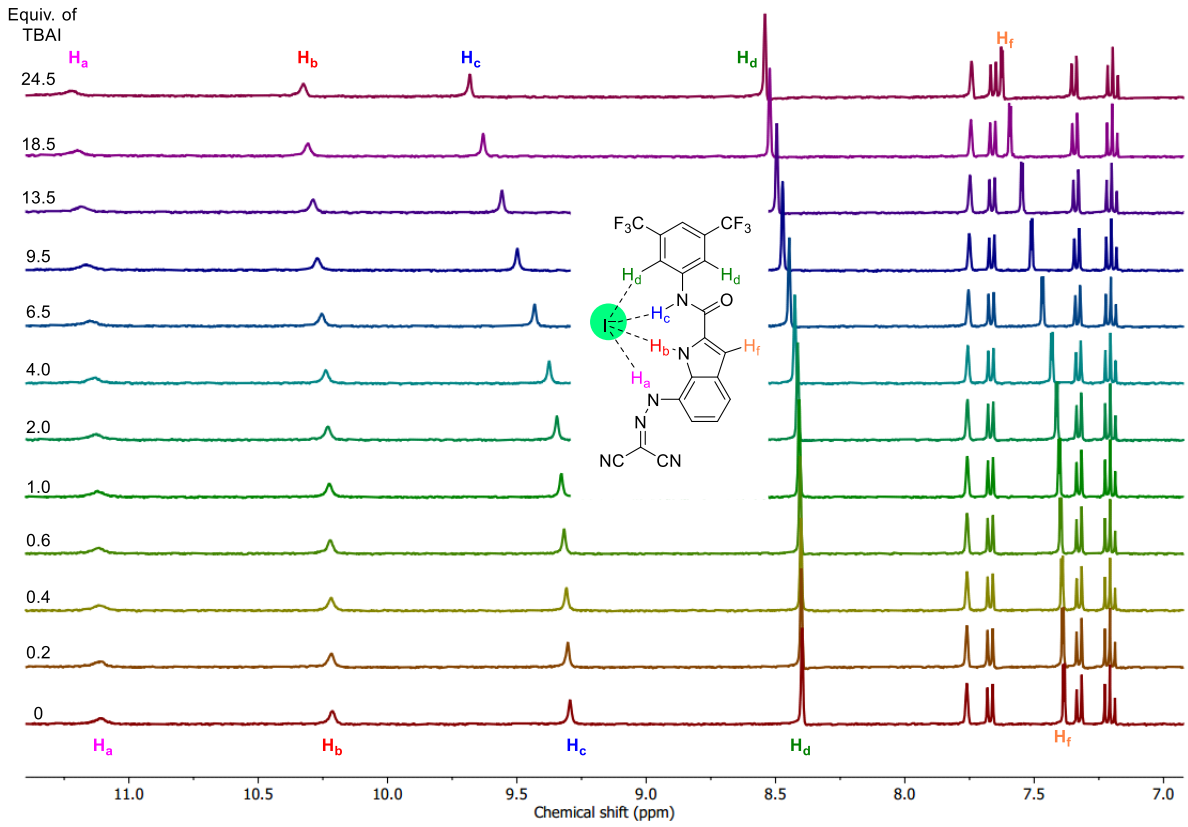

Fig. S5 The stacked plot of ^{1}H NMR titration experiment (400 MHz, acetonitrile–d_3) of **1a** (2 mM) with the sequential addition from TBAI salt at 25 °C.

5. Ion transport studies[S5–S7]

5.1.0 Preparation of HEPES buffer for HPTS assay

10 mM HEPES (4–(2–hydroxyethyl) piperazine–1–ethane sulfonic acid) buffer and 100 mM NaCl solution were prepared by using autoclave water. Further, the solution pH was elevated to 7.0 by adding the aliquots of NaOH from a 0.5 M stock solution. 1 mM HPTS (8–hydroxypyrene–1,3,6–trisulfonic acid trisodium salt) solution was made by adding the NaCl buffer solution into HPTS dye.

5.1.1 Preparation of EYPC–LUVs⊃HPTS

25 mg Egg Yolk Phosphatidylcholine (EYPC) lipid in 1 mL $CHCl_3$ solution was taken in a clean and dry 10 mL round bottom (RB) flask. A thin layer of EYPC lipid was made on the RB wall by slowly purging a stream of N_2. RB containing EYPC lipid was fitted to a vacuum pump for 4 h to remove traces of chloroform. 1 mM HPTS dye buffer solution (10 mM HEPES, 100 mM NaCl, pH = 7.0) was added to RB containing EYPC. The solution in RB was vortexed 6 times at intervals of 10 min for homogenizing suspended lipids with buffer solution. Then, the lipid suspension was subjected to 19 freeze/thaw cycles from −78 °C into liquid nitrogen to a 55 °C water bath and put for to age for 10 min. The EYPC lipid suspension was extruded (*Avanti polar Lipids Inc.*) through a 100 nm polycarbonate membrane (*Whatman Nuclepore*™). Extravesicular dye was removed using Sephadex–50 gel chromatography and washed with a prepared buffer solution. The eluted vesicles were diluted to 6 mL. (Final condition: ~ 5.4 mM EYPC lipid; intravesicular solution: 1 mM HPTS, 10 mM HEPES, 100 mM NaCl pH 7.0; extravesicular solution: 10 mM HEPES, 100 mM NaCl pH 7.0)

5.1.2 Ion transport activity by HPTS assay

In a clean and dry fluorescence cuvette accompanied by a magnetic bar, 1975 μL of buffer (10 mM HEPES, 100 mM NaCl, pH = 7.0) was added, followed by the addition of 25 μL EYPC–LUVs⊃HPTS vesicles. The cuvette was inserted into a fluorescence instrument equipped with a magnetic stirrer at $t = 0$. The fluorescence kinetics was monitored for 350 s at $\lambda_{em} = 510$ nm ($\lambda_{ex} = 450$ nm). An approximate pH gradient of 0.8 was created outside the vesicle by adding 20 μL of 0.5 M NaOH at $t = 20$ s. Then, at $t = 100$ s, 20 μL **1a**–**1c** as DMSO solution was added. Finally, 25 μL Triton X–100 (10% in water) was added at $t = 300$ s to lyse the vesicles to achieve complete destruction of the pH gradient. The fluorescence emission was recorded for 350 s. The time data at the X–axis was normalized according to Eq. S1, and the fluorescence

intensity data at the Y–axis was normalized to the change in percentage as the course of time using Eq. S2:

$$t = t - 100 \qquad \text{(Eq. S1)}$$

$$I_F = [(I_t - I_0) / (I_\infty - I_0)] \times 100 \qquad \text{(Eq. S2)}$$

where, I_F is the normalized fluorescence intensity in percentage. I_0 is the initial intensity just after adding the compound **1a**–**1c**, I_t is the intensity at time t, and I_∞ is the final intensity after adding Triton X–100.

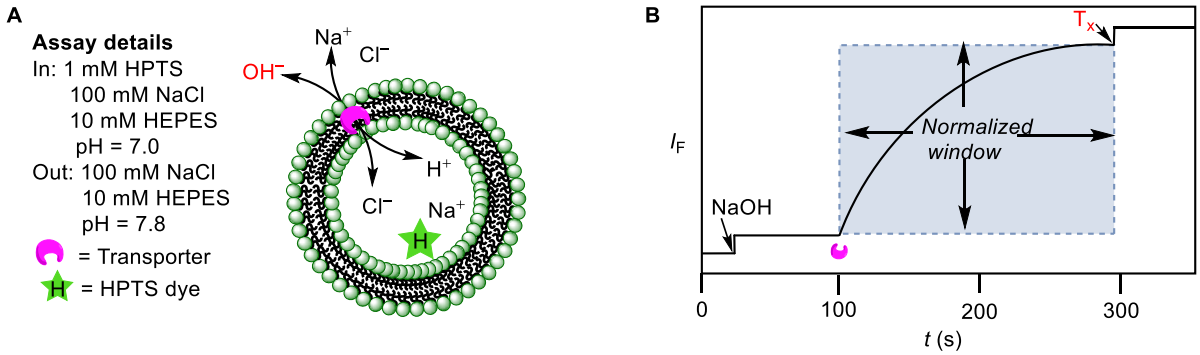

Fig. S6 Schematic representation (A) and normalized window of fluorescence kinetic (B) of EYPC–LUVs⊃HPTS vesicles.

A fluorescence kinetics study was performed at different concentrations of compound **1a**–**1c** to evaluate half–maximal concentration (EC_{50}) and Hill coefficient value (n) by using the normalized fluorescence intensity data (from 0 to 1) at 190 s after the addition of compound **1a**–**1c** from lower to higher concentration. Subsequently, those intensity values between 0 to 1 at the Y–axis against the different concentrations at the X–axis were fitted in the Hill plot by using Eq. S3:

$$Y = Y_\infty + (Y_0 - Y_\infty) / [1 + (c/EC_{50})^n] \qquad \text{(Eq. S3)}$$

where, Y is a function of the compound concentration c, Y_0 is the fluorescence intensity just before the compound addition (at t = 0 s), Y_∞ is the fluorescence intensity with excess compound concentration, and EC_{50} is the effective concentration required to reach the 50% of the maximum activity and n is the Hill coefficient value.

5.1.3 Comparison study of 1a–1c

Comparative ion transport activity of all three derivatives **1a**–**1c** was performed at 5 μM in EYPC–LUVs⊃HPTS vesicles using the above-mentioned protocol in section 5.1.2 Data divulge the activity sequence **1a** > **1b** > **1c**.

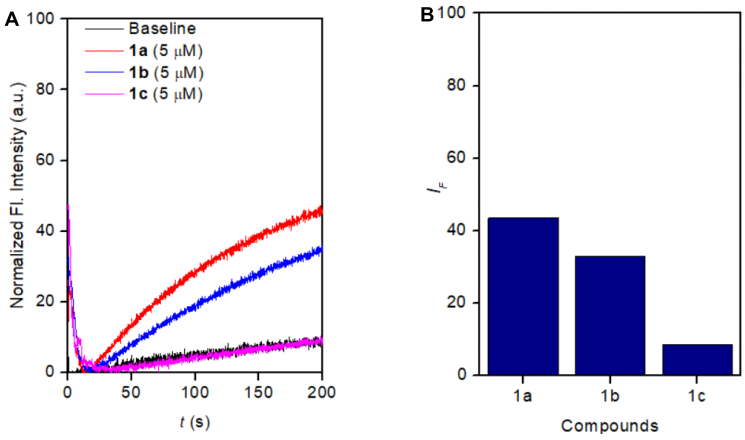

Fig. S7 Ion transport activity comparison graph of compound **1a**–**1c** (A) and fluorescence activity of compound **1a**–**1c** at 190 s (B).

5.1.4 Concentration–dependent study of 1a–1c

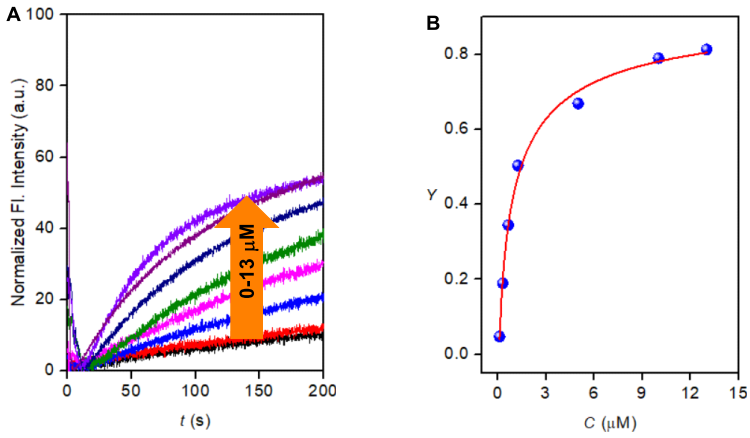

Model	Hill2 (User)		
Equation	b+(a-b)/(1+(x/EC50)^n)		
Reduced Chi-Sqr	8.50966E-4		
Adj. R-Square	0.99045		
		Value	Standard Error
P1	a	-0.16706	0.20708
	b	0.9399	0.14454
	n	0.70811	0.304
	EC50	0.79673	0.27202

Fig. S8 Representation of ion transport activity at different concentrations of compound **1a** by fluorescence kinetic of HPTS assay (A) and Hill plot analysis of fluorescence intensities at 190 s of compound **1a** to evaluate EC_{50} and Hill coefficient n (B).

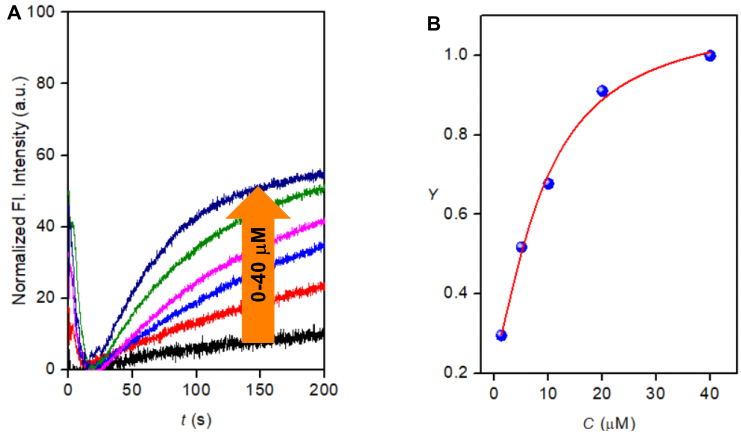

Model	Hill2 (User)		
Equation	b+(a-b)/(1+(x/EC50)^n)		
Reduced Chi-Sqr	0.00132		
Adj. R-Square	0.98403		
		Value	Standard Error
E	a	0.25017	0.07582
	b	1.10515	0.12451
	n	1.40457	0.53045
	EC50	9.23224	1.99823

Fig. S9 Representation of ion transport activity at different concentrations of compound **1b** by fluorescence kinetic of HPTS assay (A) and Hill plot analysis of fluorescence intensities at 190 s of compound **1b** to evaluate EC_{50} and Hill coefficient n (B).

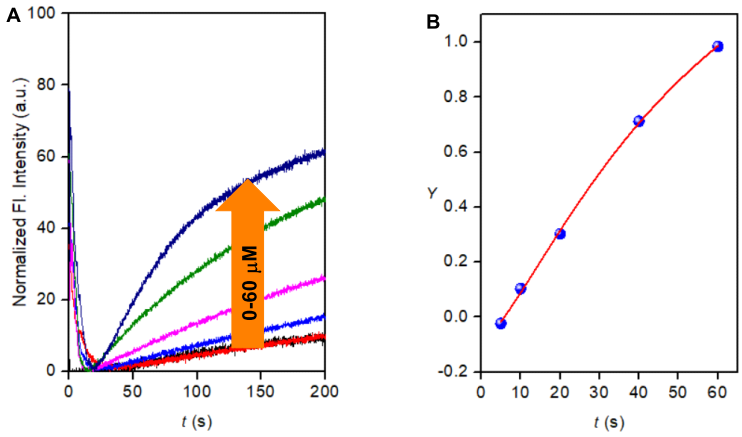

Model	Hill2 (User)		
Equation	b+(a-b)/(1+(x/EC50)^n)		
Reduced Chi-Sqr	4.50823E-4		
Adj. R-Square	0.99747		
		Value	Standard Error
C	a	-0.0907	0.05939
	b	1.98722	0.812
	n	1.35601	0.3731
	EC50	56.81098	30.68272

Fig. S10 Representation of ion transport activity at different concentrations of compound **1c** by fluorescence kinetic of HPTS assay (A) and Hill plot analysis of fluorescence intensities at 190 s of compound **1c** to evaluate EC_{50} and Hill coefficient n (B).

5.2 Determination of ion selectivity by HPTS assay[S6]

5.2.1 Preparation of buffer and stock solution for ion selectivity

All the HEPES buffers were prepared of 100 mM metal chlorides (where MCl = LiCl, KCl, RbCl, and CsCl) or sodium halides (where, NaX = NaCl, NaBr, NaI, $NaNO_3$, $NaClO_4$, and NaOAc) and 10 mM of HEPES. The pH of the solutions was adjusted to 7.0 by adding the required amount of 0.5 M NaOH solution. HPLC grade DMSO was used to prepare the stock solutions of compound **1a**.

5.2.2 Cation selectivity study by HPTS assay

The extravesicular buffer solution was changed in the cuvette with different 100 mM metal chloride (MCl) and 10 mM HEPES buffer solutions (where, $M^+ = Li^+$, Na^+, K^+, Rb^+, and Cs^+). The rest of the fluorescence measurement procedure was followed, as mentioned in section 5.1.2.

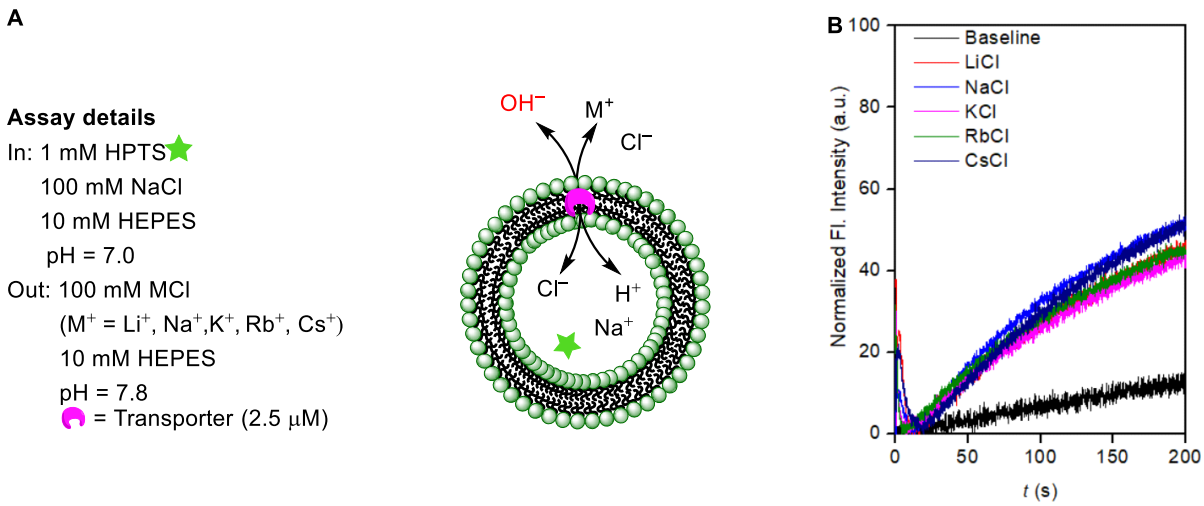

Fig. S11 The illustration shows the vesicular composition of the EYPC–LUVs⊃HPTS vesicle (A) and a graph representing alkali metal ion non-involvement during the transport process (B).

5.2.3 Anion selectivity assay

Vesicles EYPC–LUVs⊃HPTS (intravesicular composition = 100 mM NaCl, 10 mM HEPES, pH = 7.0) were prepared using the protocol mentioned in section 5.1.1 for anion selectivity studies. For that, fluorescence kinetics was performed. First, in a fluorescence cuvette, 1975 μL HEPES buffer (10 mM HEPES, 100 mM NaX, pH = 7.0, where $X^- = Cl^-$, Br^-, I^-, OAc^-, ClO_4^-, and NO_3^-) was taken, followed by the addition of 25 μL EYPC–LUVs⊃HPTS. The resulting solution was slowly stirred in a fluorescence instrument equipped with a magnetic stirrer (t = 0 s). The fluorescence intensity of HPTS was observed at λ_{em} = 510 nm (λ_{ex} = 450 nm) over the course of 350 s. pH gradient was created outside the vesicle by adding 20 μL of 0.5 M NaOH at t = 20 s, followed by the addition of compound **1a** (as a DMSO solution) at t = 100 s to initiate ion transport, and finally, the vesicle was lyzed for complete disruption of pH gradient by addition of 25 μL 10% Triton X −100 at t = 300 s. The time−dependent data were normalized to intensity change in percentage using Eq. S1 and Eq. S2.

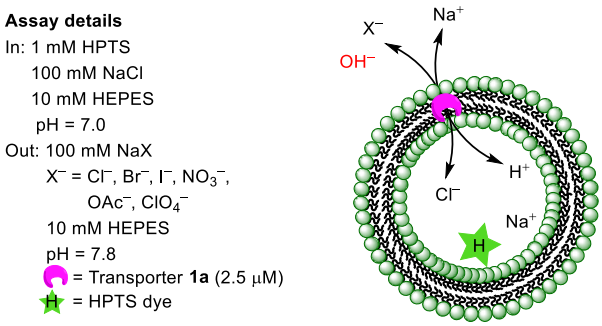

Fig. S12 Illustration of the intravesicular and extravesicular composition of EYPC−LUVs⊃HPTS for anion selectivity study with pH gradients.

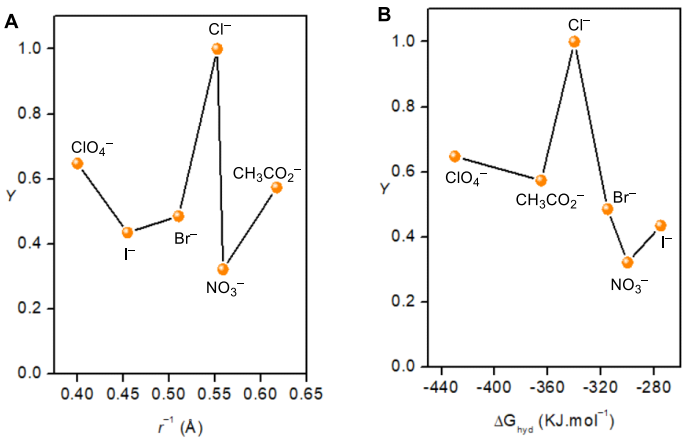

Fig. S13 Fractional activity *Y* (with respect to chloride ion) is plotted against the reciprocal of anion radius (A) and fractional activity *Y* (with respect to chloride ion) is plotted against the anion hydration energy (B).

5.2.4 Evaluation of initial rate

The initial rate of chloride exchange with different halides was calculated by fitting non-linear curve fitting analysis of the experimental measured normalized fluorescence intensity versus time (s) with the following using asymptotic function (Eq. S4) with the help of *Origin 8.5*:

$$y = a - b \cdot c^{x} \qquad \text{(Eq. S4)}$$

Where y is the normalized Fluorescence intensity corresponding to transport activity, x is time (s). The initial rate (k_{initial}) of chloride exchange with different halide anions is then derived from the Eq. S5 and is obtained in s^{-1}

$$k_{\text{initial}} = -b \cdot ln(c) \qquad \text{(Eq. S5)}$$

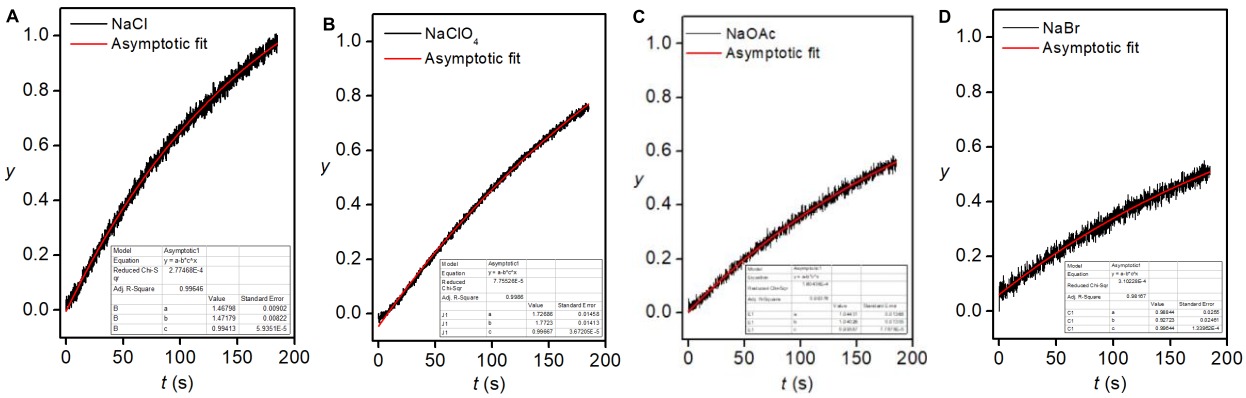

Fig. S14 Asymptotic fit to obtain the initial rate of compound **1a** (2.5 μM) with Cl^- (8.66×10^{-3} s^{-1}) (A), ClO_4^- (5.91×10^{-3} s^{-1}) (B), OAc^- (4.30×10^{-3} s^{-1}) (C), and Br^- (3.33×10^{-3} s^{-1}) (D) ions [fractional activity (y) with respect to chloride ion is plotted to compare the initial transport rate].

5.3 pH independent anion selectivity assay[S8]

Vesicles EYPC–LUVs⊃HPTS (intravesicular composition = 100 mM NaCl, 10 mM HEPES, pH = 7.0) were prepared using the protocol mentioned in section 5.1.1 for pH–independent anion selectivity studies. For that, fluorescence kinetics was performed. At first, in a fluorescence cuvette, 1975 μL HEPES buffer (10 mM HEPES, 100 mM NaX, pH = 7.0, where X^- = Cl^-, SO_4^{-2} Br^-, and NO_3^-) was taken, followed by the addition of 25 μL EYPC–LUVs⊃HPTS. The resulting solution was slowly stirred in a fluorescence instrument equipped with a magnetic stirrer (t = 0 s). The fluorescence intensity of HPTS was observed at λ_{em} = 510 nm (λ_{ex} = 450 nm) over the course of 350 s. Compound **1a** (as a DMSO solution) was added at t = 100 s to initiate ion transport, and finally, the vesicle was lyzed by the addition of 25 μL 10% Triton X –100 at t = 300 s. The time−dependent data were normalized to intensity change in relative fractional units. Where F_t is equal to the fluorescence intensity at time t, and F_0 is equal to the fluorescence intensity before the addition of transporter **1a**.

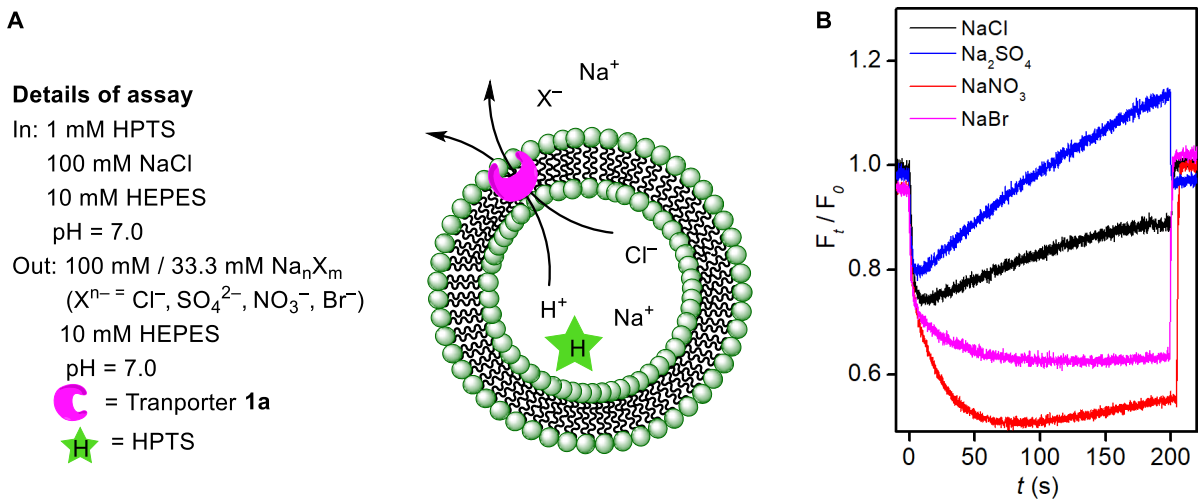

Fig. S15 Schematic representation of the anion selectivity of transporter **1a** across EYPC–LUVs⊃HPTS in the absence of any pH pulse (A) and the fluorescence kinetic experiments of the anion selectivity of transporter **1a** (1 μM) in the absence of the pH pulse (B).

5.4 pH independent extravesicular Gluconate–based HPTS assay for H^+/Cl^- transport[S9]

Vesicles EYPC–LUVs⊃HPTS (intravesicular composition = 100 mM NaCl, 10 mM HEPES, pH = 7.0) were prepared using the protocol mentioned in section 5.1.1 for Gluconate–based HPTS assay.

At first, in a fluorescence cuvette, 1975 μL HEPES buffer (10 mM HEPES, 100 mM Na–Gluconate, pH = 7.0) was taken, followed by the addition of 25 μL EYPC–LUVs⊃HPTS. The resulting solution was slowly stirred in a fluorescence instrument equipped with a magnetic stirrer (t = 0 s). The fluorescence intensity of HPTS was observed at λ_{em} = 510 nm (λ_{ex} = 450 nm) over the course of 350 s. Compound **1a** (as a DMSO solution) was added at t = 100 s to initiate ion transport, and finally, the vesicle was lyzed by the addition of 25 μL 10% Triton X –100 at t = 300 s. The time–dependent data were normalized to intensity change in relative fractional units.

Where F_t = fluorescence intensity at time t, and F_0 = fluorescence intensity before the addition of the transporter **1a**.

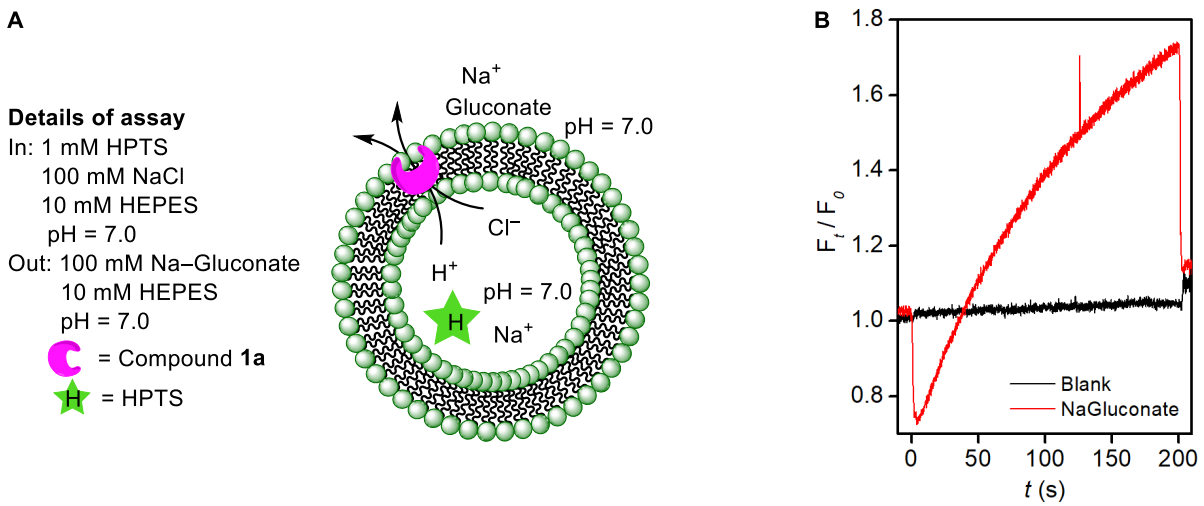

Fig. S16 Schematic representation of the H^+/Cl^- transport by transporter **1a** across EYPC–LUVs⊃HPTS in the absence of any pH pulse (A) and the fluorescence kinetic experiments of the H^+/Cl^- transport by transporter **1a** (1 μM) in the absence of the pH pulse (B).

5.5 EYPC–LUV⊃HPTS assay for electrogenic H^+ transport[S12]

5.5.1 Preparation of buffer and stock solution

10 mM HEPES buffer solution of 100 mM K–gluconate salt was prepared by maintaining pH 7.0 using 0.5 M KOH stock solution. 1 mM HPTS dye solution was made using autoclave water. 0.5 M stock solution of TBAOH was prepared to create the extravesicular pH gradient.

5.5.2 Preparation of vesicles EYPC–LUVs⊃HPTS and potassium gluconate

The 1 mM HPTS and 100 mM K–gluconate encapsulated EYPC vesicles were prepared using the standard protocol mentioned in section 5.1.1 using K–gluconate as an intravesicular buffer (Final condition: ~ 5.4 mM EYPC lipid; intravesicular solution: 1 mM HPTS, 10 mM HEPES, 100 mM K–Gluconate pH 7.0; extravesicular solution: 10 mM HEPES, 100 mM K–Gluconate pH 7.0).

5.5.3 Assay details

In a clean and dry fluorescence cuvette accompanied by a magnetic bar, 1975 μL of buffer (10 mM HEPES, 100 mM K–Gluconate, pH = 7.0) was added, followed by the addition of 25 μL EYPC–LUVs⊃HPTS vesicles. The cuvette was inserted into a fluorescence instrument equipped with a magnetic stirrer at $t = 0$. The fluorescence kinetics was monitored for 350 s at λ_{em} = 510 nm (λ_{ex} = 450 nm). An approximate pH gradient of 0.8 was created outside the vesicle by adding 20 μL of 0.5 M TBAOH at $t = 20$ s. Then, at $t = 100$ s, 20 μL compound **1a** as DMSO solution was added. Finally, 25 μL Triton X–100 (10% in water) was added at t =

300 s to lyse the vesicles to achieve complete destruction of the pH gradient. The fluorescence emission was recorded for 350 s. The time data at the X–axis was normalized according to Eq. S1, and the fluorescence intensity data at the Y–axis was normalized to the change in percentage over the course of time using Eq. S2.

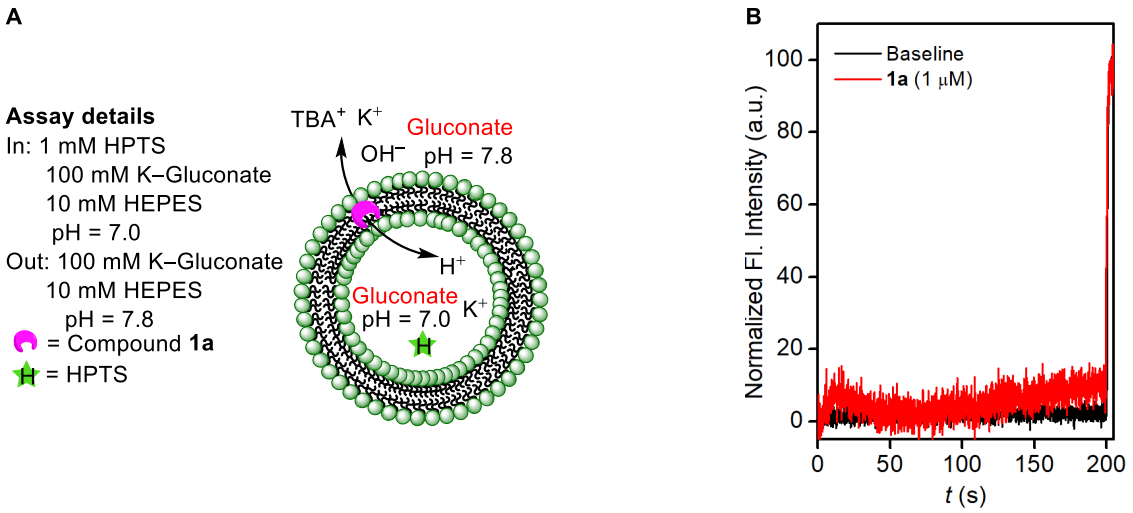

Fig. S17 Schematic representation of the proton transport assay across EYPC–LUVs⊃HPTS (A) and fluorescence kinetic experiment of the proton transport activity of the compound **1a** (1 μM) (B).

5.6 EYPC–LUV⊃ (HPTS and sodium gluconate) assay for M^+/H^+ antiport

5.6.1 Preparation of buffer and stock solution

10 mM HEPES buffer solution of 200 mM Na–gluconate and 200 mM NaCl salt was prepared by maintaining pH 7.0 using 0.5 M NaOH stock solution. 1 mM HPTS dye solution was made using autoclave water.

5.6.2 Preparation of vesicles EYPC–LUVs⊃HPTS and sodium gluconate (Na–gluconate)

The 1 mM HPTS encapsulated EYPC vesicles were prepared using the standard protocol mentioned in section 5.1.1 using Na–gluconate as an intravesicular buffer (Final condition: ~ 5.4 mM EYPC lipid; intravesicular solution: 1 mM HPTS, 10 mM HEPES, 200 mM Na–Gluconate pH 7.0; extravesicular solution: 10 mM HEPES, 200 mM Na–Gluconate or 200 mM NaCl pH 7.0).

5.6.3 Assay details

The Section 5.1.2 procedure was followed to perform a fluorescence kinetics-based experiment

for compound **1a** using EYPC–LUVs⊃HPTS and Na–gluconate by suspending this vesicle either in Na–gluconate or NaCl solution for the respective experiment.

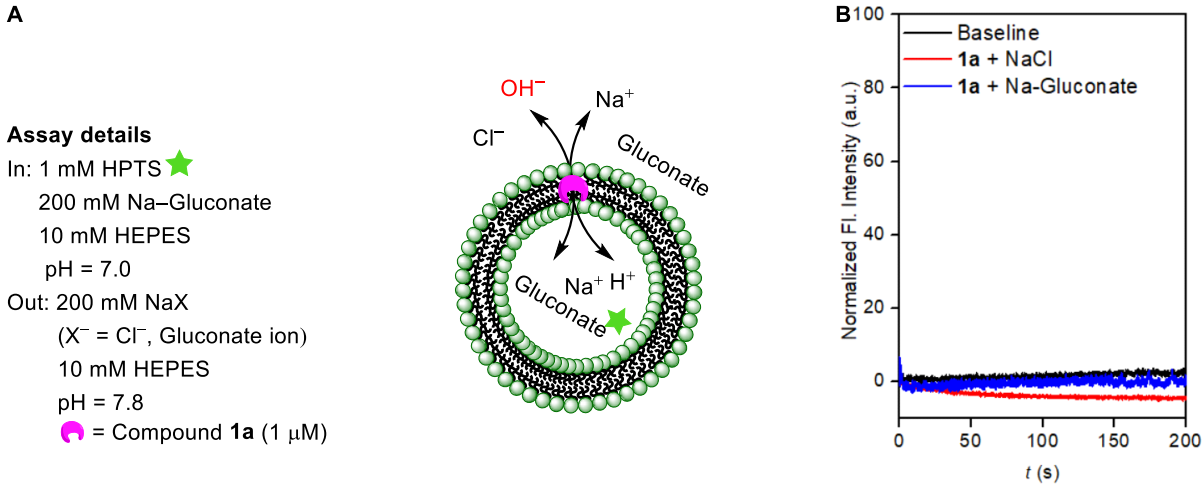

Fig. S18 The illustration shows the vesicular composition of the EYPC–LUVs⊃HPTS vesicle (A) and the graph demonstrates that no change in HPTS pH corresponds to non-exchange of gluconate/Cl^- nor Na^+/H^+ ion (B).

5.7 Lucigenin assay for determination of chloride influx[S6]

5.7.1 Preparation of salt solution and stock for lucigenin assay

The buffer solution (200 mM $NaNO_3$, 10 mM HEPES, pH = 7.0) was prepared using autoclaved water. Using the above buffer solution, 1 mM of lucigenin solution was prepared from solid lucigenin. The stock solution of compound **1a** for the lucigenin assay was prepared from a solid compound using HPLC grade CH_3CN.

5.7.2 Preparation of EYPC–LUVs⊃Lucigenin vesicles

25 mg Egg Yolk Phosphatidylcholine (EYPC) lipid in 1 mL $CHCl_3$ solution was added in a clean and dry 10 ml round bottom flask. A gentle blow of the N_2 stream made a thin layer of EYPC lipid. RB containing EYPC lipid was further connected to a vacuum pump for 4 h to remove chloroform traces. After that, 1 mM Lucigenin dye buffer solution (10 mM HEPES, 200 mM $NaNO_3$ pH = 7.0) was added to the RB. The lucigenin lipid suspension was vortexed 6 times at intervals of 10 min to make a homogenized suspension of lipids with buffer solution. Further, the lipid suspension was subjected to 19 freeze/thaw cycles from −78 °C into liquid nitrogen to a 55 °C water bath and put for 10 min of aging. The EYPC lipid suspension was extruded (*Avanti Polar Lipids Inc.*) through a 200 nm polycarbonate membrane (*Whatman Nuclepore*™). Extravesicular dye was removed using Sephadex−50 gel chromatography and

washed with a prepared buffer solution. The eluted vesicles were diluted with buffer solution (200 mM $NaNO_3$, 10 mM HEPES, pH = 7.0) to 4 mL. (Final Condition: 8.1 mM EYPC lipids; intravesicular solution: 1 mM Lucigenin, 200 mM $NaNO_3$, 10 mM HEPES, pH = 7.0; extravesicular solution: 200 mM $NaNO_3$, 10 mM HEPES, pH = 7.0).

5.7.3 Ion transport activity by Lucigenin assay

In a clean and dry fluorescence cuvette, 1975 μL 200 mM $NaNO_3$ buffer solution and 25 μL EYPC–LUVs⊃Lucigenin (200 mM $NaNO_3$, 10 mM HEPES, pH = 7.0) were taken. This suspension was placed in a slow stirring condition in a fluorescence instrument equipped with a magnetic stirrer (t = 0 s). The change in fluorescence intensity of Lucigenin was monitored at λ_{em} = 535 nm (λ_{ex} = 450 nm) over the course of 350 s. The extravesicular chloride gradient was created by adding 33.3 μL NaCl (2.0 M) at t = 20 s, and compound **1a** was added at t = 100 s. Finally, vesicles were lysed by adding Triton X–100 at t = 300 s for the complete disruption of the chloride gradient.

The time–dependent data were normalized to the percent change in fluorescence intensity using Eq. S6.

$$I_F = [(I_t - I_0) / (I_\infty - I_0)] \times (-100) \qquad \text{(Eq. S6)}$$

Where I_0 is the initial intensity, I_t is the intensity at time t, and I_∞ is the final intensity after adding Triton X–100.

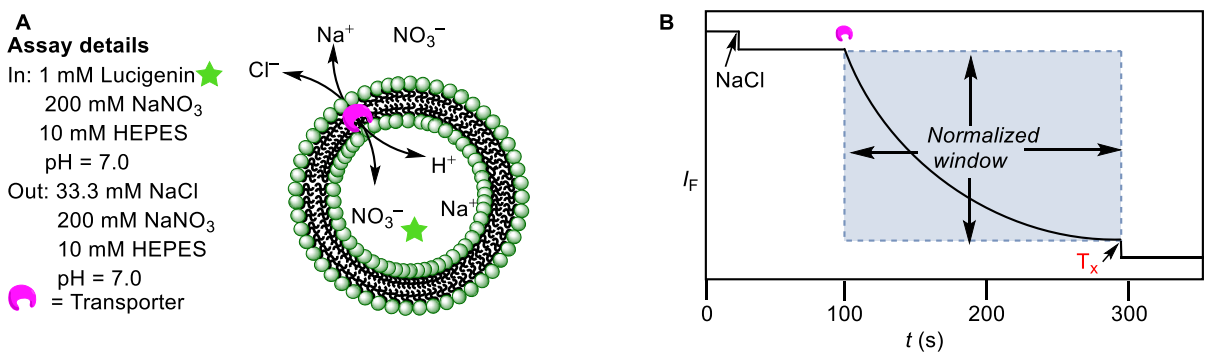

Fig. S19 Schematic presentation of the EYPC–LUVs⊃Lucigenin vesicle (A) and a normalized fluorescence–based kinetics graph window for ion transport activity(B).

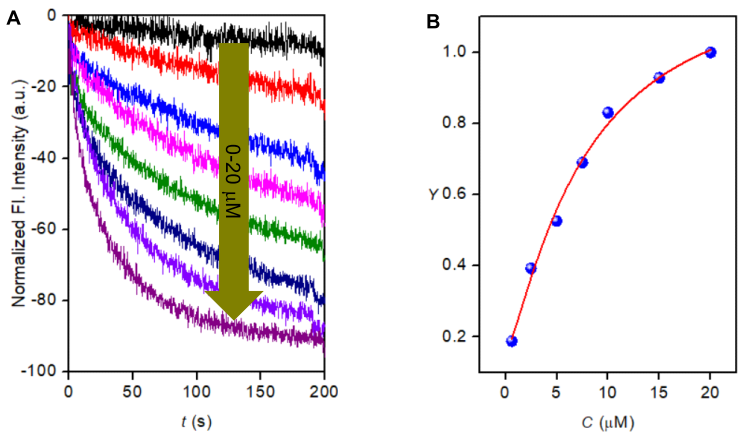

Model	Hill2 (User)		
Equation	b+(a-b)/(1+(x/EC50)^n)		
Reduced Chi-Sqr	9.85554E-4		
Adj. R-Square	0.98883		
		Value	Standard Error
E	a	0.15173	0.05931
	b	1.25651	0.20495
	n	1.27878	0.37525
	EC50	7.61293	2.13064

Fig. S20 The concentration profile of chloride influx was presented by fluorescence−based kinetic assay for compound **1a** (A) and Hill plot analysis graph for fluorescence intensity at 190 s of compound **1a** to evaluate EC_{50} and Hill coefficient n (B).

5.7.4 Cation selectivity assay across EYPC−LUVs⊃lucigenin vesicles

The vesicles were prepared by following the protocol as stated above in section 5.7.2. The vesicles mentioned above (intravesicular and extravesicular = 200 mM $NaNO_3$, 10 mM HEPES, pH = 7.0) were used for cation selectivity studies.

In a clean and dry fluorescence cuvette, 1975 μL vesicles were kept for the slow stirring condition in a fluorescence instrument equipped with a magnetic stirrer at t = 0 s. The quenching of fluorescence intensity of Lucigenin was monitored as a course of 350 s at λ_{em} = 535 nm (λ_{ex} = 450 nm). At t = 20 s, the chloride gradient was created by the addition of 33.3 μL of MCl (where $M^+ = Li^+$, Na^+, K^+, Rb^+, and Cs^+) salt from a 2 M stock solution. Compound **1a** was added at t = 100 s, and a change in the fluorescence activity of the Lucigenin dye was investigated over time. Finally, vesicles were lyzed by adding 10% Triton X−100 (25 μL) at t = 300 s to complete the disruption of the chloride gradient. The time−dependent fluorescence intensity data were normalized to fluorescence intensity change in the percentage using Eq. S6.

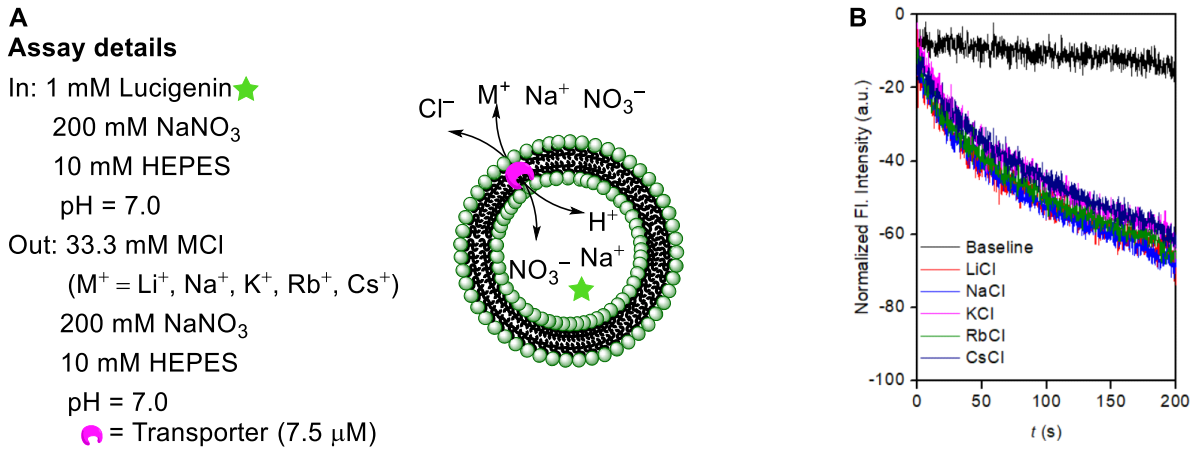

Fig. S21 The intravesicular and extravesicular components details of the EYPC−LUVs⊃Lucigenin vesicle (A), and the graph shows fluorescence intensity quenching after the addition of metal chloride (B).

5.8 pH−based study using EYPC−LUVs⊃Lucigenin vesicle

5.8.1 Preparation of buffer and stock solution

Different pH buffer solutions (200 mM $NaNO_3$, (5 mM citrate buffer for pH = 4.0; 5 mM phosphate buffer for pH = 5.0, 6.0, and 10 mM HEPES buffer for pH = 7.0) were prepared using autoclave water. The corresponding pH of the buffer was maintained with either the addition of 0.5 M NaOH or 0.5 M HNO_3.

5.8.2 Chloride influx across EYPC−LUVs⊃lucigenin vesicles at different pH

In a clean and dry fluorescence cuvette, 1975 μL vesicles were added in 200 mM $NaNO_3$ buffer solutions (200 mM $NaNO_3$, pH = 4.0–7.0) and kept for the slow stirring condition in a fluorescence instrument. The ion transport study was conducted using fluorescence kinetics at varying pH levels, following the protocol outlined in Section 5.7.3.

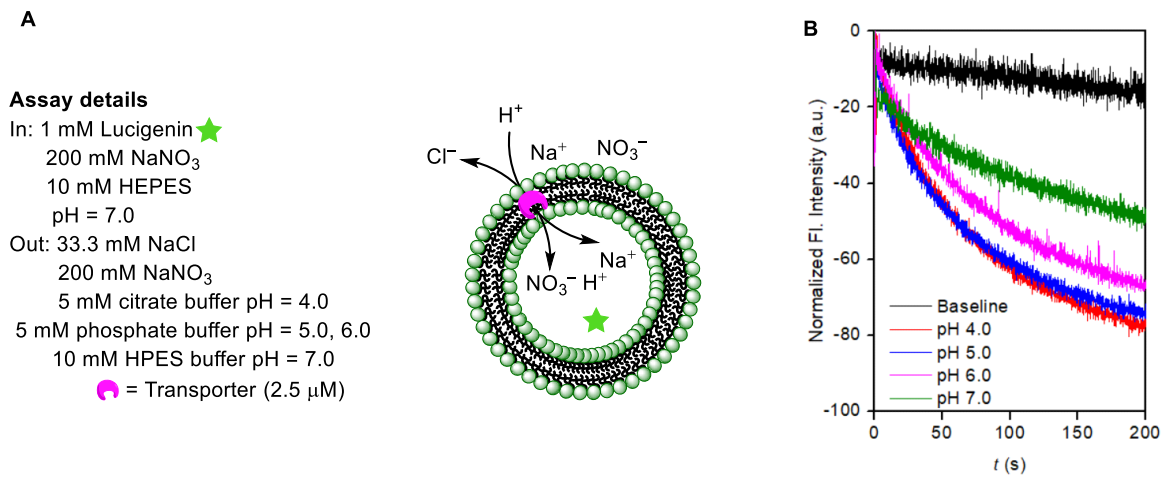

Fig. S22 Intravesicular and extravesicular components details of EYPC−LUVs⊃Lucigenin for pH–dependent study (A) and graph demonstrated the effect of pH of Lucigenin quenching activity by compound **1a** (B).

5.9 Preparation of EYPC–LUVs⊃5(6)−carboxyfluorescein[S10]

1 mL EYPC lipid (chloroform solution) was taken in 10 mL RB, and the solid lipid thin layer was created by a gentle blow of nitrogen gas. Further, the traces of chloroform were removed by putting RB under reduced pressure on the high vacuum pump for 4 h. Following that, the lipid was hydrated with buffer solution (50 mM 5(6)−carboxyfluorescein, 10 mM HEPES, 100 mM NaCl, pH = 7.0) and vortexed six times in the interval of 10 min to homogenize the suspension. Further, the suspension was passed through 19 freeze−thaw cycles, freezing at −78 °C in liquid nitrogen and thawing at 55 °C in a hot water bath. The lipid suspension was aged for 10 min. Then, the lipid suspension was passed through a 200 mM polycarbonate membrane (*Whatman Nuclepore*™) using an extruder setup. Finally, the extravesicular unentrapped dye was removed by Sephadex−50 column chromatography. The vesicles were eluted with a buffer solution and diluted up to 6 mL. (Final Condition: ~ 5.4 mM EYPC lipid; intravesicular solution: 50 mM CF, 10 mM HEPES, 10 mM NaCl, pH 7.0; extravesicular solution: 10 mM HEPES, 100 mM NaCl, pH 7.0)

5.9.1 Leakage experiments details

In a clean and dry fluorescence cuvette, 1975 μL of buffer (10 mM HEPES, 100 mM NaCl, pH 7.0) was added, followed by the addition of 25 μL EYPC−LUVs⊃CF (50 mM CF, 10 mM HEPES, 100 mM NaCl, pH = 7.0) vesicles and kept in slowly stirring condition on magnetic stirrer equipped with spectrofluorometer ($t = 0$). The change in fluorescence emission intensity due to CF leakage was continuously observed at $\lambda_{em} = 517$ nm. ($\lambda_{ex} = 492$ nm). Compound **1a**

(as DMSO solution) was added at different concentrations at t = 50 s. Finally, 10% Triton X−100 (25 μL) was added at t = 300 s to lyse the vesicles to achieve maximum fluorescence emission of CF under dilute conditions. The fluorescence emission was monitored up to 350 s. The time data was normalized according to Eq. S1. Then, the fluorescence intensity data was normalized to the percentage change in fluorescence intensity over the course of time using Eq. S2.

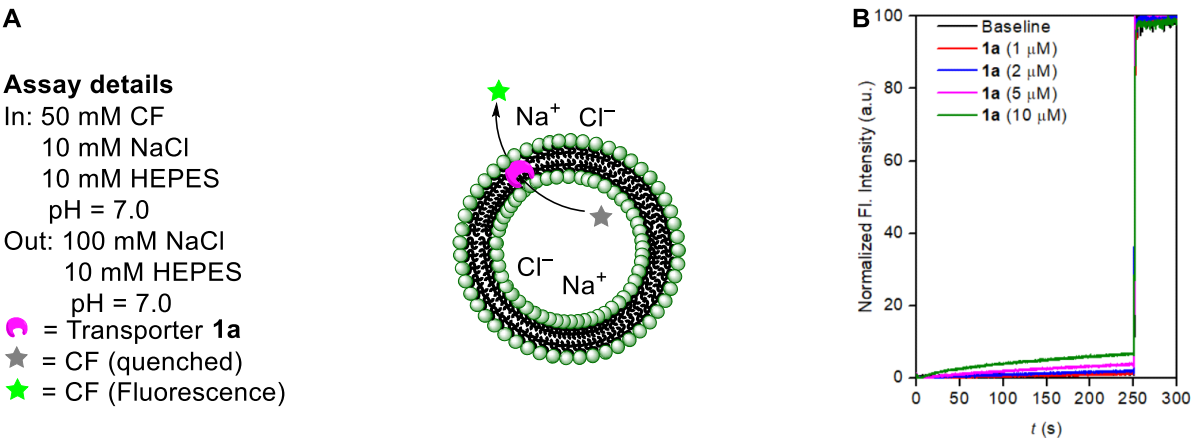

Fig. S23 Schematic presentation of EYPC−LUV⊃CF vesicle (A) and corresponding fluorescence kinetics experiment of compound **1a** at different concentrations (B).

6. U–tube experiment[S8]

One U−shaped tube was chosen for this experiment, in which the solution of both the source (S) and receiver (R) arm (6 mL each) was separated by chloroform (12 mL) containing 1 mM compound **1a**. The source arm consists of 100 mM HCl and the receiver arm contains 100 mM $NaNO_3$. A small magnetic bar was set up inside the U−shaped tube. The U−tube setup was placed on a magnetic stirrer with slow stirring. The pH in the source arm was checked initially just after starting the magnetic bar rotation (t = 0 s). The change in chloride ion concentration and pH was monitored in the receiver arm over time using the chloride selective electrode and pH meter, respectively. A time–dependent increment of the chloride ion concentration and a decrease in the pH value at the receiver arm validated the effective transport of both Cl^- and H^+/Cl^- ions from the source arm to the receiver arm.

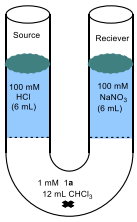

Fig. S24 Schematic representation of U−tube experiment.

7. pH dependant study by ISE[S11]

7.1.0 Preparation of buffer solutions

A buffer solution of 500 mM $NaNO_3$ and 500 mM NaCl with different pH (5 mM citrate buffer for pH = 4.0; 5 mM phosphate buffer for pH = 5.0, 6.0, and 7.0; 5 mM tris buffer for pH = 8, and 10) were prepared using autoclave water. All stock solutions for compound **1a** were prepared using the HPLC grade DMSO solution.

7.1.1 Preparation of vesicles

In a 10 mL round–bottomed flask, 0.5 mL EYPC chloroform solution (25 mg/mL) was taken. A lipid−thin layer was created by the slow purging of the nitrogen gas. It was further dried under a high vacuum pump for 4 h to remove traces of chloroform. Then, the lipid was rehydrated by intravesicular NaCl buffer solution of a particular pH (pH = 4.0, 5.0, 6.0, 7.0, 8.0, and 10.0) and subjected to a vortex to mix lipid suspension properly. 19 freeze−thaw cycles were performed on the lipid suspension by alternatingly freezing lipid suspension in −78 °C liquid nitrogen, thawing it to a 55 °C water bath, and keeping it for aging for 10 min. The suspension was extruded 23 times through a 200 nm polycarbonate membrane (*Whatman Nuclepore*™). Subsequently, the vesicles were dialyzed (*Spectra/Pore*® membrane MWCO 1 kD) twice against 500 mM $NaNO_3$ to remove extravesicular NaCl. (Final condition: 32.4 mM EYPC lipid; intravesicular solution: 500 mM NaCl, 5 mM citrate buffer (pH 4.0), 5 mM phosphate buffer (pH 5.0, 6.0, and 7.0), 5 mM tris buffer (pH 8.0 and 10.0); extravesicular solution: 500 mM $NaNO_3$, 5 mM citrate buffer (pH 4.0), 5 mM phosphate buffer (pH 5.0, 6.0, and 7.0), 5 mM tris buffer (pH 8.0 and 10.0).

7.1.2 Assay details

A 50 μL of vesicles was added in 1950 μL of $NaNO_3$ buffer solution having different pH, and chloride efflux was monitored by using a chloride-selective electrode (t = 0 s). Compound **1a** (80 μM) was added at t = 60 s, and chloride efflux was monitored up to 660 s. Finally, 25 μL Triton X–100 (10 % in water) was added at t = 600 s to lyze the vesicles and obtain the maximum chloride efflux. The time at 60 s was normalized to zero using Eq. S7, where t_x is a normalized time, and the chloride efflux recorded by ISE was converted into chloride efflux in percentage using Eq. S8:

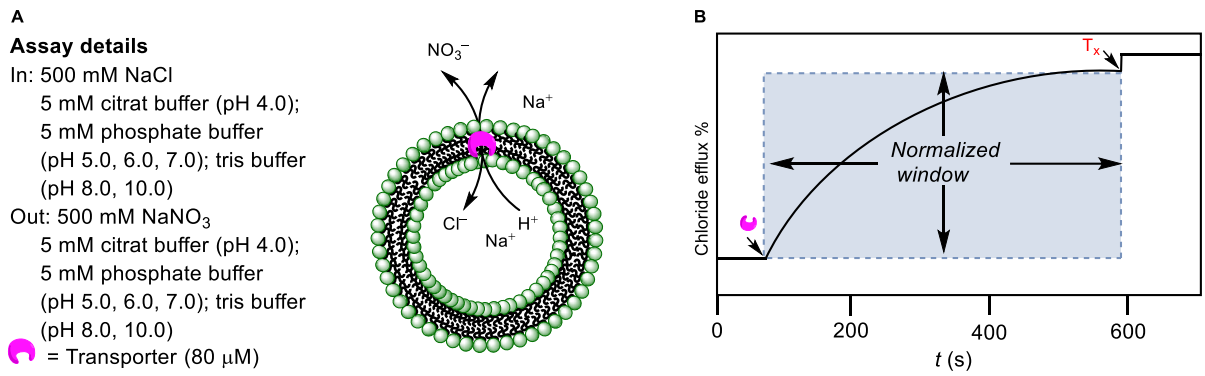

Fig. S25 The intravesicular and extravesicular details of EYPC−LUVs (A) and normalized window of ISE experiment for chloride efflux in percentage (B).

$$t_x = t - 60 \qquad \text{(Eq. S7)}$$

where, t_x and t are normalized time and time when the experiment was initiated.

$$\%\ \text{chloride efflux} = \frac{X_c - X_i}{X_f} \times 100 \qquad \text{(Eq. S8)}$$

where X_c is chloride efflux in a given time, and X_i is chloride efflux recorded at 0 s, and X_f is chloride efflux measured at 600 s.

7.2 Mechanistic studies by ISE[S12]

7.2.1 Preparation of buffer solutions

300 mM KCl as an intravesicular solution and 300 mM potassium gluconate (K–gluconate) as an extravesicular solution buffered at pH 5.0 by 5 mM appropriate mixture of KH_2PO_4 (monobasic potassium phosphate) and K_2HPO_4 (dibasic potassium phosphate).

7.2.2 Preparations of vesicles

The 300 mM KCl entrapped vesicles were prepared following standard protocol.[S12] 25 mg EYPC/1 mL $CHCl_3$ was added in a 10 mL RB. The chloroform was evaporated by a blow of nitrogen gas followed by 4 hours of high vacuum pump exposure. After that, the lipid was hydrated by 1 mL 300 mM buffer solution and vortexed for homogenized mixing of lipid suspension. The lipid suspension was then subjected to 19 freeze−thaw cycles, in which it was frozen at −78 °C into liquid nitrogen and thawed at 55 °C in the hot water bath. After that, the lipid suspension was aged for 30 min. Then, the lipid suspension was passed through a 200 mM polycarbonate membrane (*Whatman Nuclepore*™) using an extruder (*Avanti Polar Lipids,*

Inc.) setup. The extruded vesicles were dialyzed (*Spectra/Pore*® membrane MWCO 1 kD) twice by external 300 mM K–gluconate buffer to replace the external KCl buffer solution. Finally, the vesicle offered 32.4 mM EYPC−LUVs (intravesicular solution: 300 mM KCl, 5 mM phosphate buffer pH = 5.0; extravesicular solution: 300 mM K–gluconate, 5 mM phosphate buffer pH = 5.0).

7.2.3 Assay details

The unilamellar vesicles containing 300 mM KCl were suspended in 300 mM K−Gluconate buffer solution, and 0.8 mM vesicle concentration was maintained in the cuvette. The cuvette solution was kept for stirring for up to 660 s. Just after 30 s of stirring, 1 μM of either monensin or valinomycin as DMSO solution was added, and after 60 s, 40 μM compound **1a** as DMSO solutions were added. The chloride efflux was observed through the *Accumet* chloride selective electrode. At 600 s, triton X–100 (10% in water) was added to rupture the vesicles completely. Chloride efflux at 60 s was normalized to zero, and 100% chloride efflux was set at 660 s using Eq. S8.

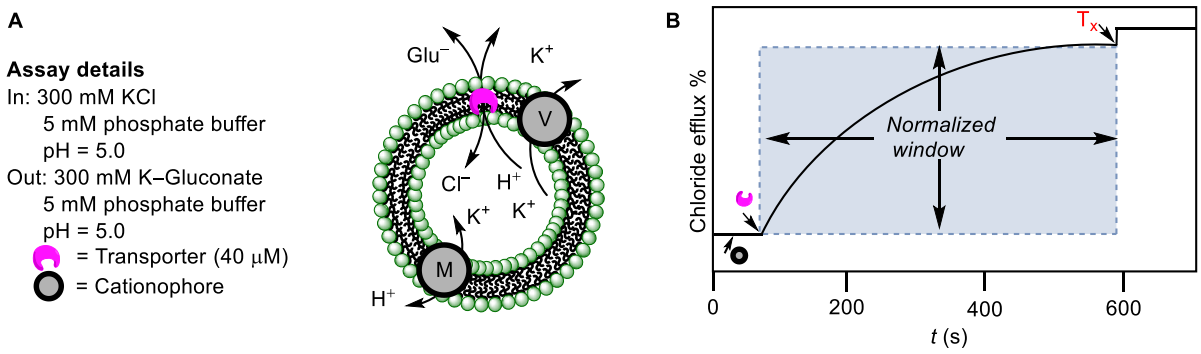

Fig. S26 The intravesicular and extravesicular details of EYPC−LUVs (A) and normalized window of ISE experiment for chloride efflux in percentage (B).

8. pK_a determination[S13,S14]

Experimentally, the pK_a value of the most acidic proton was established for all derivatives (**1a**–**1c**) using spectrophotometric titration with the help of a UV−Visible absorbance spectrophotometer (*SHIMADZU UV−2600*). The pH of the solution was monitored using an *Accumet* pH meter (*accuTuPH*). A 15 mL acetonitrile/water (9:1) solution was prepared having 50 mM $TBAPF_6$, 50 μM of **1a**–**1c**, pH = 2.0 by addition of 1 M HNO_3. Initial absorbance spectra were recorded with 2 mL of the prepared solution having the lowest pH value. A sequential addition of 0.1 M NaOH was added into the 15 mL prepared solution to increase the required pH value, and subsequent absorbance was recorded by an aliquot of 2 mL of the

solution. The changes in the absorbance value with respect to the pH was plotted by using OriginPro 8.5 software. The corresponding pK_a value of compound **1a**–**1c** was determined by using the sigmoid curve function Eq. S9.

$$Y = \frac{\max + (min - max)}{1 + 10^{(pKa - x)}} \qquad \text{(Eq. S9)}$$

where, Y is the dependent (pH of the solution during titration) variable, and x is a point of inflection which indicates the point where half of the compound is dissociated.

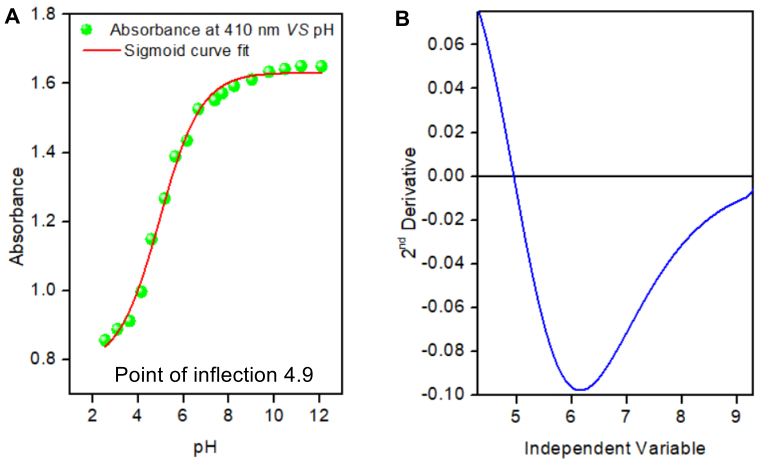

Fig. S27 Four–parameter sigmoid curve fit for absorbance at 410 nm against the different pH values and point of inflection is designated as pK_a (A) and 2nd derivative plot of the sigmoid curve for compound **1a** (B).

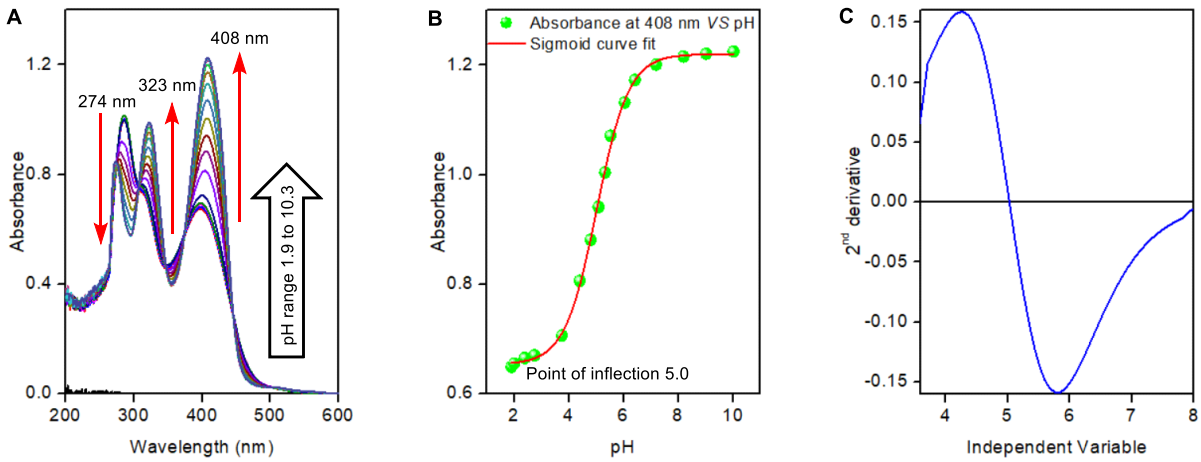

Fig. S28 The stacked UV–Vis absorbance spectra of **1b** (50 μM) for different pH ranges (A), four-parameter sigmoid curve fit for absorbance at 408 nm against the different pH values and point of inflection is designated as pK_a (B), and 2nd derivative plot of the sigmoid curve for compound **1b** (C).

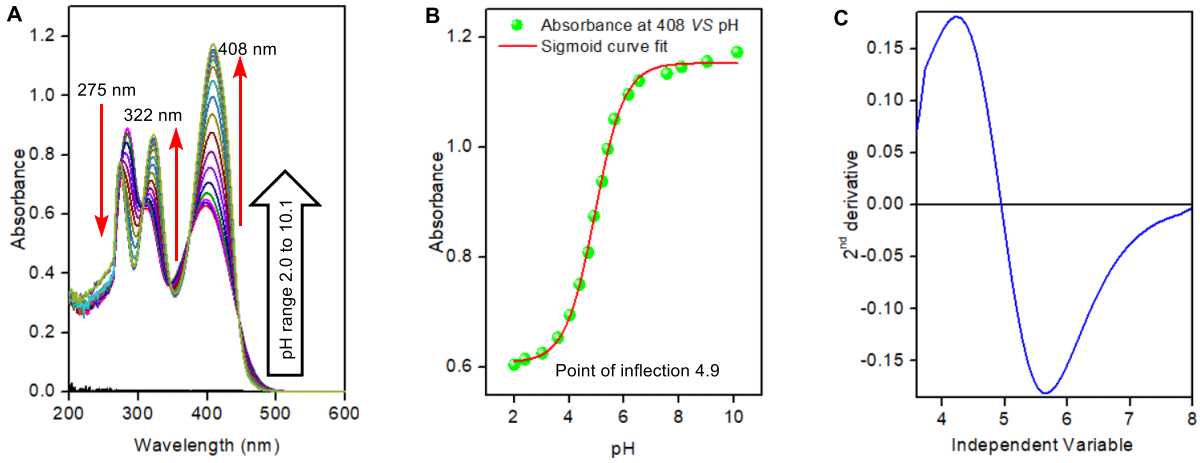

Fig. S29 The stacked UV–Vis absorbance spectra of **1c** (50 μM) for different pH ranges (A), and four parameters of the sigmoid curve fit for absorbance at 408 nm against the different pH values, and the inflection point is designated as pK_a (B), and 2nd derivative plot of the sigmoid curve for compound **1c** (C).

9. Single crystal X–ray diffraction

The compound **1a** and **1b** were crystallized as a yellow solid by slow evaporation of methanol and acetonitrile solvent, respectively, to get a single crystal appropriate for X–ray examination. The single crystal data were obtained on a *Bruker* Smart Apex Duo diffractometer using Mo Kα radiation (λ = 0.71073 Å) for compound **1a** at 296 K. Olex 2 graphical interface was used with SHELXT to solve the structure using intrinsic phasing and refined with SHELXL with full matrix least square minimization on F^2. All non–hydrogen atoms were refined anisotropically except for those in minor disordered parts. Crystallographic parameters for **1a** are summarised in Table S1. Crystallographic data for compounds **1a** and **1b** have been deposited at the Cambridge Crystallographic Data Centre (CCDC) under deposition numbers 2381721 and 2389545, respectively. [S15,S16]

Table S1. Data collection parameters for compound **1a**.

Compound	**1a**
Chemical formula	$C_{20}H_{10}F_6N_6O$
Formula weight	464.34 g/mol
Temperature	296(2) K
Wavelength	0.71073 Å
Crystal system	Triclinic
Space group	*P-1*

Unit cell dimensions	a = 9.475(2)) Å b = 10.104(2) Å c = 13.666(3) Å α = 91.019(6)° β = 106.311(6)° γ = 112.839(5)°
Volume	1145.3(4) $Å^3$
Z	2
Density (calculated)	1.346 g/cm^3
Absorption coefficient	0.121 mm^{-1}
F (000)	468
Theta range for data collection	2.21 to 20.53°
Index ranges	−11<=h<=11, −11<=k<=11, −16<=l<=16
Reflections collected	31919
Independent reflections	3872 [R(int) = 0.1948]
Coverage of independent reflections	99.7%
Function minimized	Σ w $(F_o^2 - F_c2)^2$
Data/restraints/parameters	3872 / 0 / 306
Goodness–of–fit on F2	1.631
Δ/σ max	0.016
Final R indices	1889 data; [I>2σ(I)] R1 = 0.1247, wR_2 = 0.2849
	all data, R_1 = 0.2175, wR_2 = 0.3141
Largest diff. peak and hole	0.225 and −0.175 $eÅ^{-3}$
R.M.S. deviation from mean	0.028 $eÅ^{-3}$
CCDC number	2381721

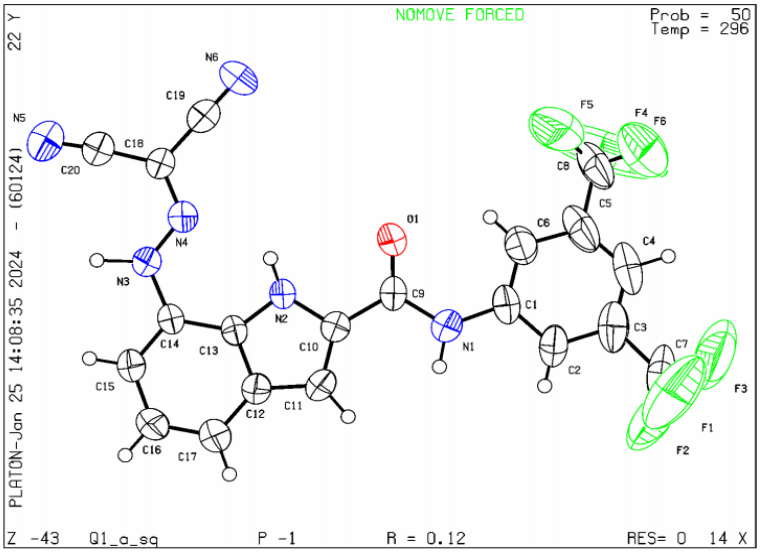

Fig. S30 ORTEP diagram of compound **1a** with 50% probability ellipsoids established by single X−ray crystallography.

Table S2. Data collection parameters for compound **1b**.

Compound	**1b**
Chemical formula	$C_{21}H_{17}N_7O$
Formula weight	383.42 g/mol
Temperature	150(2) K
Wavelength	0.71073 Å
Crystal system	Triclinic
Space group	*P-1*
Unit cell dimensions	a = 10.1964(16) Å b = 10.2846(15) Å c = 10.8304(15) Å α = 109.588(4)° β = 90.363(4)° γ = 116.248(4)°.
Volume	943.5(2) Å^3
Z	2
Density (calculated)	1.350 g/cm^3
Absorption coefficient	0.089 mm^{-1}
F (000)	400.0

Crystal size	0.240 x 0.150 x 0.090 mm^3
Theta range for data collection	2.030 to 28.436°.
Index ranges	−13<=h<=13, −13<=k<=13, −14<=l<=14
Reflections collected	42964
Independent reflections	4735 [R(int) = 0.0926]
Coverage of independent reflections	100.0 %
Absorption correction	Semi-empirical from equivalents
Refinement method	Full-matrix least-squares on F^2
Data/restraints/parameters	4735 / 0 / 276
Goodness–of–fit on F^2	0.792
Final R indices	R1 = 0.0668, wR2 = 0.1611
	all data, R1 = 0.1202, wR2 = 0.1980
Largest diff. peak and hole	0.371 and -0.522 e.$Å^{-3}$
CCDC number	2389545

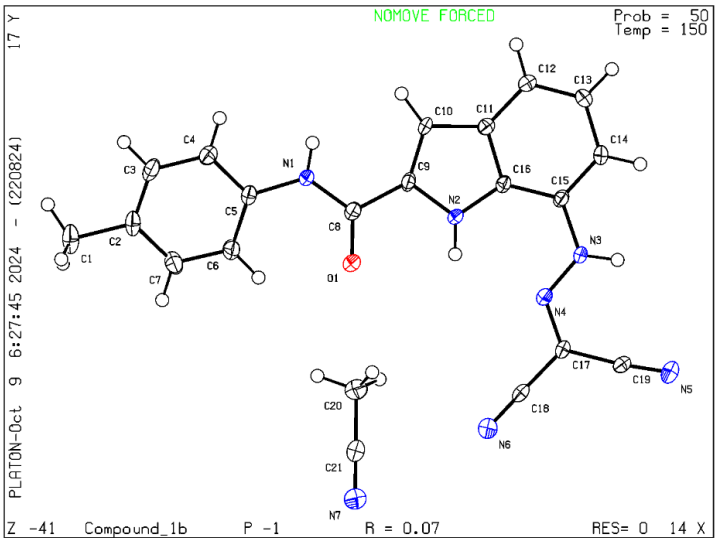

Fig. S31 ORTEP diagram of compound **1b** with 50% probability ellipsoids established by single X−ray crystallography.

10. Theoretical studies[S17]

Based on the ^{1}H NMR titration (Host : Guest = 1:1) and Hill co−efficient value of $n \sim 1$ obtained from dose−response studies of compounds **1a**−**1c**, geometry optimization of the highest active compound **1a** and [**1a**+Cl^-] was performed. Initially, the most probable conformers of **1a** and [**1a**+Cl^-] were obtained using the CONFLEX–8 software program, and subsequently, their geometry optimization was carried out using the Gaussian 09 program package. The geometry optimized [**1a**+Cl^-] confirmed the formation of H−bonding interactions between the chloride anion and the three N−H groups, i.e., $H_a \cdots Cl^-$ = 2.420 Å, $H_b \cdots Cl^-$ = 1.954 Å, $H_c \cdots Cl^-$ = 2.317 Å, and also with H_d, i.e., $H_d \cdots Cl^-$ = 2.876 Å. The binding energy of the geometrically optimized [**1a**+Cl^-] complex was calculated to be −47.44 kcal/mol.

To visualize the different conformers of compound **1a** and [**1a**+Cl^-] complex, several free compounds and complex geometries were obtained using the CONFLEX−8 software package using MMFF94S force field. The calculation provided the 5 possible conformers of compound **1a**. The Boltzmann populations of the two highest populated conformations are **Conf-I** with 97.50% and **Conf-II** with 2.49%. For the [**1a**+Cl^-] complex, 7 possible conformers were obtained. The Boltzmann populations of the four highest populated conformations are **Conf-I** with 50.47% and **Conf-II** with 49.53%.

1a (**Conf-I**, **Conf-II**) and [**1a**+Cl^-] (**Conf-I**, **Conf-II**) were further geometry optimized by the Gaussian 09 program package using B3LYP functional and 6−311++G (d,p) basis set. For structures **1a** and [**1a**+Cl^-], the vibrational frequency calculation during the geometry optimization has not shown any imaginary frequencies, indicating that all optimized structures are ground−state minima.

The Gaussian 09 program was used to calculate the zero−point energy (ZPE) and basis set superposition error (BSSE) corrected bonding energy of [**1a**+Cl^-], which was used for the calculation of binding energy (*BE*) using the following Eq.S10. Geometry−optimized energetically more stable **Conf-I** of structure **1a** and **Conf-I** of [**1a**+Cl^-] complexes were used during the binding energy (*BE*) calculation.

$$BE = [HF_{[\mathbf{1a}+Cl^-]} + ZPE_{[\mathbf{1a}+Cl^-]} + BSSE_{[\mathbf{1a}+Cl^-]}] - [HF_{\mathbf{1a}} + ZPE_{\mathbf{1a}}] - [HF_{Cl^-}] \qquad \text{(Eq. S10)}$$

where, $HF_{[\mathbf{1a}+Cl^-]}$ = electronic energy of [**1a**+Cl^-] complex, $ZPE_{[\mathbf{1a}+Cl^-]}$ = zero−point energy of [**1a**+Cl^-] complex, $BSSE_{[\mathbf{1a}+Cl^-]}$ = BSSE of [**1a**+Cl^-] complex, $HF_{\mathbf{1a}}$ = electronic energy of the receptor **1a**, $ZPE_{\mathbf{1a}}$ = zero−point energy of the receptor **1a**, HF_{Cl^-} = electronic energy of cation Cl^-.

Table S3. The electronic energy (HF), zero−point energy (ZPE), basis set superposition error (BSSE) corrected energy (in Hartree unit) for all structures and complexes are calculated at the DFT B3LYP/6–311++G(d,p) level of theory.

Parameters	Energy
$HF_{[\mathbf{1a}+Cl^-]}$ (in Hartree)	−2231.79685
$ZPE_{[\mathbf{1a}+Cl^-]}$ (in Hartree)	0.280907
$BSSE_{[\mathbf{1a}+Cl^-]}$ (in Hartree)	0.001946507
$HF_{\mathbf{1a}}$ (in Hartree)	−1771.415539
$ZPE_{\mathbf{1a}}$ (in Hartree)	0.280868
HF_{Cl^-} (in Hartree)	−460.3037272
BE (in Hartree)	−0.075598593
BE (in kcal/mol)	−47.43834369

Table S4. Atomic coordinates of compound **1a** after geometry optimization by Gaussian 09 program using B3LYP functional and 6−311++G(d,p) basis set.

Charge = 0 Multiplicity = 1

Atom number	Atom type	X	Y	Z
1	C	−5.14003	−3.7861	−0.02604
2	C	−5.75164	−2.52071	−0.01585
3	C	−4.99712	−1.35199	−0.00763
4	C	−3.59567	−1.469	−0.00983
5	C	−2.97573	−2.75112	−0.01987

6	C	−3.76266	−3.91649	−0.02807
7	N	−2.60581	−0.52588	−0.00383
8	N	−5.66284	−0.11621	0.002534
9	C	−1.37855	−1.15145	−0.0093
10	C	−1.56687	−2.51826	−0.01918
11	C	−0.18201	−0.28097	−0.00403
12	O	−0.29622	0.934967	0.001353
13	C	4.700993	−0.85415	−0.02094
14	C	3.390843	−1.31443	−0.02108
15	C	2.322195	−0.40862	−0.00268
16	C	2.587181	0.9663	0.017306
17	C	3.910438	1.403219	0.017263
18	C	4.978026	0.511193	−0.00191
19	N	1.024642	−0.94706	−0.00476
20	N	−5.02734	1.024163	0.011378
21	C	−5.70356	2.152578	0.021292
22	C	5.833241	−1.84802	0.024035
23	F	5.499683	−3.02383	−0.55615
24	F	6.193432	−2.13406	1.299442
25	F	6.937257	−1.39023	−0.59994
26	C	4.180859	2.888199	−0.02209
27	F	3.263184	3.589874	0.67248
28	F	4.158359	3.359591	−1.29274
29	F	5.393609	3.195913	0.486608
30	C	−4.98424	3.380562	0.030914
31	N	−4.42965	4.394444	0.038949
32	C	−7.13046	2.167333	0.022749
33	N	−8.28132	2.043025	0.022862
34	H	−5.76886	−4.66785	−0.03226
35	H	−6.83446	−2.45193	−0.01436
36	H	−3.2985	−4.89541	−0.0359
37	H	−2.7297	0.476798	0.003481
38	H	−6.68391	−0.13218	0.003355

39	H	−0.80524	−3.28309	−0.0258
40	H	3.19979	−2.38121	−0.04069
41	H	1.770111	1.670497	0.035999
42	H	5.998513	0.868155	−0.00189
43	H	0.977165	−1.95472	−0.0105

Table S5. Atomic coordinates of [**1a**+Cl^-] after geometry optimization by Gaussian 09 program using B3LYP functional and 6−311++G (d, p) basis set.

Charge = −1 Multiplicity = 1

Atom number	Atom type	X	Y	Z
1	C	5.389318	−3.41205	0.070268
2	C	5.499608	−2.008	0.058451
3	C	4.368821	−1.19937	0.035598
4	C	3.114117	−1.83887	0.027383
5	C	2.99574	−3.26106	0.046516
6	C	4.159985	−4.04983	0.066584
7	N	1.861215	−1.30754	0.002484
8	N	4.453531	0.217958	0.0269
9	C	0.93725	−2.332	0.012199
10	C	1.597363	−3.54451	0.036441
11	C	−0.52751	−2.12325	0.004819
12	O	−1.29789	−3.07667	−0.01738
13	C	−3.6991	1.618703	−0.03189
14	C	−2.4241	1.072154	−0.01231
15	C	−2.25644	−0.32636	0.006346
16	C	−3.39055	−1.15015	0.005053
17	C	−4.65992	−0.57042	−0.01478
18	C	−4.83582	0.807198	−0.03313
19	N	−0.94313	−0.80417	0.026335
20	N	5.625543	0.763692	−0.10045
21	C	5.842869	2.056293	−0.06954

22	C	−3.87542	3.112922	0.009745
23	F	−2.82902	3.78007	−0.50815
24	F	−4.03926	3.565556	1.282284
25	F	−4.98061	3.511704	−0.67347
26	C	−5.85607	−1.48226	−0.05375
27	F	−5.78726	−2.46264	0.87789
28	F	−5.9834	−2.10737	−1.25348
29	F	−7.02075	−0.82341	0.158796
30	C	7.203217	2.46424	−0.24079
31	N	8.295264	2.821553	−0.37651
32	C	4.891786	3.101675	0.143138
33	N	4.185704	3.998089	0.331235
34	H	6.300883	−3.99899	0.087862
35	H	6.474652	−1.54125	0.067784
36	H	4.094746	−5.13202	0.079904
37	H	1.658803	−0.28671	−0.01298
38	H	3.588723	0.784539	0.105885
39	H	1.116269	−4.50907	0.047774
40	H	−1.54601	1.710108	−0.01488
41	H	−3.26534	−2.22163	0.020384
42	H	−5.82508	1.241036	−0.05165
43	H	−0.23573	−0.06169	0.055073
44	Cl	1.328594	1.648018	0.060646

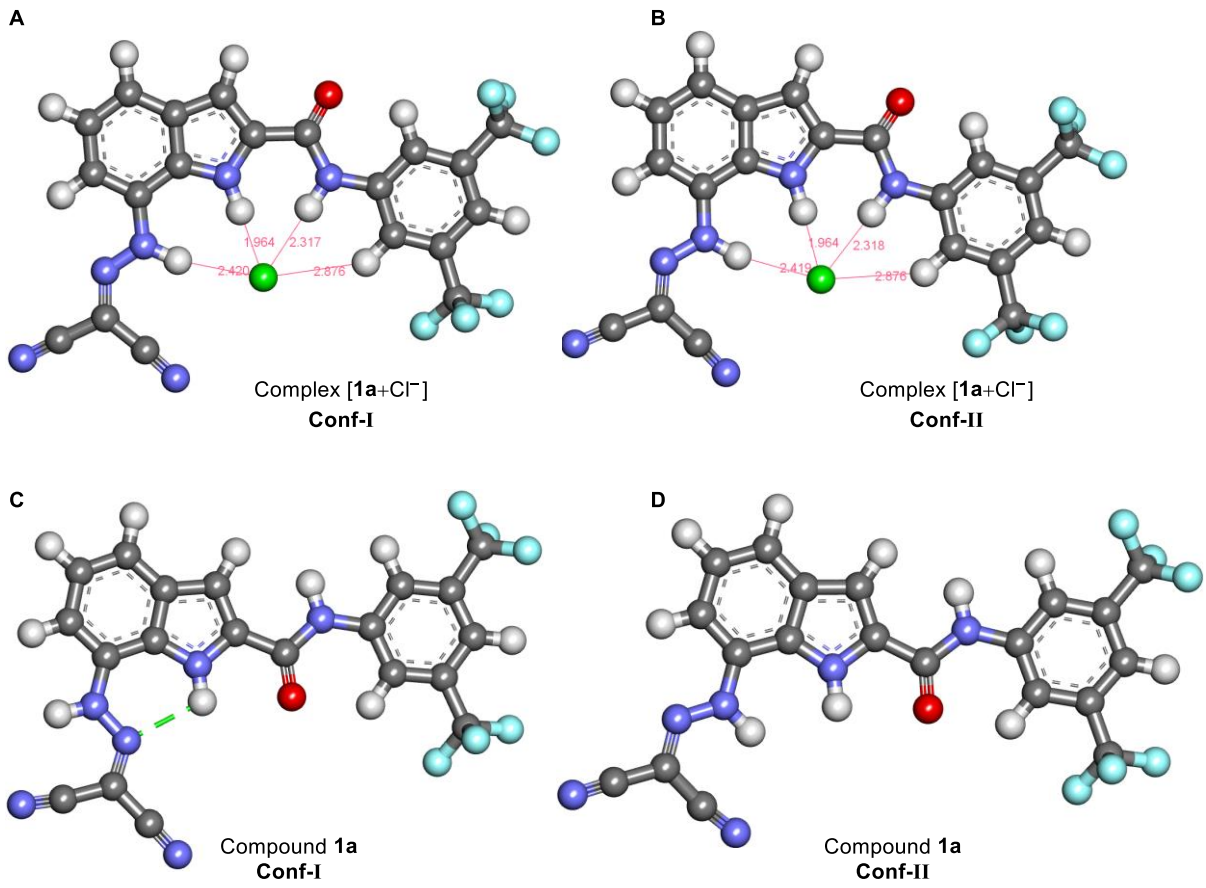

Fig. S32 Geometry–optimized structure of complex [**1a**+Cl^-] (A, B) and compound **1a** (C, D) by using Gaussian 09 program using B3LYP functional and 6−311++G(d,p) basis set.

11. HPLC analysis

The purity of all the final compounds **1a**–**1c** was tested by employing HPLC (High-performance liquid chromatography) *Agilent* 1260 infinity II LC system fitted with C18 reverse phase column and diode array detector (DAD). The absorbance of pure trace was monitored at λ_{max} 320 nm. The stock solution of compounds **1a**–**1c** (2 mM) was prepared, and 10–50 µL samples were injected into the C18 reverse phase column. The experimental method was optimized for up to 20 min by keeping 0.5 mL/min flow rate. H_2O/MeOH (with 0.5% HCOOH) mobile phase system was used to elute the compound. The solvent flow was started with 100% H_2O, then sequentially, the methanol percentage was increased at 1.5 min by 5%, followed by 100% between 3 min–12 min, 5 % between 12 min–16.5 min, and 0% between 16.5 min–20 min.

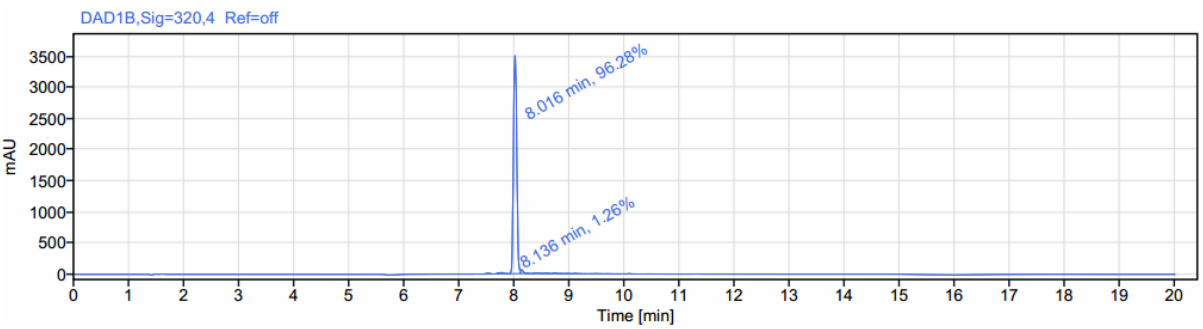

Peak Results (Area Percent at least 1%)

RT (min)	Signal Description	Width (min)	Area	Height	Area%
8.016	DAD1B,Sig=320,4 Ref=off	0.200	14604.0	3531.9	96.28
8.136	DAD1B,Sig=320,4 Ref=off	0.103	190.8	59.3	1.26
		Sum DAD1B	14794.8		

Fig. S33 Purity analysis of compound **1a** by HPLC using H_2O/MeOH (0.5% HCOOH) as mobile phase has demonstrated 96.28% purity.

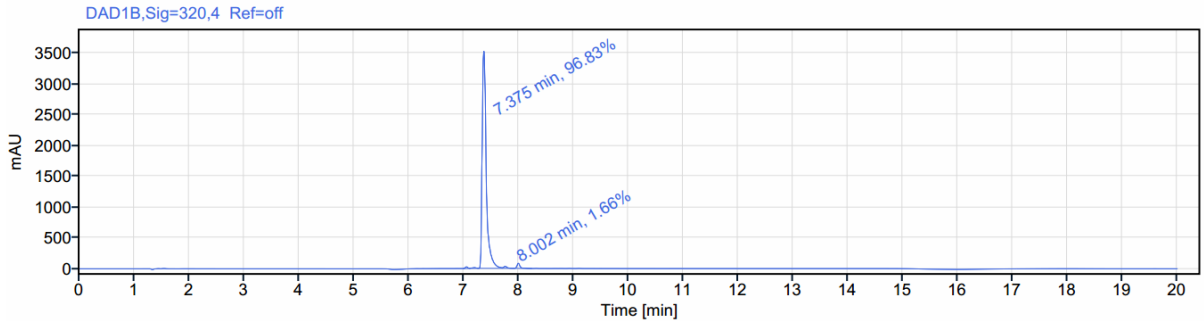

Peak Results (Area Percent at least 1%)

RT (min)	Signal Description	Width (min)	Area	Height	Area%
7.375	DAD1B,Sig=320,4 Ref=off	0.431	18406.2	3537.3	96.83
8.002	DAD1B,Sig=320,4 Ref=off	0.334	316.4	82.2	1.66
		Sum DAD1B	18722.6		

Fig. S34 Purity analysis of compound **1b** by HPLC using H_2O/MeOH (0.5% HCOOH) as mobile phase has demonstrated 96.83% purity.

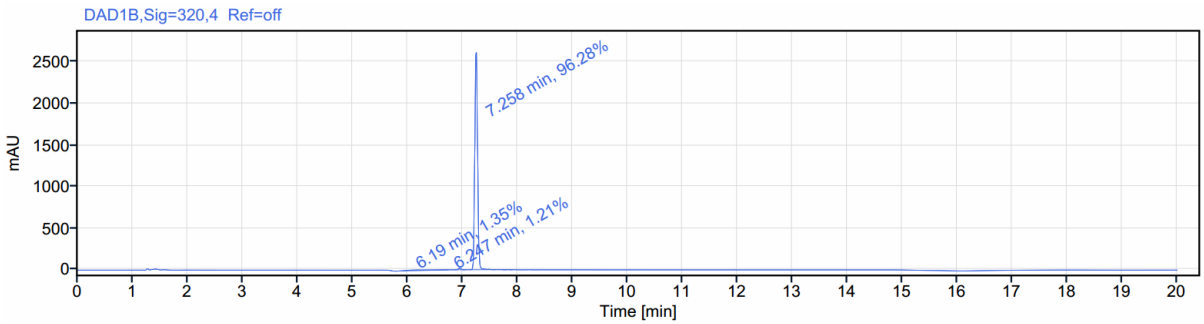

Peak Results (Area Percent at least 1%)

RT (min)	Signal Description	Width (min)	Area	Height	Area%
6.190	DAD1B,Sig=320,4 Ref=off	0.445	129.9	8.0	1.35
6.247	DAD1B,Sig=320,4 Ref=off	0.509	116.1	6.5	1.21
7.258	DAD1B,Sig=320,4 Ref=off	0.311	9251.6	2629.6	96.28
		Sum DAD1B	9497.6		

Fig. S35 Purity analysis of compound **1c** by HPLC using H_2O/MeOH (0.5% HCOOH) as mobile phase has demonstrated 96.28% purity.

12. NMR data

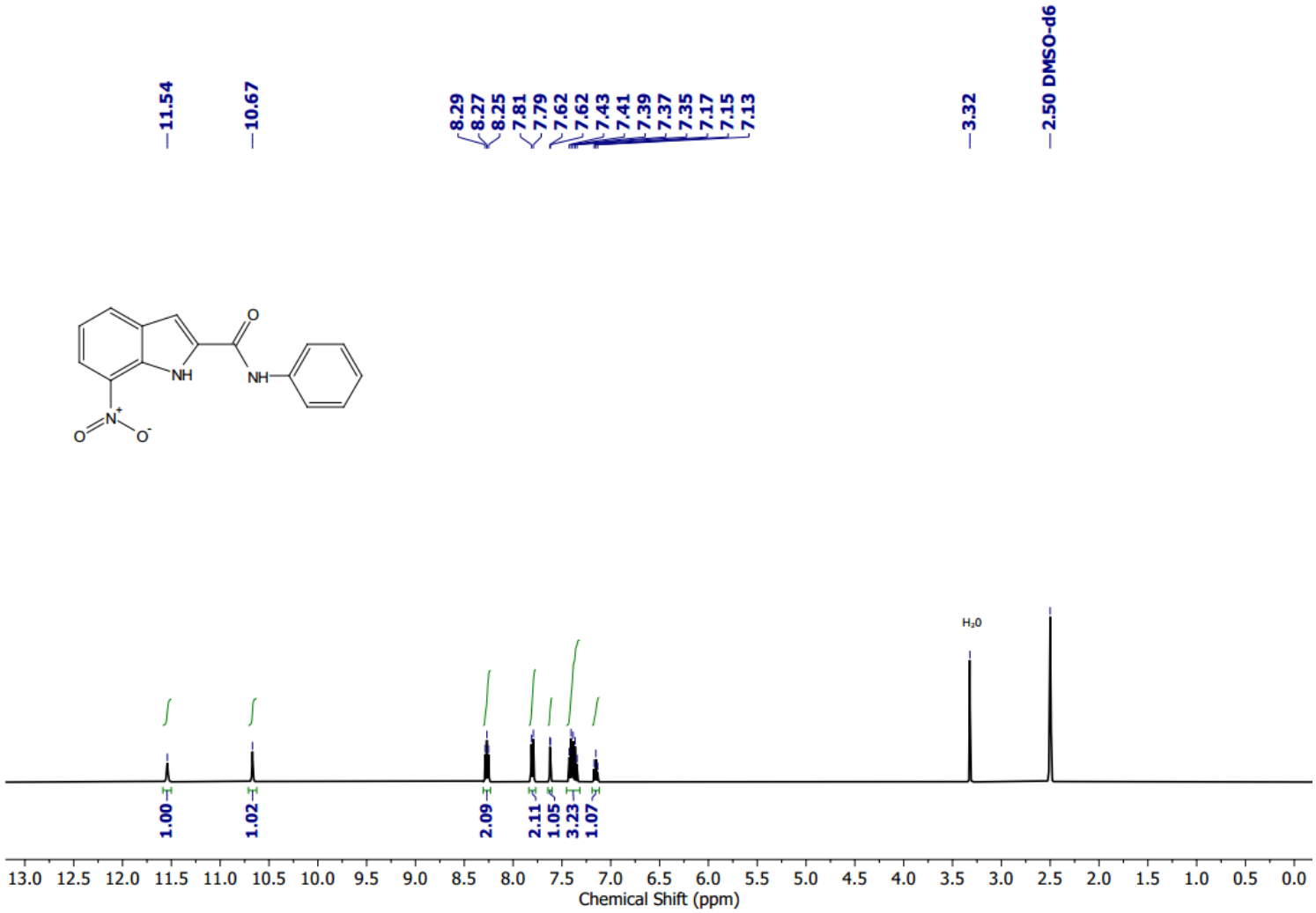

Fig. S36 ^{1}H NMR (400 MHz) of **4c** in DMSO−d_6 at 25 °C.

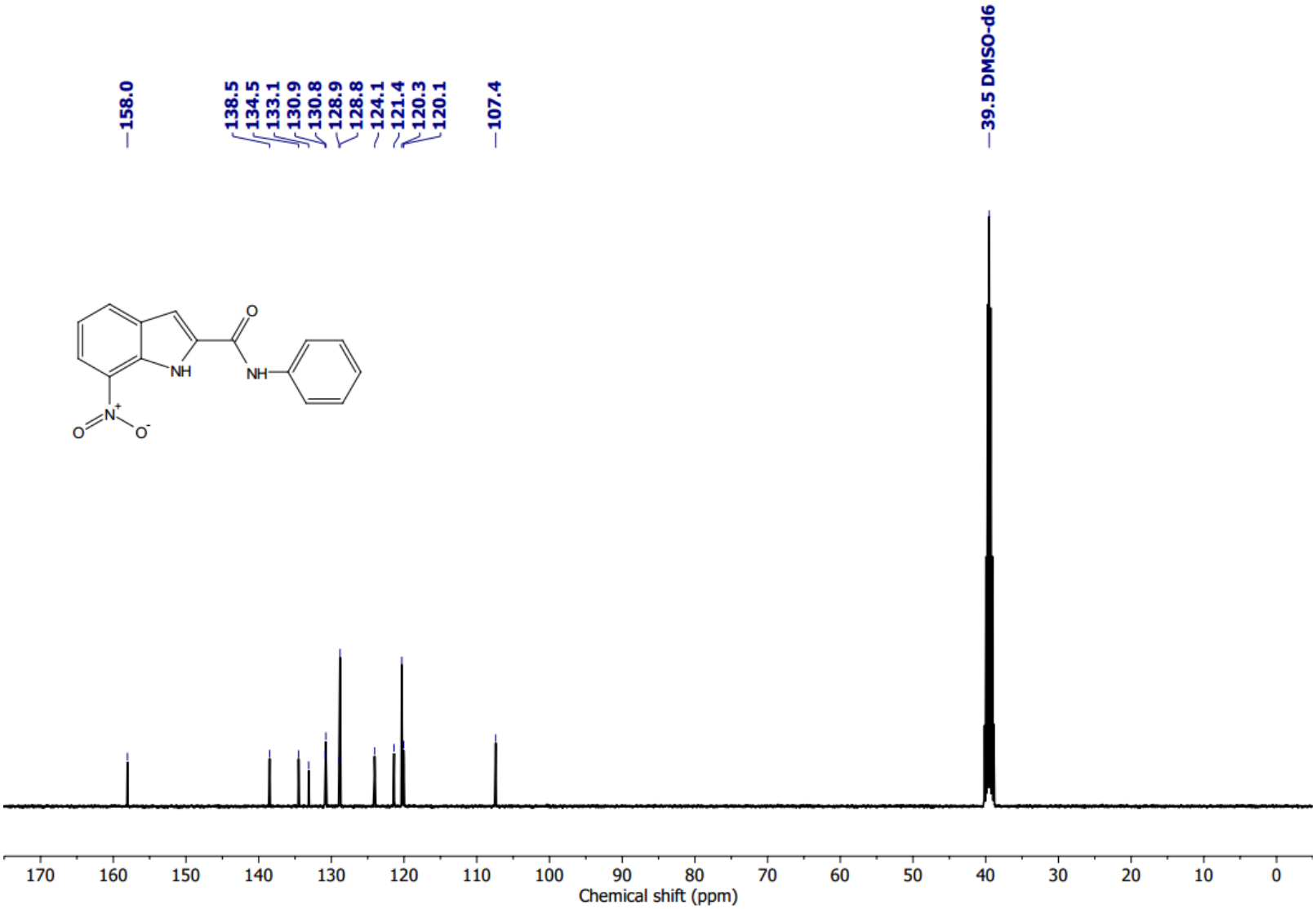

Fig. S37 ^{13}C NMR (101 MHz) of **4c** in DMSO−d_6 at 25 °C.

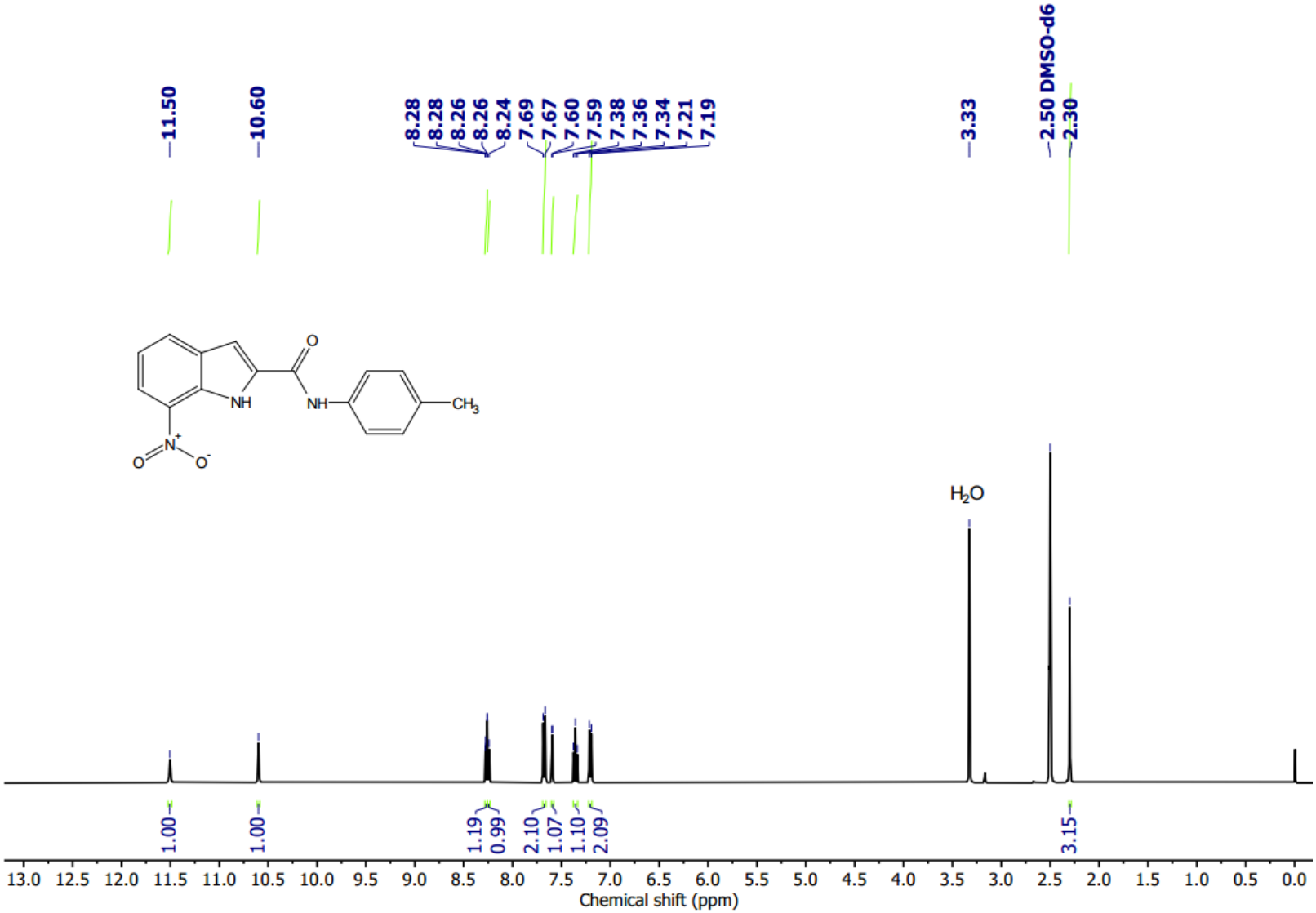

Fig. S38 ^{1}H NMR (400 MHz) of **4b** in DMSO−d_6 at 25 °C.

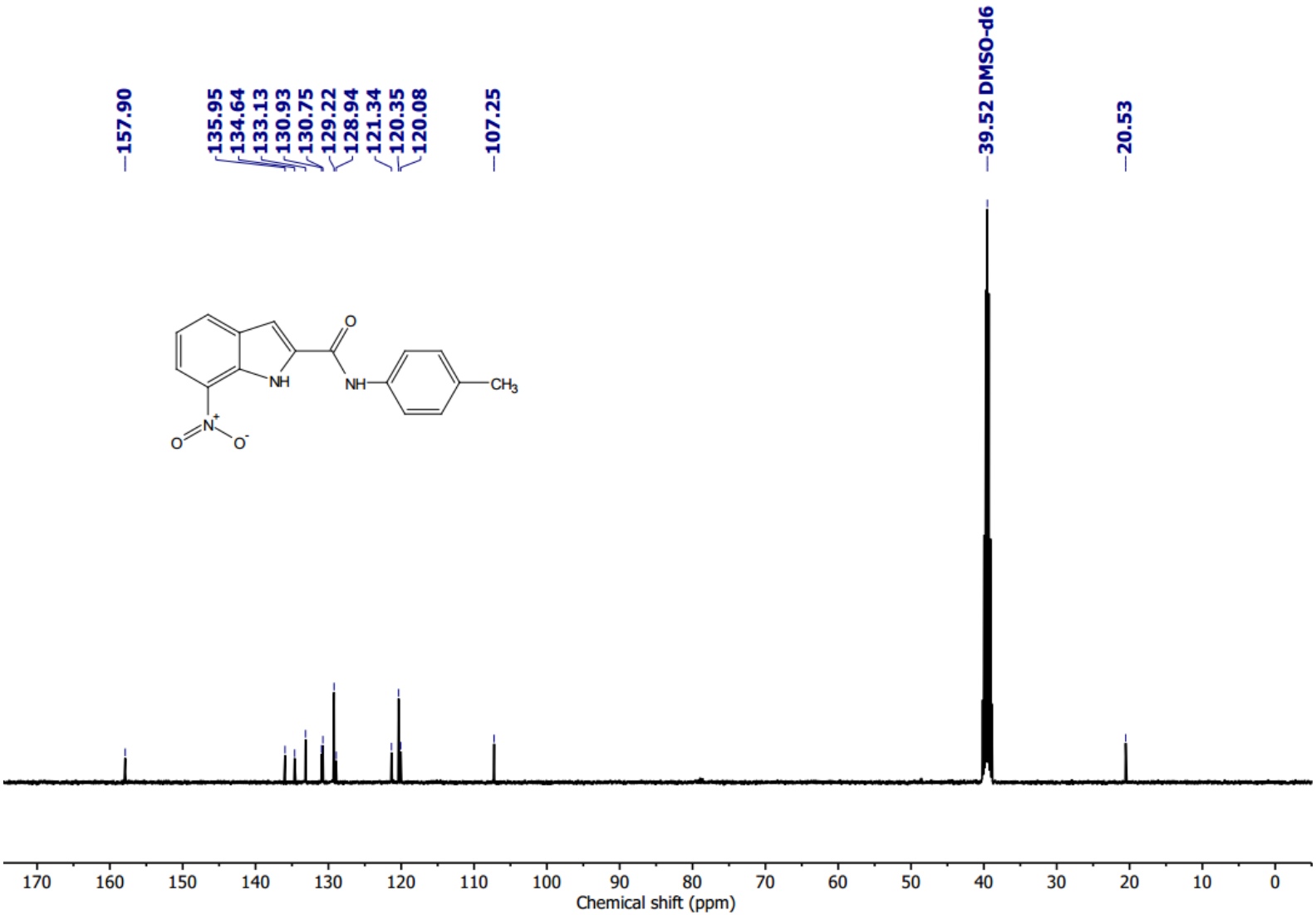

Fig. S39 ^{13}C NMR (101 MHz) of **4b** in DMSO−d_6 at 25 °C.

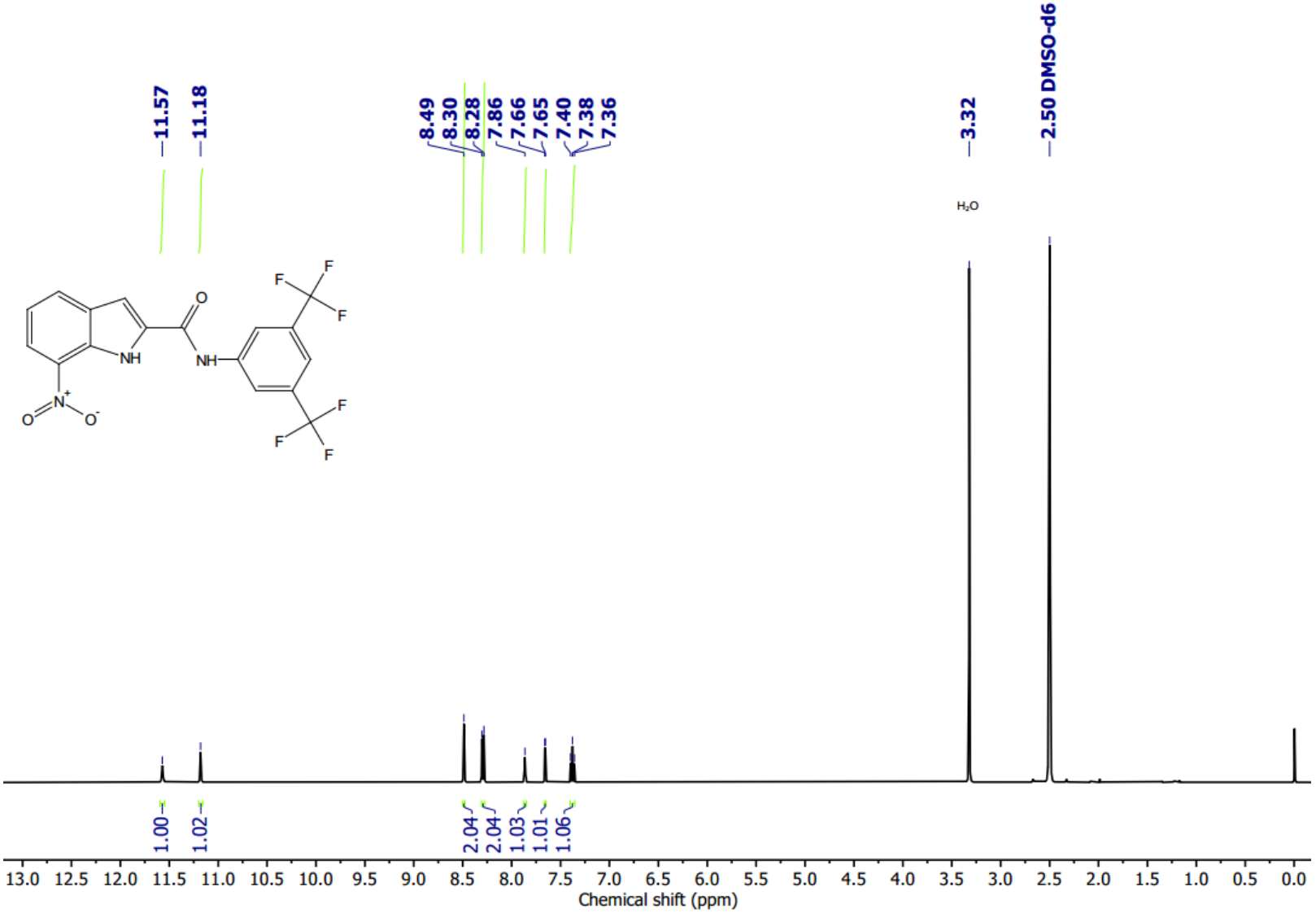

Fig. S40 ^{1}H NMR (400 MHz) of **4a** in DMSO−d_6 at 25 °C.

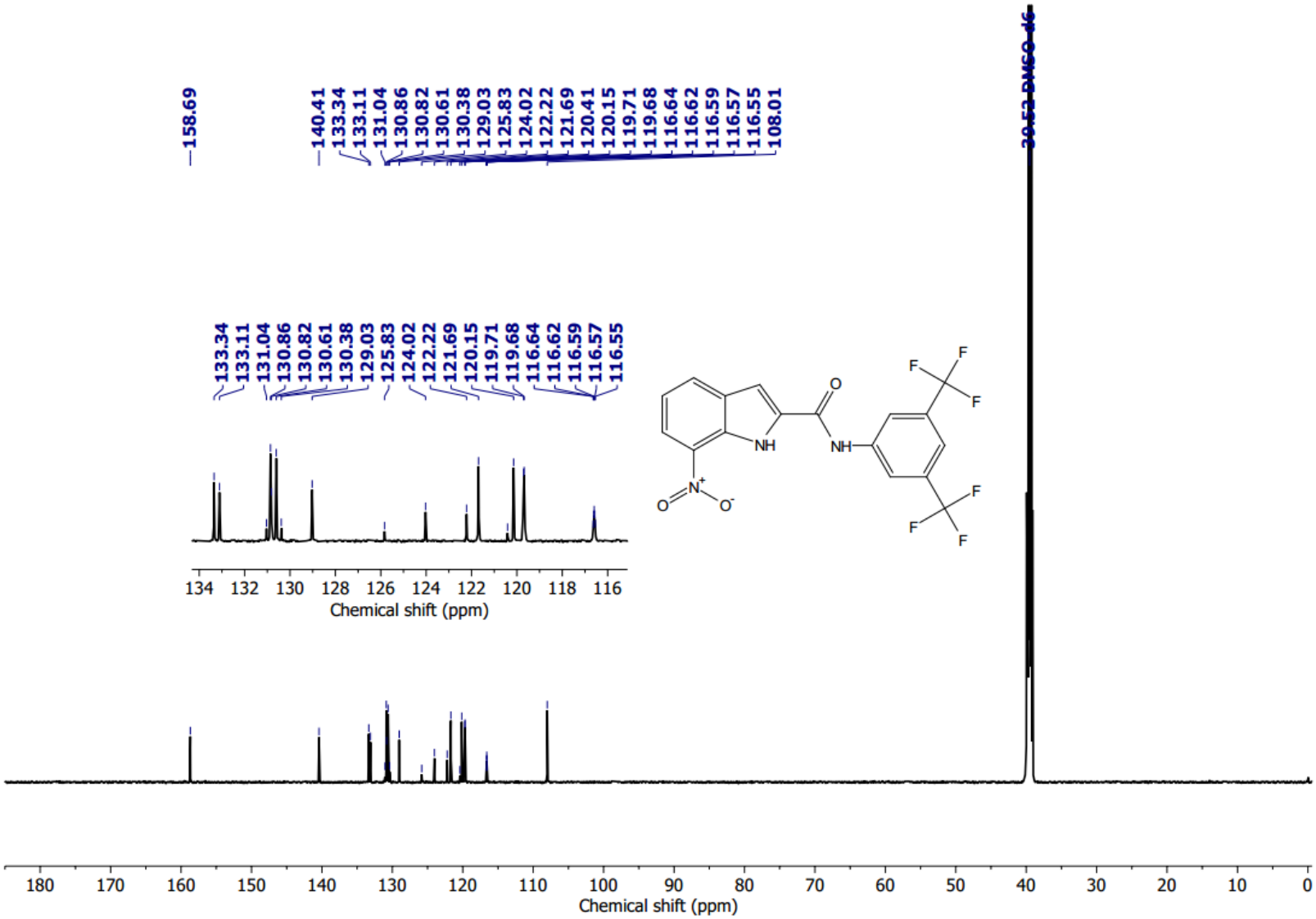

Fig. S41 ^{13}C NMR (101 MHz) of **4a** in DMSO−d_6 at 25 °C.

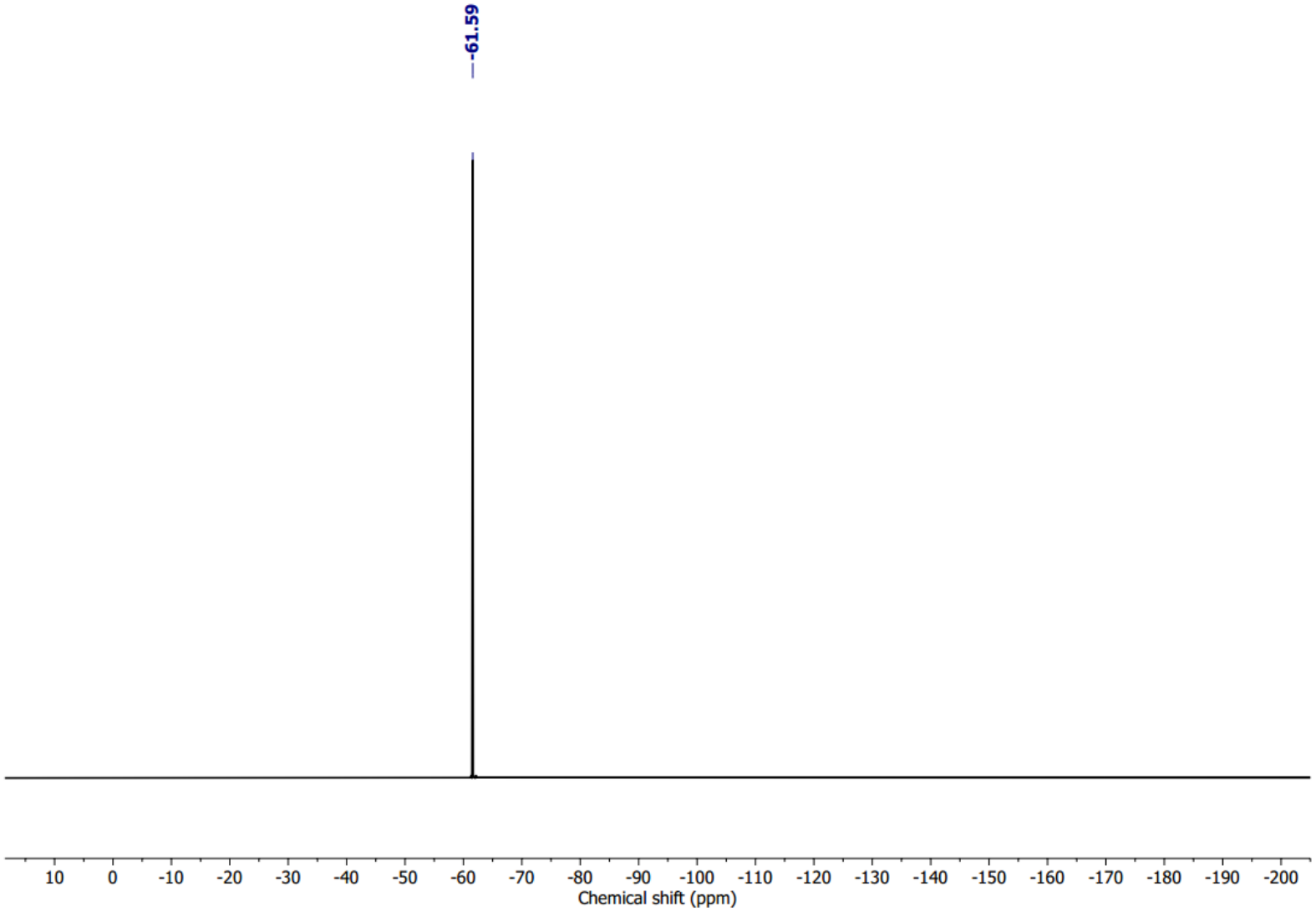

Fig. S42 ^{19}F NMR (376.8 MHz) of **4a** in DMSO−d_6 at 25 °C.

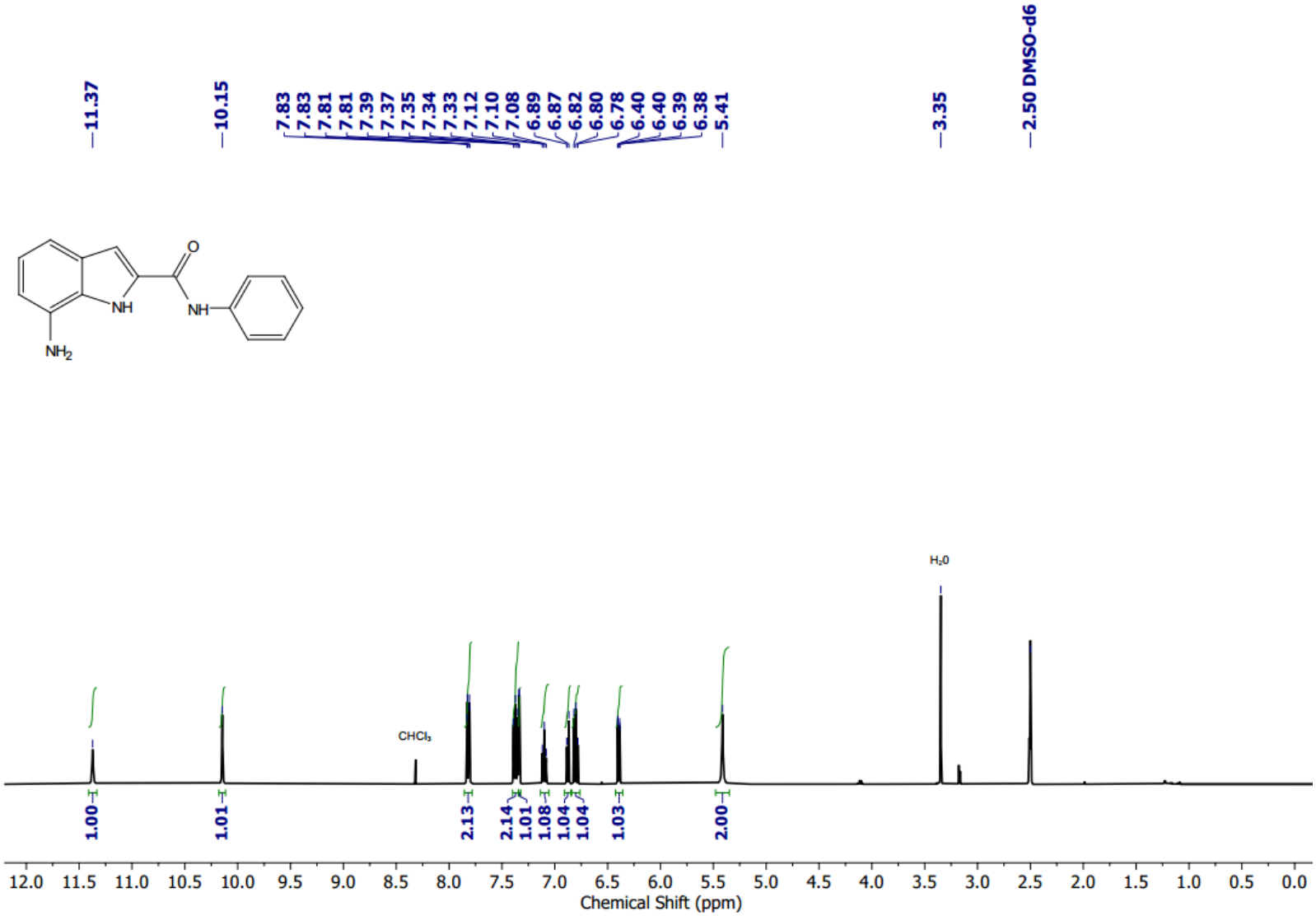

Fig. S43 ^{1}H NMR (400 MHz) of **5c** in DMSO−d_6 at 25 °C.

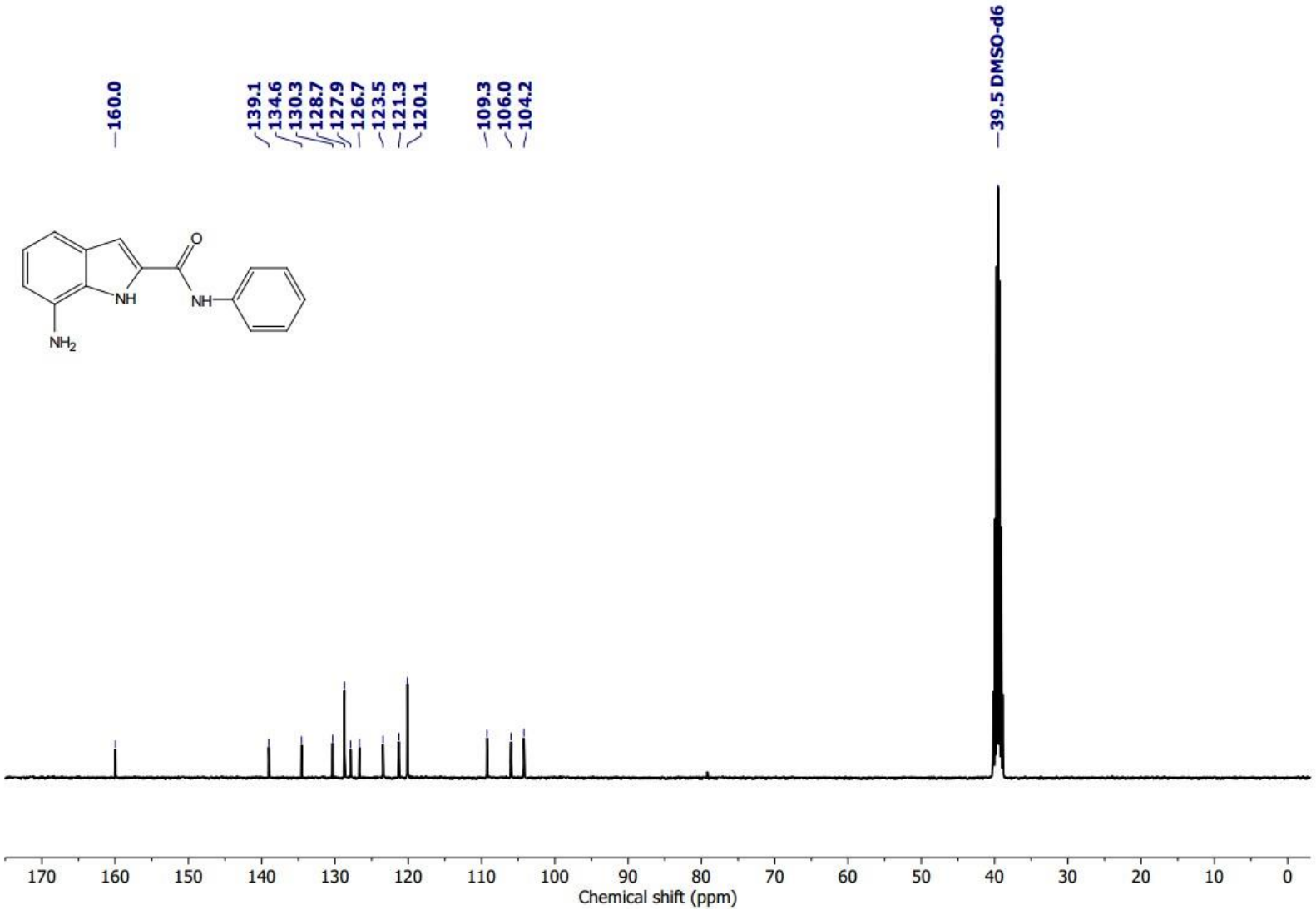

Fig. S44 ^{13}C NMR (101 MHz) of **5c** in DMSO−d_6 at 25 °C.

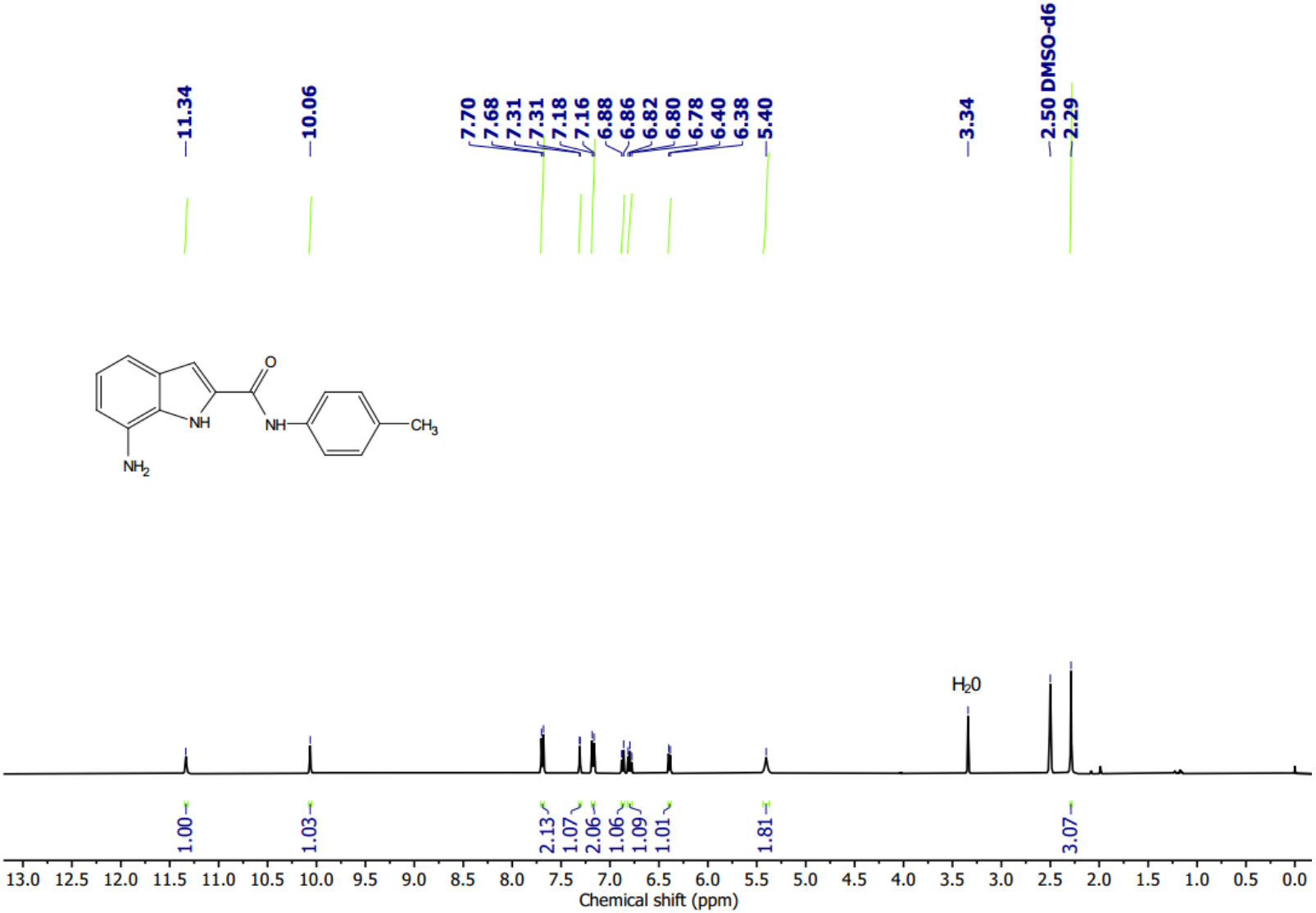

Fig. S45 ^{1}H NMR (400 MHz) of **5b** in DMSO−d_6 at 25 °C.

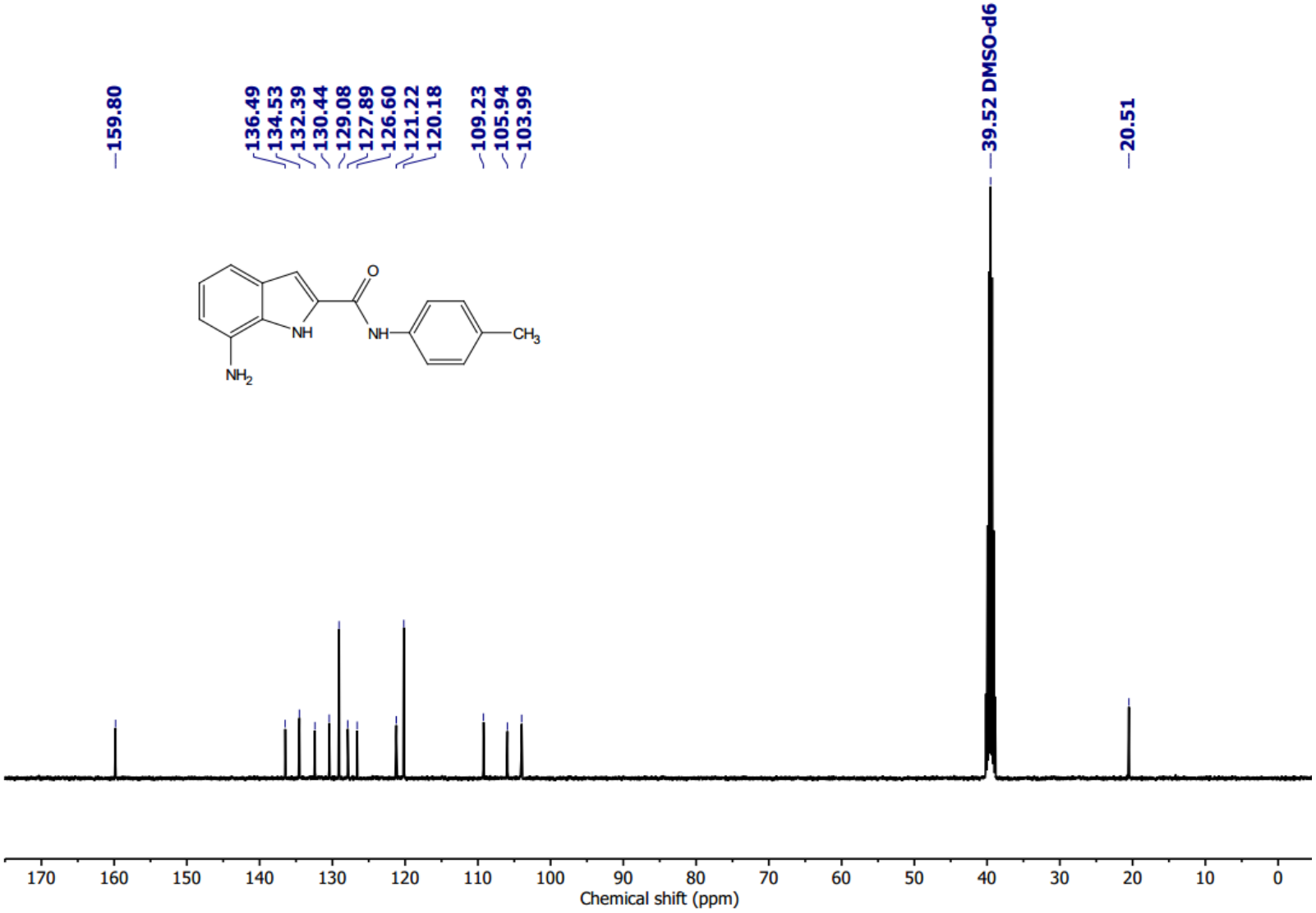

Fig. S46 ^{13}C NMR (101 MHz) of **5b** in DMSO−d_6 at 25 °C.

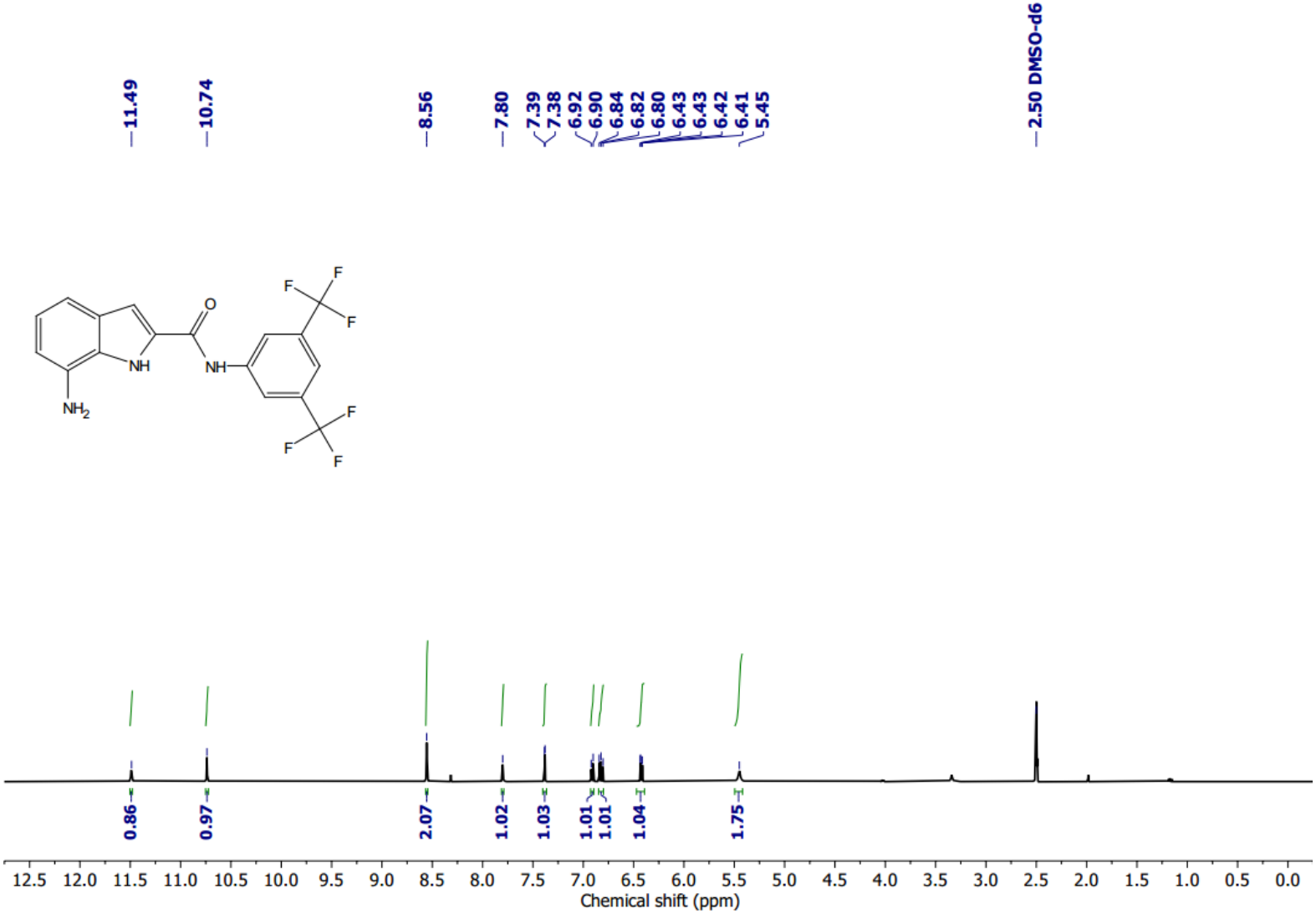

Fig. S47 ^{1}H NMR (400 MHz) of **5a** in DMSO−d_6 at 25 °C.

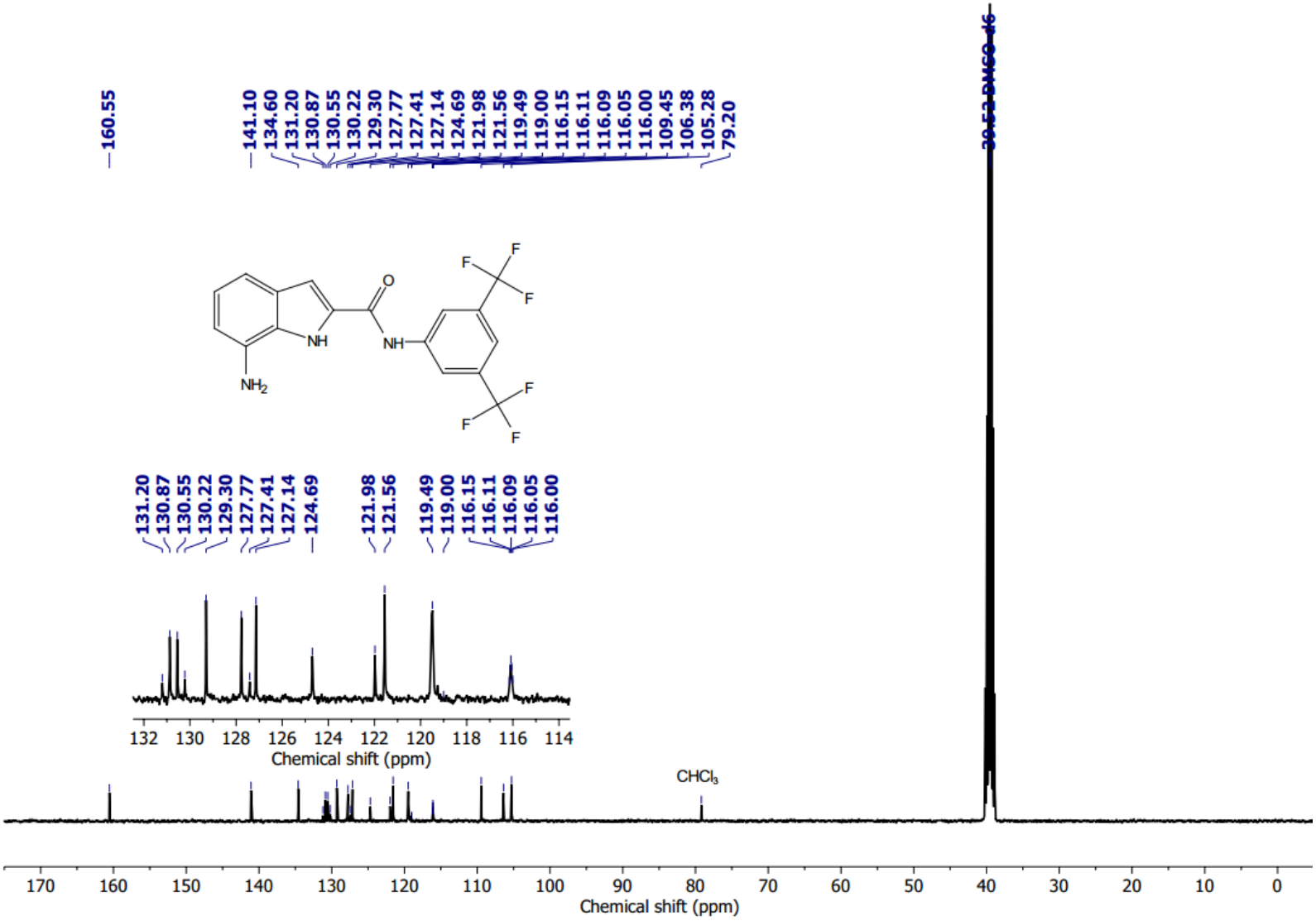

Fig. S48 ^{13}C NMR (101 MHz) of **5a** in DMSO−d_6 at 25 °C.

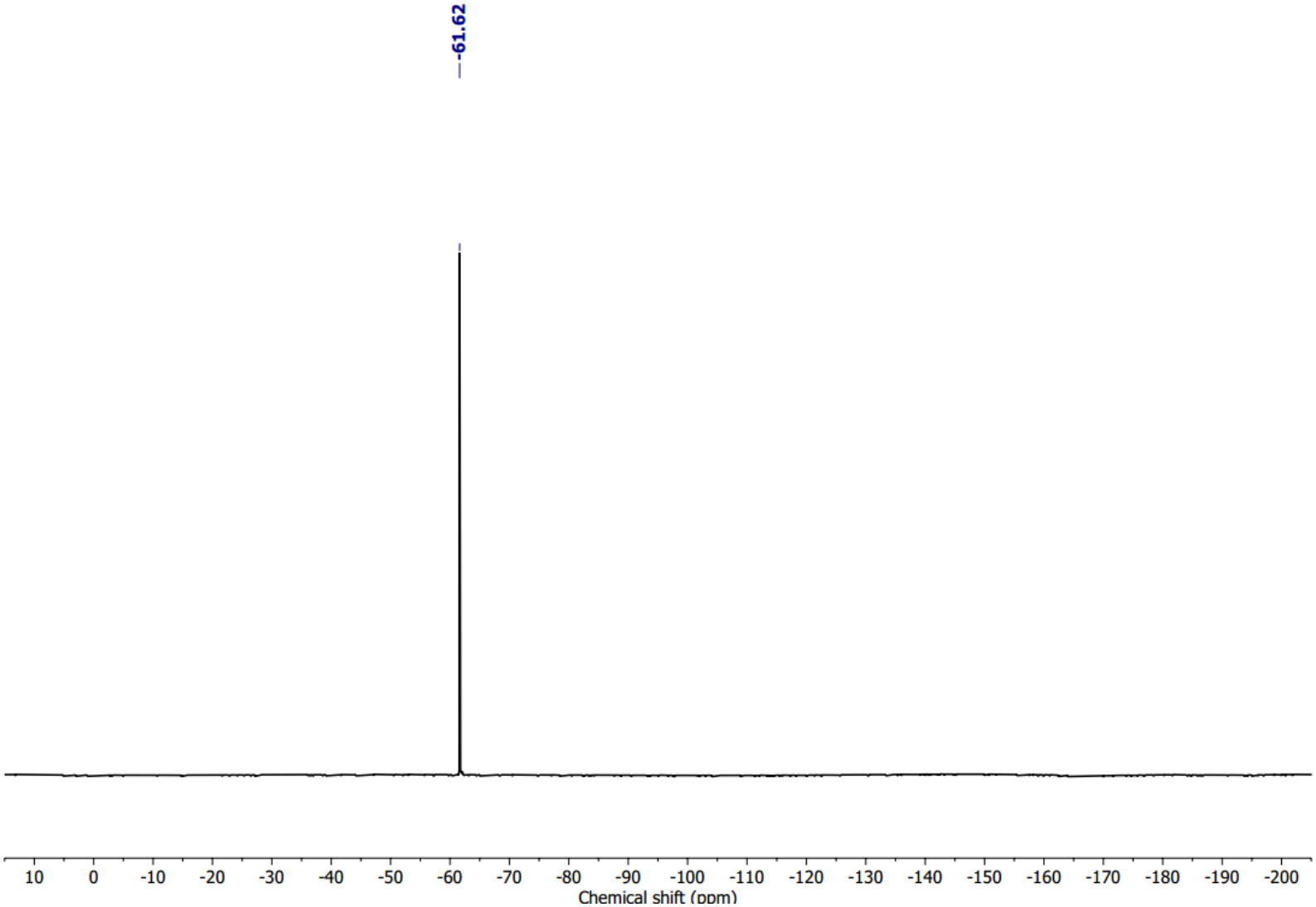

Fig. S49 ^{19}F NMR (376.8 MHz) of **5a** in DMSO−d_6 at 25 °C.

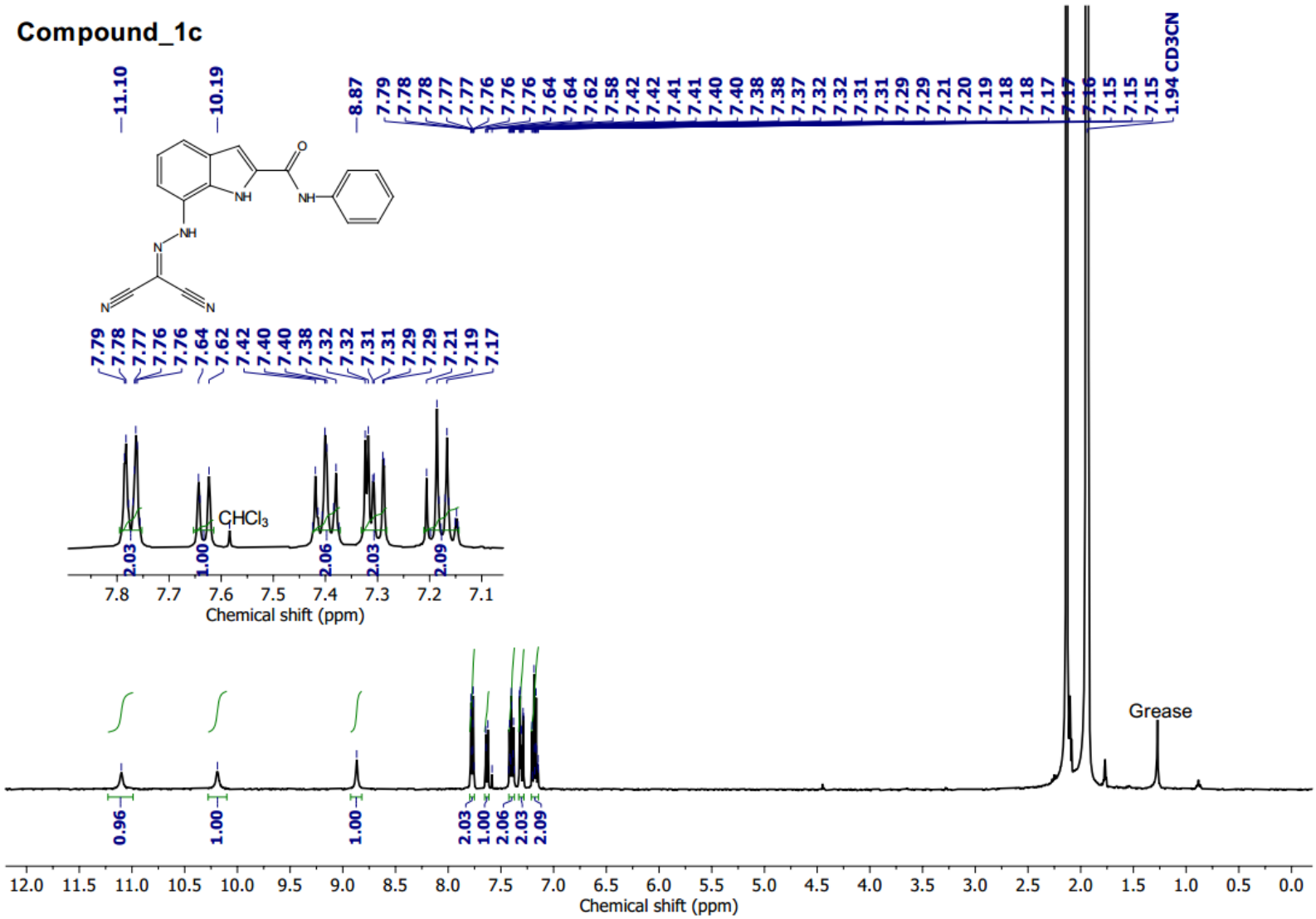

Fig. S50 ^{1}H NMR (400 MHz) of **1c** in acetonitrile−d_3 at 25 °C.

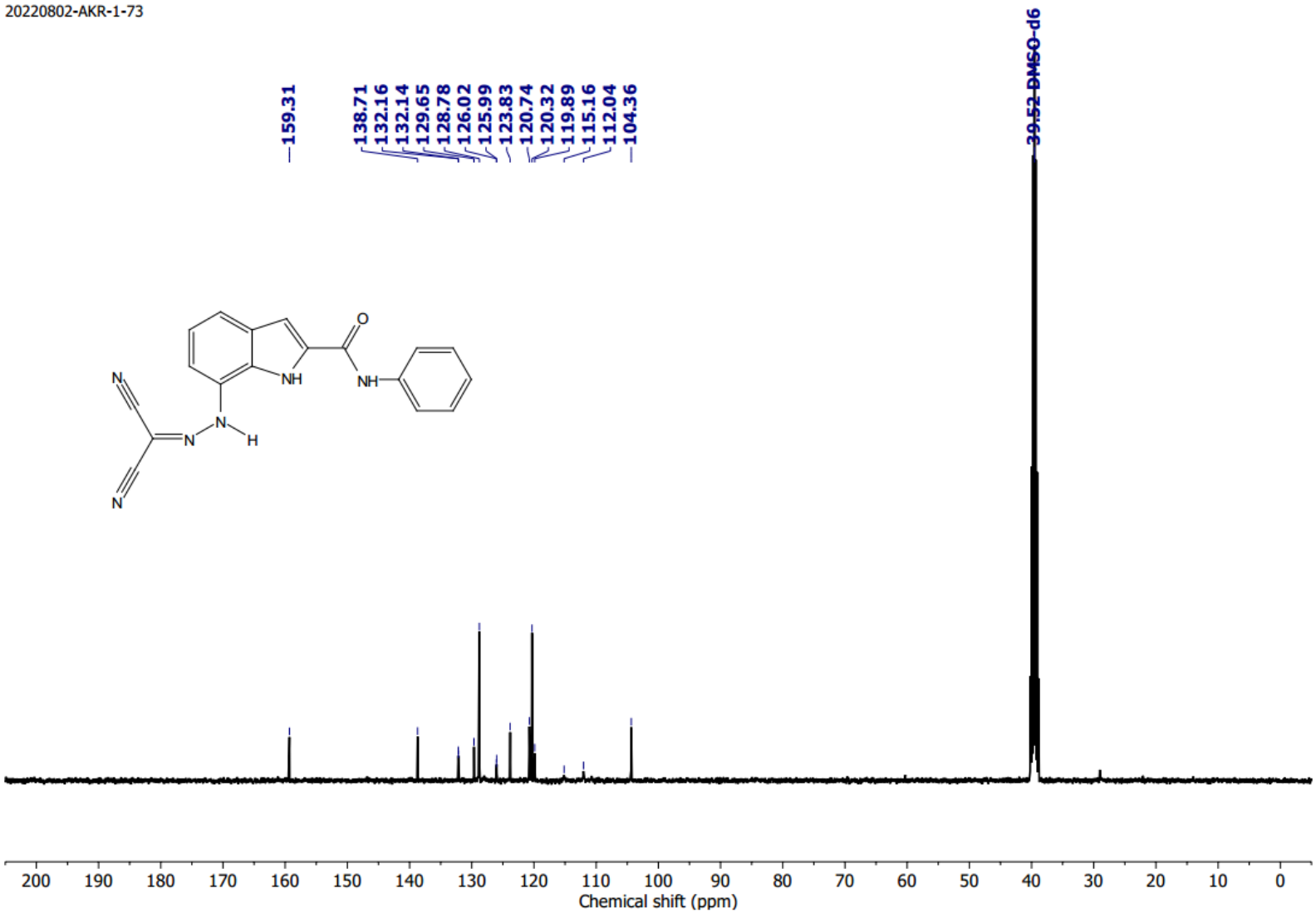

Fig. S51 ^{13}C NMR (101 MHz) of **1c** in DMSO−d_6 at 25 °C.

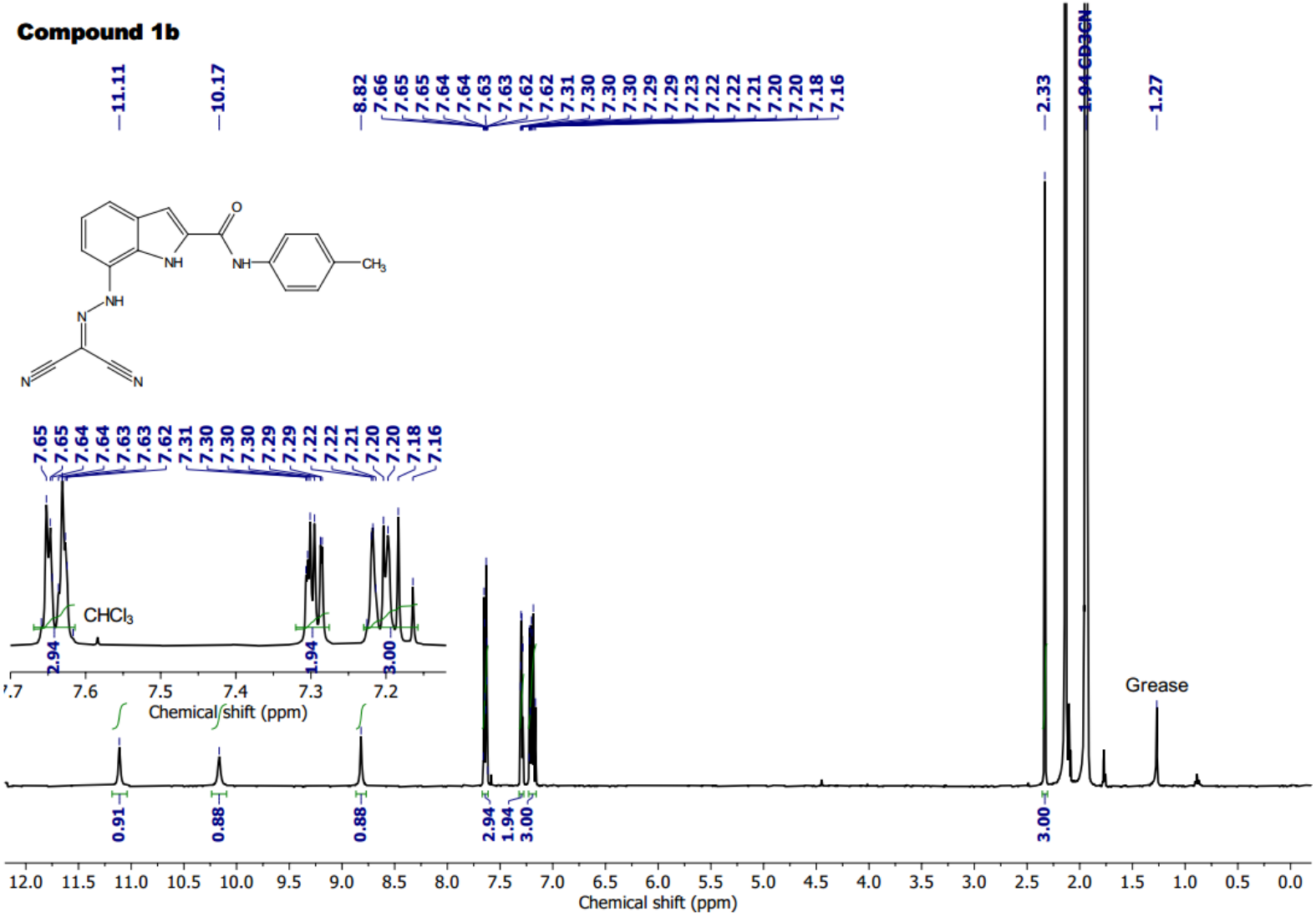

Fig. S52 ^{1}H NMR (400 MHz) of **1b** in acetonitrile−d_3 at 25 °C.

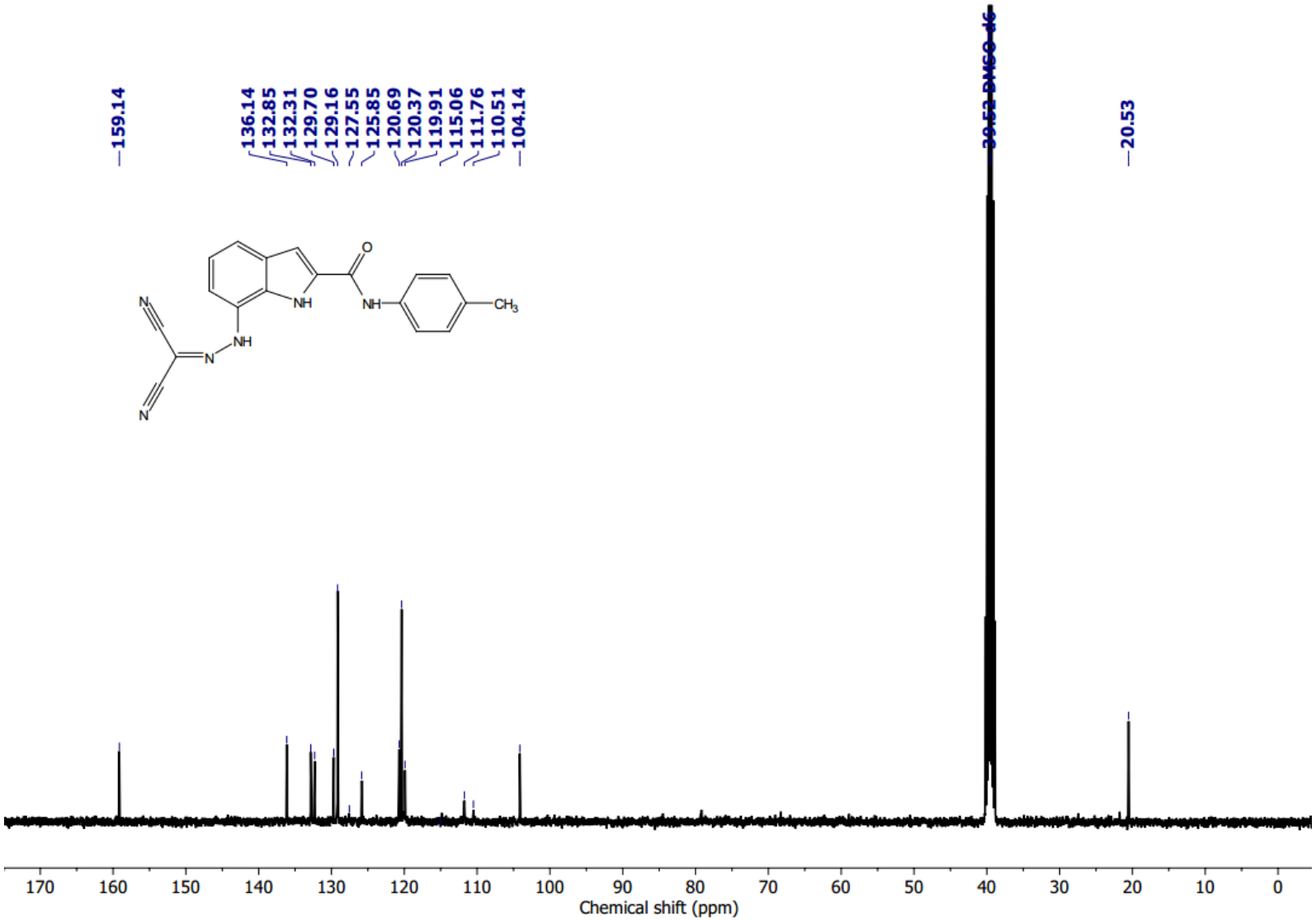

Fig. S53 ^{13}C NMR (101 MHz) of **1b** in DMSO−d_6 at 25 °C.

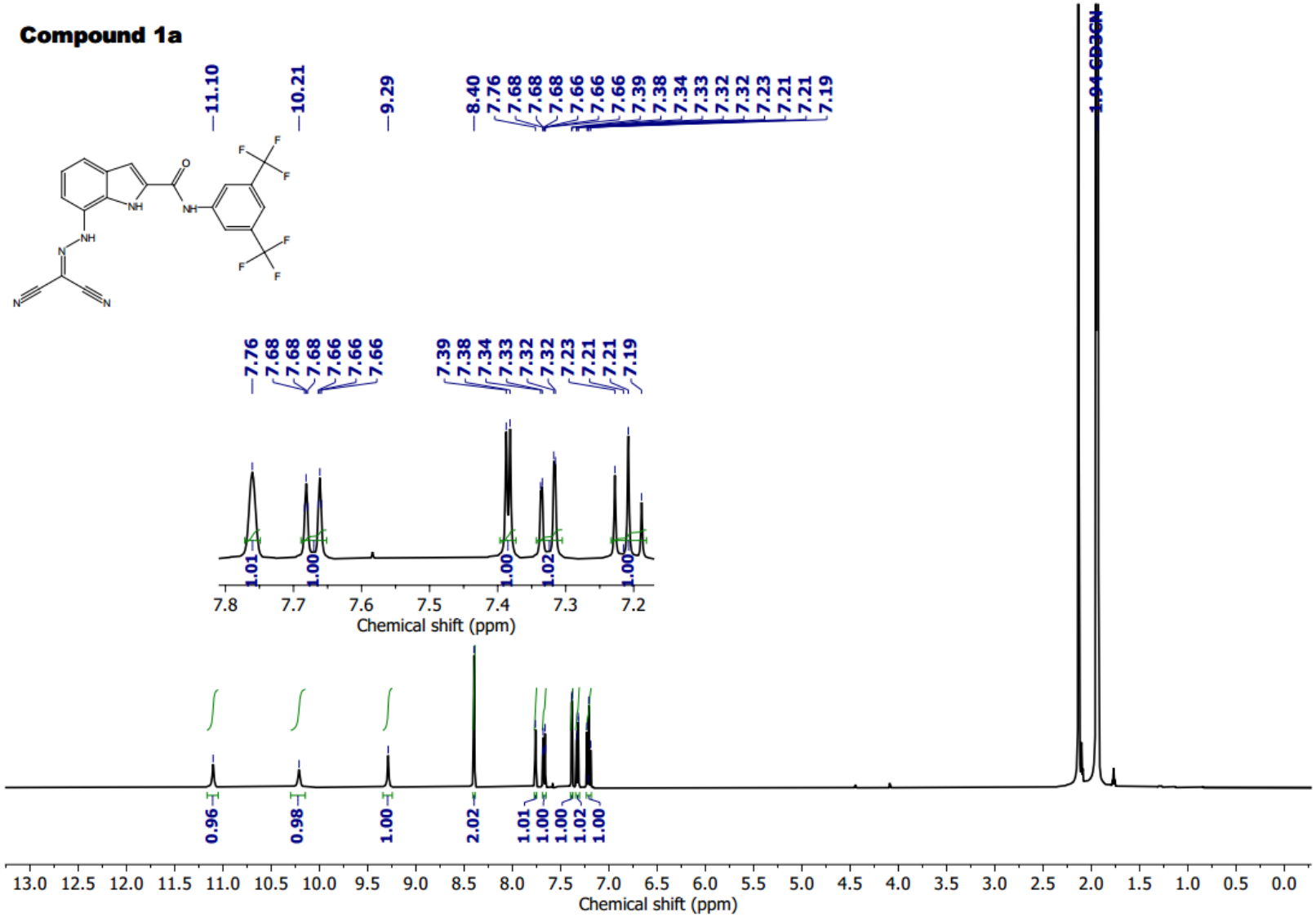

Fig. S54 ^{1}H NMR (400 MHz) of **1a** in acetonitrile−d_3 at 25 °C.

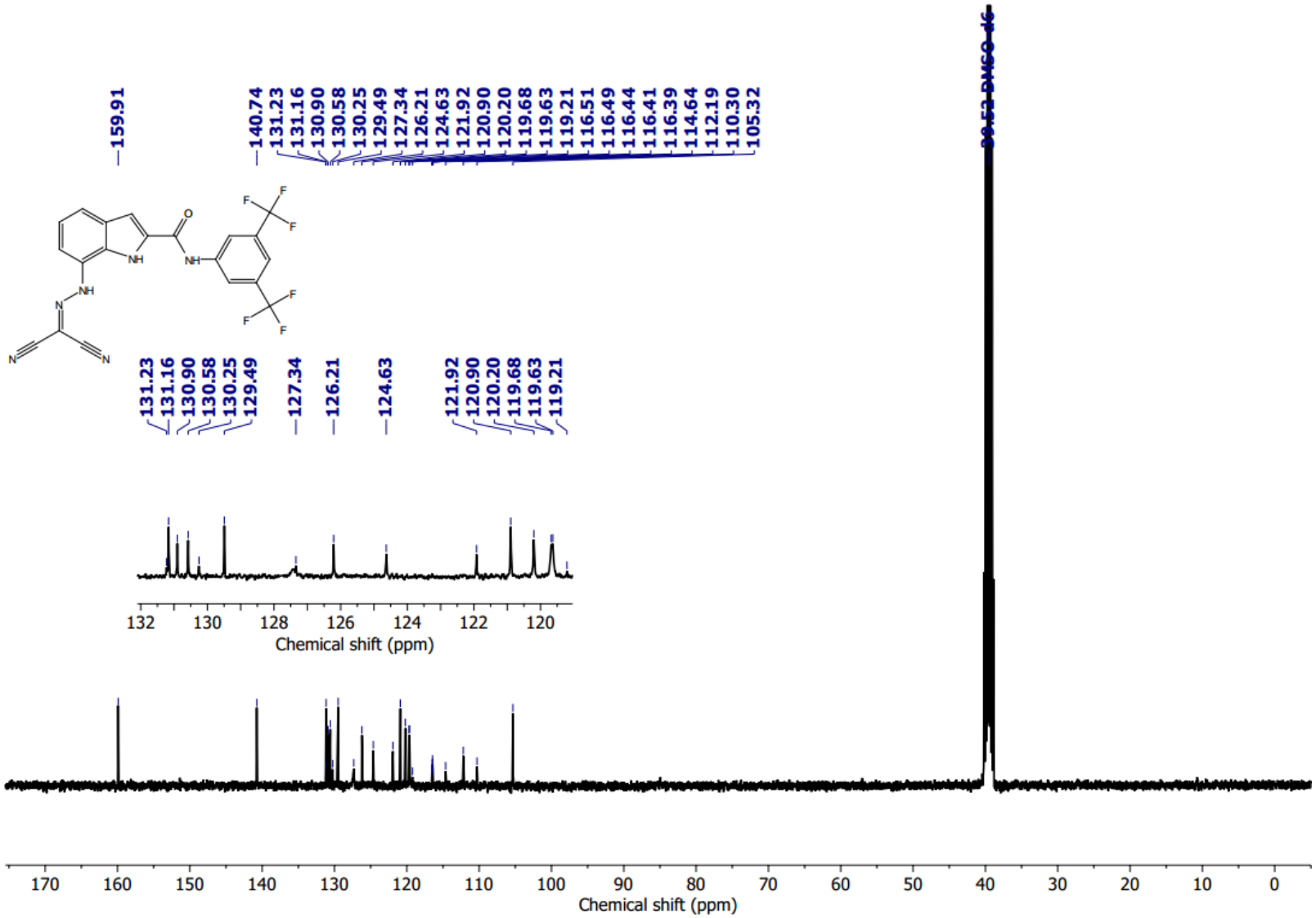

Fig. S55 ^{13}C NMR (101 MHz) of **1a** in DMSO−d_6 at 25 °C.

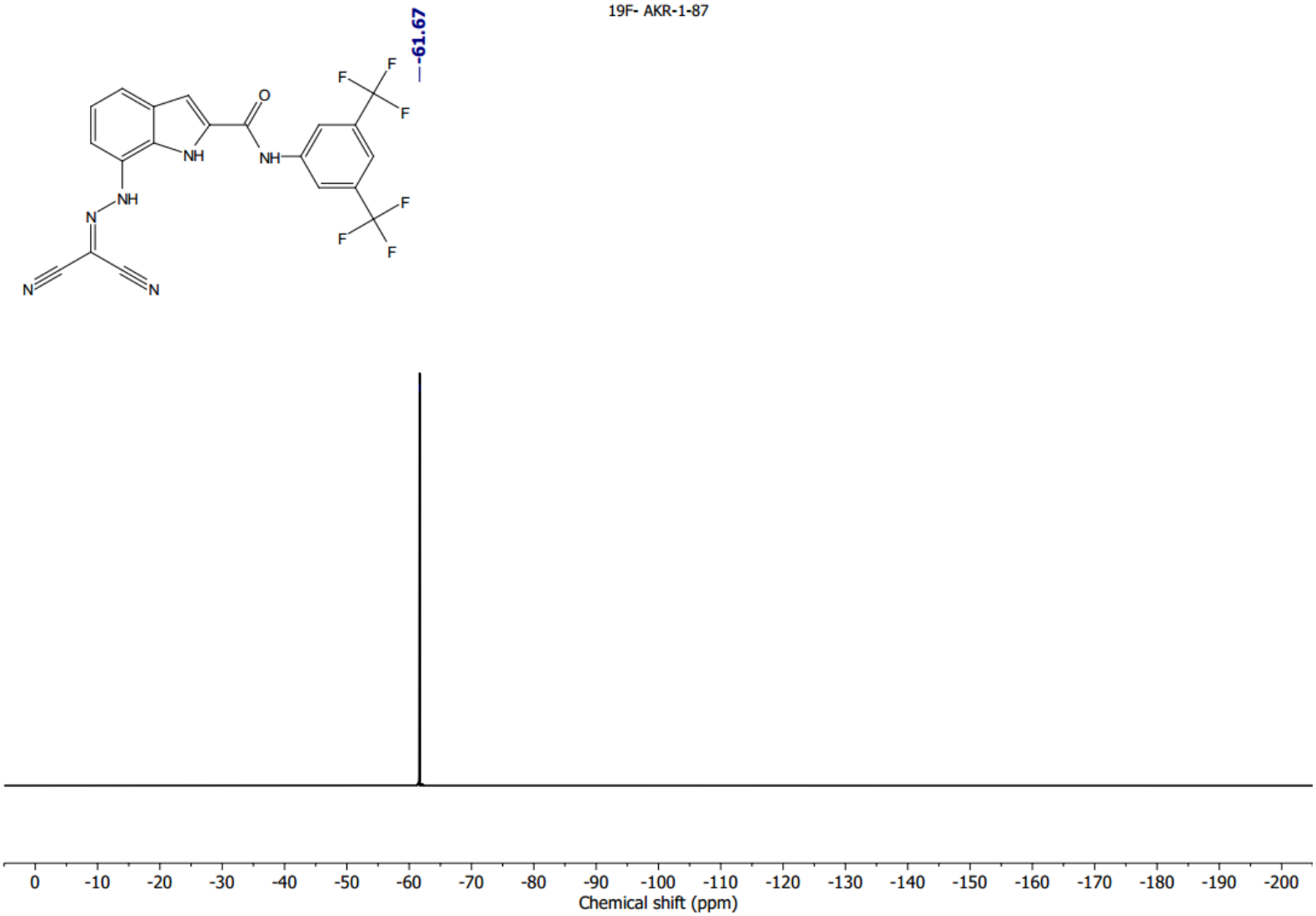

Fig. S56 ^{19}F NMR (376.8 MHz) of **1a** in DMSO−d_6 at 25 °C.

13. References

S1 R. Xu, R. Xia, M. Luo, X. Xu, J. Cheng, X. Shao and Z. Li, *J. Agric. Food Chem.*, 2014, **62**, 381–390.

S2 D. Mondal, M. Ahmad, B. Dey, A. Mondal and P. Talukdar, *Nat. Commun.*, 2022, **13**, 1–11.

S3 M. L. Sciú, V. Sebastián-Pérez, L. Martinez-Gonzalez, R. Benitez, D. I. Perez, C. Pérez, N. E. Campillo, A. Martinez and E. L. Moyano, *J. Enzyme Inhib. Med. Chem.*, 2019, **34**, 87–96.

S4 http://app. supramolecular. org/bindfit.

S5 L. A. Weiss, N. Sakai, B. Ghebremariam, C. Ni and S. Matile, *J. Am. Chem. Soc.*, 1997, **119**, 12142–12149.

S6 T. Saha, M. S. Hossain, D. Saha, M. Lahiri and P. Talukdar, *J. Am. Chem. Soc.*, 2016, **138**, 7558–7567.

S7 P. Talukdar, G. Bollot, J. Mareda, N. Sakai and S. Matile, *J. Am. Chem. Soc.*, 2005, **127**, 6528–6529.

S8 S. V. Shinde, P. Talukdar, *Angew. Chem., Int. Ed.*, 2017, **56**, 4238–4242.

S9 X. Wu, E. N. W. Howe and P. A. Gale, *Acc. Chem. Res.*, 2018, **51**, 1870–1879.

S10 J. A. Malla, A. Upadhyay, P. Ghosh, D. Mondal, A. Mondal, S. Sharma and P. Talukdar, *Org. Lett.*, 2022, **24**, 4124–4128.

S11 A. Roy, O. Biswas and P. Talukdar, *Chem. Commun.*, 2017, **53**, 3122–3125.

S12 N. Busschaert, S.-H. Park, K.-H. Baek, Y. P. Choi, J. Park, E. N. W. Howe, J. R. Hiscock, L. E. Karagiannidis, I. Marques, V. Félix, W. Namkung, J. L. Sessler, P. A. Gale and I. Shin, *Nat. Chem.*, 2017, **9**, 667–675.

S13 N. Busschaert, R. B. P. Elmes, D. D. Czech, X. Wu, I. L. Kirby, E. M. Peck, K. D. Hendzel, S. K. Shaw, B. Chan, B. D. Smith, K. A. Jolliffe and P. A. Gale, *Chem. Sci.*, 2014, **5**, 3617–3626.

S14 V. Amendola, L. Fabbrizzi, L. Mosca and F. -P. Schmidtchen, *Chem. Eur. J.*, 2011, **17**, 5972–5981.

S15 A. Raza, S. Chattopadhayay, D. Mondal and P. Talukdar, CCDC 2381721: Experimental Crystal Structure Determination, 2025, DOI: 10.5517/ccdc.csd.cc2kycqm.

S16 A. Raza, S. Chattopadhayay, D. Mondal and P. Talukdar, CCDC 2389545: Experimental Crystal Structure Determination, 2025, DOI: 10.5517/ccdc.csd.cc2l6j3g.

S17 M. J. Frisch, G. W. Trucks, H. B. Schlegel, G. E. Scuseria, M. A. Robb, J. R. Cheeseman, G. Scalmani, V. Barone, B. Mennucci, G. A. Petersson, H. Nakatsuji, M. Caricato, X. Li, H. P. Hratchian, A. F. Izmaylov, J. Bloino, G. Zheng, J. L. Sonnenberg, M. Hada, M. Ehara, K. Toyota, R. Fukuda, J. Hasegawa, M. Ishida, T. Nakajima, Y. Honda, O. Kitao, H. Nakai, T. J. Vreven, M. J.A., J. E. Peralta, F. Ogliaro, M. Bearpark, J. J. Heyd, E. Brothers, K. N. Kudin, V. N. Staroverov, R. Kobayashi, J. Normand, K. Raghavachari, A. Rendell, J. C. Burant, S. S. Iyengar, J. Tomasi, M. Cossi, N. Rega, J. M. Millam, M. Klene, J. E. Knox, J. B. Cross, V. Bakken, C. Adamo, J. Jaramillo, R. Gomperts, R. E. Stratmann, O. Yazyev, A. J. Austin, R. Cammi, C. Pomelli, J. W. Ochterski, R. L. Martin, K. Morokuma, V. G. Zakrzewski, G. A. Voth, P. Salvador, J. J. Dannenberg, S. Dapprich, A. D. Daniels, O. Farkas, J. B. Foresman, J. V. Ortiz and D. J. Cioslowski, J. and Fox, *Gaussian 09, Revis. B.01. Gaussian Inc., Wallingford*.